Assessment of the Water Mass Dynamics Over the Algero-Provencal Basin (Western Mediterranean Sea) in the MEDRYS1V2 Reanalysis

Quentin-boris Barral, Bruno Zakardjian, Franck Dumas, Pierre Garreau, Jonathan Beuvier

JGR Oceans

RESEARCH ARTICLE
10.1029/2023JC020260

Assessment of the Water Mass Dynamics Over the Algero-Provencal Basin (Western Mediterranean Sea) in the MEDRYS1V2 Reanalysis

Quentin-Boris Barral[1], Bruno Zakardjian[1], Franck Dumas[2,3], Pierre Garreau[2], and Jonathan Beuvier[4]

[1]Université de Toulon, Aix-Marseille Université, CNRS, IRD, MIO, Toulon, France, [2]SHOM, Service Hydrologique et Océanographique de la Marine, Brest, France, [3]Laboratoire d'Océanographie Physique et Spatiale (LOPS), IFREMER, UNIV. Brest, CNRS UMR 6523, IRD, IUEM, Plouzané, France, [4]CNRM, Université de Toulouse, Météo-France, CNRS, Toulouse, France

Abstract We present an assessment of the water mass dynamics in a reanalysis of the Mediterranean Sea with a focus on the Algero-Provencal basin. We use a θ-S-based algorithm to compute the fractions of the main western Mediterranean water masses: Atlantic and modified Atlantic Waters (AW and mAW), Western and Eastern Intermediate Waters (WIW and EIW), Tyrrhenian and Western Mediterranean Deep Water (TDW and WMDW). The reanalysis retains the known mean characteristics of the water masses, their seasonal to interannual variabilities, and main circulation patterns when compared with the literature. The imprint of winter mixing is particularly obvious with coherent variations of water mass volumes, mainly the yearly creation of WIW from mAW on northernmost shelves and of WMDW from all surface and intermediate layers during years of deep water formation (DWF). The results also highlight some unrealistic events of variability of the WMDW volume that are likely due to the data assimilation process. Recomputation of water mass volumes and transports without these altered years allowed to highlight the possible disruption of large-scale barotropic cyclonic circulation in the East Algerian basin in response to major DWF events over the Gulf of Lion and the induced surface consequence on Algerian Eddies' trajectories.

Plain Language Summary Defined as the large-scale oceanic circulation driven by surface heat and freshwater flows, oceanic thermohaline circulation plays a major role in the Earth's climate, as it distributes excess heat and carbon dioxide due to human activities into the deeper layers of the ocean over the long term. The Mediterranean Sea is unique in that it has its own thermohaline circulation due to its semi-enclosed configuration, a climate-driven evaporation (∼1 m/y) balanced by an influx of Atlantic Water, and significant winter heat loss leading to the formation of heavy water masses at the surface and their sinking toward the intermediate and bottom layers. This thermohaline circulation has a time scale of less than 100 years, more than 10 times smaller than the global circulation, and has been shown to respond rapidly to climate variability in the Northern Hemisphere. We have used a 20-year ocean reanalysis—a simulation assimilating observations—to characterize and quantify water mass circulation in the Algero-Provencal basin, from seasonal to interannual scales. Our study reveals that the main weakness of reanalysis lies in deep-water dynamics, whereas it has a marked impact on surface and intermediate circulations. Understanding the Mediterranean's future requires a better representation of its deep-water dynamics.

Key Points:

- We study the dynamics of seven water masses in a 20-year reanalysis using a linear mixing algorithm based on θ-S based fractions
- The method allows detecting spurious events of deep water formation, destruction and surface impact, likely due to the assimilation process
- Results show that the Provencal deep water formation could slow down the deep Algerian gyre, inducing an effect on the surface eddies' path

Correspondence to:
Q.-B. Barral,
qbarral@ik.me

Citation:
Barral, Q.-B., Zakardjian, B., Dumas, F., Garreau, P., & Beuvier, J. (2024). Assessment of the water mass dynamics over the Algero-Provencal basin (western Mediterranean Sea) in the MEDRYS1V2 reanalysis. *Journal of Geophysical Research: Oceans*, *129*, e2023JC020260. https://doi.org/10.1029/2023JC020260

Received 27 JUL 2023
Accepted 28 OCT 2024

Author Contributions:
Conceptualization: Quentin-Boris Barral, Bruno Zakardjian, Franck Dumas, Pierre Garreau
Data curation: Quentin-Boris Barral, Bruno Zakardjian, Jonathan Beuvier
Formal analysis: Quentin-Boris Barral, Bruno Zakardjian, Franck Dumas, Pierre Garreau
Funding acquisition: Bruno Zakardjian
Investigation: Quentin-Boris Barral, Bruno Zakardjian
Methodology: Quentin-Boris Barral, Bruno Zakardjian, Pierre Garreau
Project administration: Bruno Zakardjian
Resources: Jonathan Beuvier
Software: Jonathan Beuvier
Supervision: Bruno Zakardjian, Franck Dumas, Pierre Garreau

1. Introduction

The Mediterranean Sea has the unique particularity of having its own and well-defined thermohaline circulation, almost independent from the global one. This is due to its particular configuration: a semi-enclosed sea suffering a dry, windy, and relatively warm regional climate that makes it a concentration basin where evaporation exceeds precipitation and run-offs (Bethoux, 1980; Nof, 1979). This climate-driven deficit of water (∼0.5–1.0 m/year) is balanced by a net inflow through the Strait of Gibraltar between in-flowing AW and deeper out-flowing salty Mediterranean water (Bethoux & Gentili, 1999; Jorda et al., 2017; Mariotti et al., 2002; Millot, 1987; Nof, 1979; Pellet et al., 2019; Sammartino et al., 2015; Schroeder et al., 2023). The incoming AW flows cyclonically in all the Mediterranean sub-basins toward the easternmost Levantine Basin and is continuously modified all along its path by mixing with saltier resident waters and air-sea exchanges. Simultaneously, severe heat loss and evaporation due to harsh atmospheric conditions in autumn and winter over the northern parts of the Mediterranean Sea

Validation: Quentin-Boris Barral, Bruno Zakardjian, Franck Dumas, Pierre Garreau, Jonathan Beuvier
Visualization: Quentin-Boris Barral, Bruno Zakardjian
Writing – original draft: Quentin-Boris Barral, Bruno Zakardjian
Writing – review & editing: Franck Dumas, Pierre Garreau, Jonathan Beuvier

causes convection to intermediate and deep layers (the deep water formation, DWF) in several areas and so to the recurrent formation of different intermediate and deep water masses. Those areas are mainly the Gulf of Lion for Western Mediterranean Deep Water (WMDW), the Adriatic Sea and the Aegean Sea for the Eastern Mediterranean Deep Water (EMDW) and in the northern Levantine Basin for the very salty Levantine Intermediate Water (LIW). All those locally produced water masses mix and spread all together with the AW to set up and maintain the Mediterranean thermohaline circulation (MTHC, Bergamasco & Malanotte-Rizzoli, 2010; Robinson & Golnaraghi, 1994; Waldman et al., 2018; Pinardi et al., 2019). The MTHC has a time scale of about 50–100 years (10–30 times less than the global ocean, 1000–1500 years, e.g., Bond et al., 1997; Cacho et al., 2001; Millot & Taupier-Letage, 2005a, 2005b) and has been shown to quickly respond to Northern Hemisphere climate variability, be it during the last glacial period (Cacho et al., 2000, 2001; Cortina-Guerra et al., 2021; Incarbona et al., 2016) or more recently in the early 90s when an abrupt shift in the intermediate and deep part of the eastern MTHC, called the Eastern Mediterranean Transient (EMT), has affected the water masses in both parts of the Mediterranean for at least a decade (Bergamasco & Malanotte-Rizzoli, 2010; Cardin et al., 2015; Li & Tanhua, 2020; Roether et al., 2007; Sisma-Ventura et al., 2021). Subsequent to the propagation of the EMT signal in the western Mediterranean and after a lack of intermediate and deep convection in the early 00's, the sudden return of DWF events in 2005 and after has led to a cooling and freshening of the intermediate waters associated with a warming and salting of the deep waters called the Western Mediterranean Transition (WMT, Amitai et al., 2021; López-Jurado et al., 2005; Piñeiro et al., 2019, 2021; Schroeder et al., 2006, 2010, 2016).

All climate models predict increased precipitation variability in the Mediterranean, significant warming and drying, and an increase in the frequency, intensity, and duration of both continental and marine heat waves (Darmaraki et al., 2019; de Sherbinin, 2014; Giorgi, 2006; IPCC AR6 WGI Full Report, 2023; Martinez et al., 2023; Somot et al., 2008). The western part of the MTHC has already been shown to be undergoing changes, with historical observations showing that the western DWF has declined by 40% since 1969, whereas worst-case scenario future predictions show that it could collapse by mid-century due to weakening heat loss and stronger stratification (Adloff et al., 2015; Herrmann et al., 2008; Josey & Schroeder, 2023; Margirier et al., 2020; Parras-Berrocal et al., 2022; Somot et al., 2006). Indeed, recent studies have shown the surface Mediterranean waters to have warmed at a rate four times larger than the global ocean over the last decades (~0.04°C/year vs. ~0.01°C/year, Bensoussan et al., 2019; Bethoux et al., 1998; Nykjaer, 2009; Pisano et al., 2020; Vargas-Yanez et al., 2008), affecting all layers throughout the Mediterranean. These warning signals have led, over the last 20 years or so, to an unprecedented effort of sampling, modeling, and analysis. However, an integrated and quantitative view of the MTHC able to improve the monitoring and future predictions of climate-induced changes still remains a challenge (CIESM, 2002, 2022; Fox-Kemper et al., 2019; Somot et al., 2008; Theocharis, 2008). Here, we focus on the Algero-Provencal basin which is known to be a multilayered system (surface, winter subsurface, intermediate, deep and bottom waters, Juza et al., 2015) and at least has six main water masses which are commonly used and identified in the literature: the recent and an older Atlantic Water (both 0–200 m) in near surface layers, the Western and Eastern Intermediate Waters (WIW, ~200 m and EIW, 300–600 m) in the intermediate layers, and the Tyrrhenian and Western Mediterranean Deep Waters (TDW, 500–1,500 m and WMDW, deeper than 1,500 m) at greater layers down to the bottom (Juza et al., 2013, 2019; Manzella & La Violette, 1990; Millot, 1987; Millot & Taupier-Letage, 2005a, 2005b; Pinot et al., 1995; Wüst, 1961).

The AW incoming from the strait of Gibraltar (0.6–1.0 Sv, Peliz et al., 2013; Skliris et al., 2018; Soto-Navarro et al., 2010) is the first input of the western MTHC and, except the Rhône and Ebro rivers plumes, is the lightest and freshest water of the western Mediterranean (S ~ 36.0 at the Strait of Gibraltar). It flows along the North African coast within the Algerian Current (AC, Figure 1), being spread and partially mixed northward in the Algerian basin by the Algerian Eddies (AEs, e.g., Escudier et al., 2016; Millot, 1990; Puillat et al., 2002; Testor, Send, et al., 2005) before flowing eastward toward the Tyrrhenian and through the strait of Sicily toward the Eastern Mediterranean (Béranger et al., 2004; Jebri et al., 2016). MAW or mAW, for modified Atlantic Water is an acronym commonly used by many authors to designate the saltier AW due to its aging in the Mediterranean (e.g., Hassoun et al., 2015; Millot, 1999; Onken & Sellschopp, 2001; Puillat et al., 2002; Theocharis et al., 1993). It is sometimes also called old AW, (typical) Mediterranean Water or Mediterranean Surface Water (Millot, 2007, 2009; Millot et al., 2006). Some others consider both the AW and mAW as a single entity (e.g., Béranger et al., 2005; CIESM, 2001; Fedele et al., 2022; Millot, 2013; Millot & Taupier-Letage, 2005a, 2005b). Both the AW and mAW are restricted to the upper (0–200 m) layers but significantly differ in terms of salinity values, the latter at least reaching two salinity units greater values (~38.2–38.4) for the saltier ones in the Tyrrhenian and

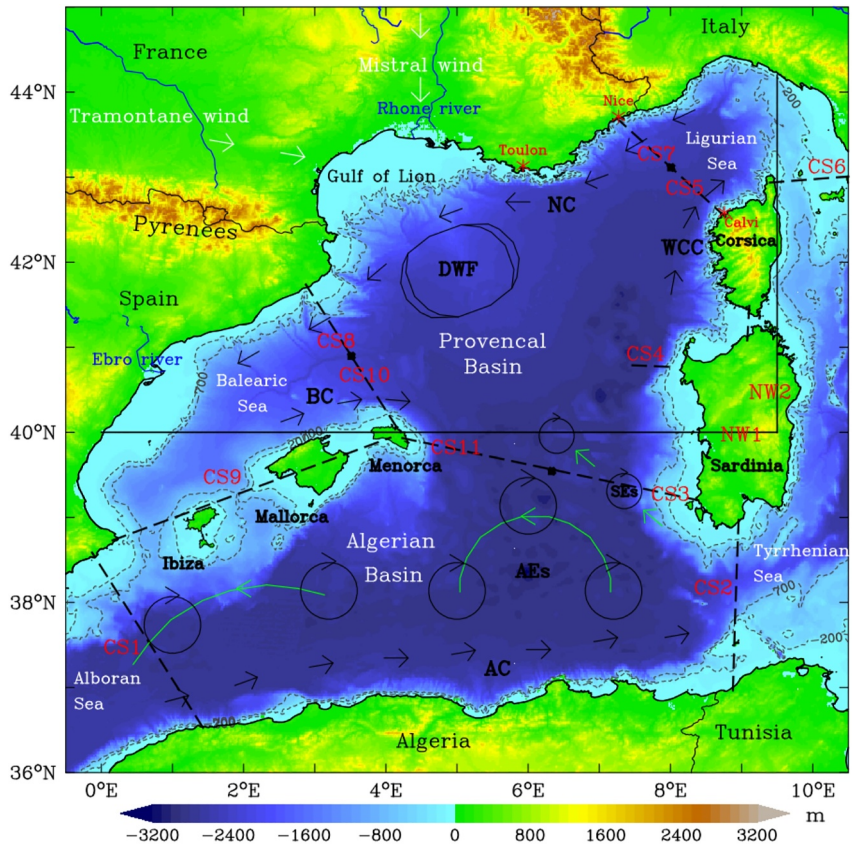

Figure 1. Map of the western Mediterranean bathymetry and major circulations features. AC, BC, NC, and WCC denote, respectively, the Algerian, Balearic, Northern, and West Corsican currents. Large and small black arrow circles denote the Algerian and Sardinian Eddies, respectively, (AEs and SEs) whereas green arrows represent their paths. The black oval shape locates the Deep-Water Formation area. The red-labeled cross-sections locate where the transports of Table 3 have been calculated. The studied domain is the Algero-Provencal basin which is located between CS1, CS2, and CS6 for the calculations of Table 2, Figures 6, 7c, and 7d. The NW1 section locates the section of Figures 3 and 4, and with NW2, both define the NWMED domain, such as in Somot et al. (2018) for calculations in Figures 7a and 7b. Bathymetry data are detailed in the Open Research section.

Ligurian Seas; hence, the use of the appellation mAW for the present work. The saltier mAW from the Tyrrhenian fuels the East Corsican Current (ECC) and joins with the West Corsican Current (WCC) to feed the Northern Current (NC) that flows from the Ligurian Sea to the Balearic Sea (Figure 1).

The Eastern Intermediate Water (EIW) is the second major input of the western MTHC. EIW is the preferred used term for all intermediate water that crosses the Sicily channel (Millot, 2013), being mainly composed of two water masses among others. Levantine and Cretan Intermediate Waters (LIW and CIW) are produced in the Eastern Mediterranean by intermediate (~200–700 m) convection in winter and are the saltier ($S > 39$) of the Mediterranean (Kubin et al., 2019; Millot, 2013; Ozer et al., 2017; Velaoras et al., 2013, 2014). These flow cyclonically along the continental slope at intermediate depths throughout the eastern basin and either more or less pass the Strait of Sicily according to a seasonal cycle and the mode of the Bimodal Oscillating System of the Ionian Sea (where they mix within a turbulent dispersion) before to entering the western basin and then forms the EIW (Ben Ismail et al., 2014; Estournel et al., 2021; Millot, 2013; Velaoras et al., 2014). When EIW enters the Tyrrhenian Sea, it mixes with resident deep waters (mostly WMDW) and forms the TDW (Astraldi & Gasparini, 1994; Gasparini et al., 2005; Sparnocchia et al., 1999), but still keeping a pronounced salinity signature ($S > 38.8$ between 300 and 600 m). Both the EIW and TDW follow a counterclockwise circulation in the Tyrrhenian (Falco et al., 2016; Iacono et al., 2021; Vara et al., 2019) before they leave through the Sardinia Channel to enter the Algero-Provencal basin where it flow northwestward along the western coasts of Sardinia and Corsica or are

spread out westward in the central basin by the Sardinian eddies (SEs) (Bosse et al., 2015; Rhein et al., 1999; Send & Testor, 2017; Testor, Béranger, & Mortier, 2005).

The WIW is a product of intermediate convection, a winter cooled mAW due to cold and dry winds (Mistral and Tramontane) blowing over the shelf of the Gulf of Lion (GoL), the Provencal basin, and the Ligurian Sea. Although not originally the saltiest of the mAW (~38.3), its cooling is sufficient to increase its potential density so as to make it sit between the warmer mAW and the deeper EIW at an intermediate depth of about 200–300 m. It flows then mostly along the continental slope across the Balearic Sea and later through the Ibiza and Mallorca channels down to the Alboran Sea (Juza et al., 2019; Puig et al., 2013; Salat & Font, 1987; Vargas-Yanez et al., 2012, 2020). Stronger winter wind forcing over the GoL and the Provencal basin regularly causes vertical convection that goes beyond WIW formation, mixes with EIW and can reach the seabed in some years, leading to WMDW renewal (Keller Jr. et al., 2022; MEDOC GROUP, 1970; Millot, 1999; Schroeder, Ribotti, et al., 2008; Schroeder, Taillandier, et al., 2008; Testor et al., 2018; Waldman, Herrmann, et al., 2017; Waldman, Somot, et al., 2017; Waldman et al., 2016). Intermediate convection during less severe winters produces a slightly less dense water that stands and stacks between the EIW and older deep water with thermohaline characteristics similar to the TDW. Constrained by the southward increasing bathymetry, the denser WMDW ($\sigma_\theta > 29.10\,kg.m^{-3}$) then spreads mostly southward across the whole Algero-Provencal basin up till the Alboran Sea. The WMDWs can sometimes pass through the Sardinia Channel to enter the Tyrrhenian when exceptional DWF uplifts the older and lighter WMDW up to the strait sill, as following the WMT (e.g., Beuvier et al., 2012; Li & Tanhua, 2020; Schroeder et al., 2016).

To better understand the dynamics of these water masses, it is necessary to be able to follow their behavior and interactions, their entry or exit, their propagation, and their mixing through the numerous mesoscale to submesoscale eddies that are found throughout the NW Mediterranean. This challenge is hardly achievable with at-sea observations alone, while numerical modeling may not be free of biases and unrealistic trends due to uncertainties in forcing, initial conditions, and unresolved sub-grid processes. By combining, thanks to data assimilation systems, modeling, and observations in a coherent physical framework, ocean reanalysis offers a good compromise, particularly for multi-decadal series which allow us to approach the climatology of the system and its inter-annual variability (Aznar et al., 2016; Balsameda et al., 2015). However, the reanalysis has its own weaknesses, mainly due to the assimilation process which, by forcing the model trajectory to converge toward independent observations, does not guarantee the pure conservation of heat and salt and can therefore alter the characteristics of the water masses.

This work is based on a reanalysis of the Mediterranean Sea, called MEDRYS1V2 (Beuvier et al., 2016; Hamon et al., 2016), with two main objectives: first, to assess the mean characteristics and distribution of water masses over the Algero-Provencal basin as produced by the reanalysis, and second, to gain insight, characterize, and quantify the circulation of these different water masses from seasonal to interannual time scales. We built a simple and efficient method to detect the water masses in the Algero-Provencal basin and track their circulation and mixing over the 20-year reanalysis (Section 2.2). The results are first analyzed using the mean thermohaline characteristics of each water mass to assess the robustness of the reanalysis in terms of water mass conservation. Climatological average of water mass volumes and transports are then assessed based on known circulation patterns (Section 3.1). In a second step, we analyze the time series of peculiar properties and volumes of surface to intermediate water masses (Section 3.2). In a third step, we focus the analysis on the intermediate to deep water mass time series in Section 3.3. These are assessed with regard to their long-term changes and averages tendencies (Section 3.3.1) before focusing on special episodes (Sections 3.3.2). We finally discuss the possible origins of these episodes (Section 4.1), the water mass detection method (Section 4.2), and the possible northern DWF impact on southern dynamics (Section 4.3) before concluding in Section 5.

2. Data and Methods

2.1. The MEDRYS1V2 Reanalysis

The study is based on the MEDRYS1V2 reanalysis which begins in October 1992 and ends in June 2013 with daily outputs (Beuvier et al., 2016; Hamon et al., 2016). These two decades give us sufficient years to produce a climatology of water mass volumes and transports of this era and to observe several different episodes. MEDRYS1V2 is a configuration of the NEMO-MED12 model (which has a spatial resolution of 1/12° and 75 z levels sharpened near the surface) that uses the SAM2 assimilation scheme (Lellouche et al., 2013). The

simulation is forced by the atmospheric ALDERA data set (Hamon et al., 2016), a downscaling of the ERA-Interim reanalysis (Dee et al., 2011) with the ALADIN-Climate regional climate model (Colin et al. (2010) for the description of the version 5 of ALADIN-Climate used to produce the ALDERA data set). Satellite SST, altimetry, and in situ temperature-salinity (θ-S) profiles are assimilated. SST data were assimilated at a resolution of 1° and comes from NOAA 1/4° gridded radiometer products (Reynolds et al., 2007). The along-track sea level anomaly (SLA) AVISO product (1992–2013) is assimilated one every three points and combined with the Mediterranean MDT from Rio et al. (2011). Both SST and SLA were assimilated without trusting any observation within 50 km off the coasts. Assimilated in situ θ-S profiles from the CORA4 database (Cabanes et al., 2013) uses only one profile within 0.1° per day per platform. The reanalysis is initialized at the end of September 1992 with the state of a twin free run (same model configuration as MEDRYS1V2 but without data assimilation), which starts in October 1979. It takes about 9 months after its beginning for the reanalysis to achieve its spin up (see Hamon et al., 2016). Following results and validation hence do not take into account the first three seasons of the reanalysis (autumn 1992–spring 1993).

2.2. The Water Mass Detection Algorithm

2.2.1. Initial Assessment of Mixing: Literature and Shape of the θ-S Diagram

The θ-S diagram is the classic physical oceanography tool used to analyze the mixing and distribution of water masses. It is based on the mixing of two water masses that form a straight line in the diagram, allowing the fraction of those to be determined for the entire depth sampled along this mixing line. The method is more complicated for the mixing of three water masses that build a curve inside a triangle instead (e.g., Mamayev, 1975; Millot, 2013; Schroeder et al., 2023) and considering that the sum of their fraction must equal unity. It becomes even more difficult for four water masses or more without considering at least one another conservative variable (e.g., de Brauwere et al., 2007; Manca et al., 2006; Schroeder, Taillandier, et al., 2008). Even in these cases, the other used variables should have to be sampled with the same spatio-temporal resolution that the θ-S data, which is a hard to achieve task. Other methods can be found in recent literature, such as more complex diagrams using variables derived from potential temperature and salinity (e.g., σ-π diagrams, Huang et al., 2018; Tailleux, 2021) and clustering based methods (e.g., Kim et al., 1991; Zhu et al., 2019), sometimes combined with EOF analysis on vertical profile of temperature and salinity (e.g., Bauch & Cherniavskaia, 2018; Gao et al., 2020; Hjelmervik & Hjelmervik, 2013), but these were not considered given their high computing cost over a 20-year reanalysis.

Instead, we rather use the fact that, with the exception of transitory convection events, the vertical distributions of the different water masses are constrained by their relative buoyancy, that is, that they are vertically ordered with increasing potential density σ_θ. Our water mass sorting algorithm is defined on the basis of the literature (Table 1 below) and the daily climatological θ-S diagram (averaged over 20 years) calculated from the reanalysis (e.g., see Figure 2 for the monthly diagram), assuming that over the Algero-Provencal basin the water column can be divided into several layers of which the surface and deep layers are the boundaries, each with its own different θ, S, or σ mixing tendency.

AW and mAW ($37 < S < 38.45$, $\theta > 13$, 5°C) are located above 200–300 m, that is, at the surface and they can be easily distinguished from each other solely by using salinity in the Algero-Provencal basin (Table 1). In this upper layer, temperature ranges seasonally from 13°C to more than 25°C (Figure 2, left, top yellow); this also helps in winter to identify the WIW as a cooled mAW ($\theta < 13.5$°C, Figure 2, left and right). Meanwhile, shelf waters are fresh and cold (Figure 2, left, bottom yellow), mostly because the river plumes undergo winds at the surface. Below these water masses of the surface layer and below 300 m (Figure 2, blue in the left panel and greater than 28.9 $kg.m^{-3}$ in the right panel), other mixings reveal the transitions from mAW-WIW toward a temperature-salinity maximum that marks the EIW core (Figure 2, right, about 29.04 $kg.m^{-3}$). Below this salinity maximum, the θ-S diagram shows a third and almost linear mixing line from the resident EIW in the Algero-Provencal at the Strait of Sardinia to the bottom WMDW of the Algerian basin (about 38.7, 14.0°C linking 38.45, 12.8°C). Between the two, TDW is present but does not form a marked inflection point, as it was produced by the mixing of EIW with WMDW outside the study area (i.e., the Tyrrhenian, Table 1, Figure 2, purple part of the right-hand panel).

The water mass sorting algorithm therefore initially uses a partitioning of the water column based on the potential density anomaly: it defines a surface layer and a deep layer, whose density fraction decreases progressively toward the middle of the intermediate layer, where they are fixed at zero. In a second step, the water masses of a

Table 1
Historical Values of Potential Temperature, Salinity, Potential Density Anomaly, and Depth Location of the Water Masses in the Western Mediterranean

Water mass	θ (°C)	S	σ_θ (kg.m^{-3})	Depth (m)	Location and period	References
AW	>15	36.0–36.4	<27	<200	Gibraltar, 1955–2007	Bryden et al. (1994), Millot (2007, 2009), Carracedo et al. (2014)
	14–25	37.5–37.8	~25	0–150	Bal. Sea and Alg.-Pro. 1996–2020	Vargas-Yanez et al. (2020), Barral et al. (2021); Fedele et al. (2022)
mAW	>13	38.0–38.5	27.5–29	0–300	Lig. Sea and Pro. area 1980–2018	Marty and Chiavérini (2010), Puig et al. (2013), Prieur et al. (2020)
WIW	11.5–13.5	37.7–38.6	28.9–29.1	100–300	Bal and Pro 1983–2019	Salat and Font (1987), Puig et al. (2013), Juza et al. (2019), Vargas-Yanez et al. (2012, 2020)
LIW	≥15	39–39.2	29.06	200–500	Lev. basin 1978–2017	Millot (2013), Ozer et al. (2017), Kubin et al. (2019)
EIW	13.1–13.9	38.5–38.7	29.05–29.1	200–800	Alg.-Pro. 2000–2019	Puillat et al. (2006), Bosse et al. (2015), Mallil et al. (2021), Fedele et al. (2022)
TDW	12.8–13.7	38.43–38.7	>29.09	>700	Tyr. Sea 1987–2018	Fuda et al. (2002), Buffett et al. (2017), Napolitano et al. (2019), Li and Tanhua (2020)
	>12.86	38.46–38.56		600–1900	Alg.-Pro. 1997–2002	Rhein et al. (1999), Send and Testor (2017), von Schuckmann et al. (2021)
WMDW	12.7–13	38.4–38.5	>29.1	>1500	Alg.-Pro. 1990–2014	Millot (1999), Fuda et al. (2000), Puig et al. (2013), Schroeder et al. (2006, 2016), Knoll et al. (2017)

Note. The locations of historical studies are indicated with Alg.-Pro., Bal., Lev., Lig., Pro. and Tyr., denoting, respectively, the Algero-Provencal basin, Balearic Sea, Levantine basin, Ligurian Sea, Provencal basin, and Tyrrhenian Sea. AW, mAW, WIW, LIW, EIW, TDW, and WMDW respectively denote Atlantic Water, modified Atlantic Water, Western Intermediate Water, Levantine Intermediate Water, Eastern Intermediate Water, Tyrrhenian Deep Water, and Western Mediterranean Deep Water.

same layer are separated thanks to ad hoc salinity and/or temperature dilution fractions along the previously identified mixing lines. As a result, some of these are sometimes multiplied by the first density fractions. The use of functions based on potential density rather than fixed depths allows this water column partitioning to be dynamically adjusted throughout the reanalysis. Similarly, dilution ratios for temperature, salinity, and density are used subsequently rather than sharp truncations (fixed-thresholds) which do not resolve the mixing of water masses. In addition, the fixed-threshold values used to discriminate between water masses generate unwelcome spurious effects due to discontinuities in their vicinity. These undesirable effects (in this study) can be seen, for example, in Figure 7b of Beuvier et al. (2012), Figure 8 in Waldman et al. (2016), and Figures 9a and 9b in Testor et al. (2018) where deep waters are separated according to different fixed density thresholds that produce significant differences in volume and formation rate.

2.2.2. The Detailed Algorithm: Sorting Water Masses by Linear Fractions of σ, S, and θ

This section outlines the main assumptions of the algorithm, the calculation steps and concise mathematical equations are set out in Appendix A, with less explanation.

At a first step, the water column is partitioned using two functions defining the fractions of surface (f_{surf}) and deep (f_{deep}) layers, which are density fractions, assuming that the EIW marks the boundary between the two. The surface layer is first defined as 100% ($f_{surf} = 1$) for the fraction of all waters with densities that are smaller than the isopycnal $\sigma_{mAW} = 28.964$ kg.m^{-3} that would mark the limit of the mAW core. Below this threshold, the algorithm considers a linear decrease between σ_{mAW} and $\sigma_{EIW} = 29.062$ kg.m^{-3} in f_{surf} from 1 to zero (Equation A1) that is assumed to account the progressive mixing of surface waters (AW-mAW-WIW) with the lower intermediate layer. Conversely, the deep layer tagging fdeep is constructed with the isopycnal $\sigma_{WMDW} = 29.1075$ kg.m^{-3}, which is often used to locate the upper bound of the WMDWs (e.g., Somot et al., 2018; Testor et al., 2018; Waldman, Herrmann, et al., 2017; Waldman, Somot, et al., 2017), and with a linear decrease between σ_{WMDW} and σ_{EIW} (Equation A2). σ_{WMDW} is defined using S = 38.45, the average minimum of salinity of WMDW (e.g.,

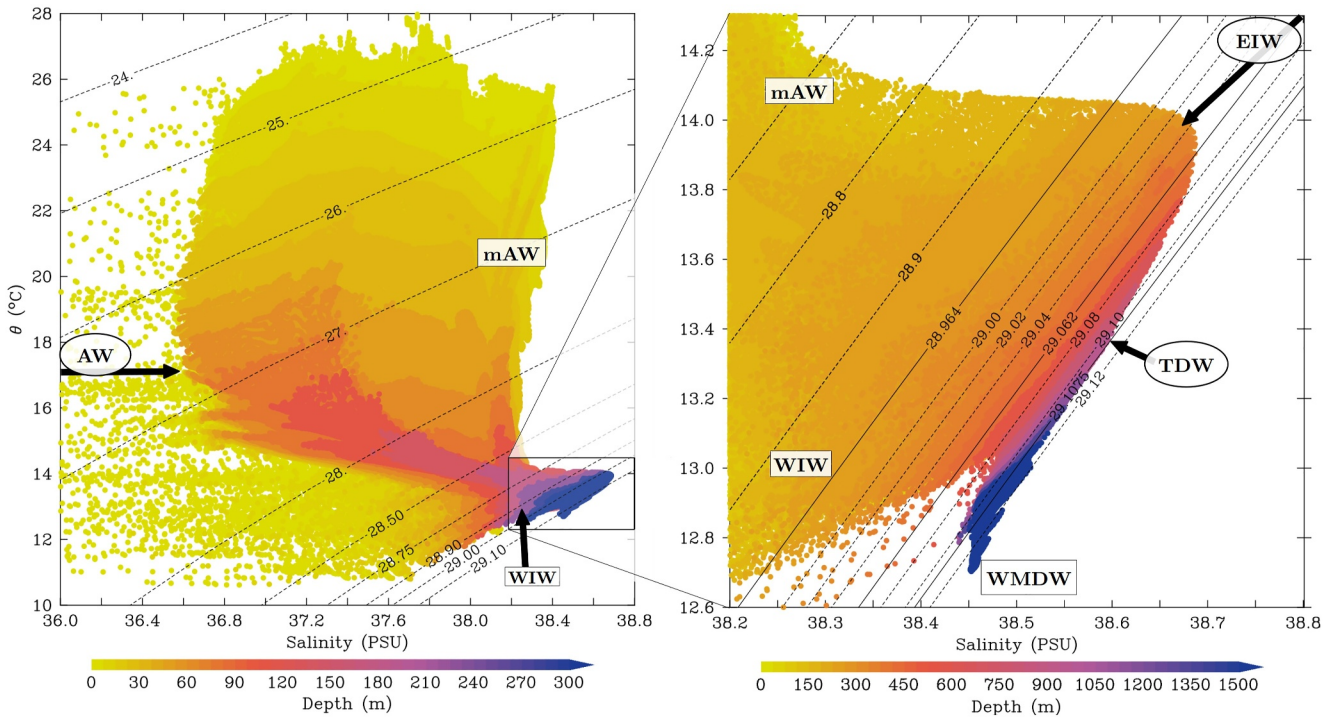

Figure 2. θ-S diagram colored by depth of the full monthly average of the 20-year MEDRYS1V2 reanalysis, illustrating the several known water masses in the western Mediterranean basin (except the Alboran and Tyrrhenian Seas' sub-basins as in Figure 1). AW, mAW, WIW, LIW, TDW, and WMDW denote, respectively, Atlantic Water, modified Atlantic Water, Western Intermediate Water, Levantine Intermediate Water, Tyrrhenian Deep Water, and Western Mediterranean Deep Water. Layer marking limits are represented by the three undotted isopycnals.

Houpert et al., 2016; Puig et al., 2013), and θ = 12.815°C. These values come from the reanalysis and corresponds to the inflection point constructed by the old WMDW on the θ-S diagram (Figure 2, right-hand panel) such as in Schroeder et al. (2016) and Testor et al. (2018). The value used for σ_{EIW} is that of the intermediate EIW at the strait of Sicily (taking S = 38.8 and θ = 14.3°C) that is globally conserved in the reanalysis along the path of the EIW spreading (Figure 2). The value of 13.3°C in the Strait of Sicily does not derive from its maximum salinity, but rather from the maximum spice in the channel (Flament, 2002; McDougall & Krzysik, 2015), better characterizing the earlier spreading of LIW + CIW along the isopycnal of about 29.06 kg.m^{-3} (Millot, 2013).

The second step sorts low-salinity water masses (freshwater vs. AW, AW vs. saltier mAW, and mAW/WIW vs. EIW) using salinity dilution functions. As we consider the surface layer, all fractions of salinity used for AW-mAW-WIW sorting are multiplied by the previous surface layer fraction. The salinity fraction of AW (frW) that is calculated between frW and AW is set to zero (1) for S = 0 and linearly increases (decreases) to be set to 1 (zero) for S_{AW} = 36 (Equation A3). 36.0 is the minimum salinity of inflowing AW through the Strait of Gibraltar (see Table 1). The frW fraction is forced to zero above 36 but the AW fraction depends on the mAW there. The salinity mixing between AW and mAW is described with a function that decreases (increases) the AW (mAW) fraction between 36 and 38.45, the upper salinity bound of mAW (Equation A4). The AW fraction is zero when the salinity is greater than S_{mAW}, whereas the mAW fraction follows a salinity linear mixing with the EIW (38.8). The mAW's salinity (38.45) used to define σ_{mAW} has been given by the maximum of time-averaged sea surface salinity in the reanalysis (Figure 2) and by observations in literature, both in the Ligurian Sea (Marty & Chiavérini, 2010; Prieur et al., 2020).

The EIW tagging uses a salinity ratio tmp_{EIW} between 38.8 and 38.45, assuming a similar salinity dilution with all surrounding layers (Equation A5) but in conjunction with the complementary fraction of deep water ($1 - f_{deep}$, i.e. intermediate waters) to discriminate between denser TDW and WMDW (Equation A6). The TDW are then tagged as the saltiest of the deeper water masses as the rest of EIW-like dilution ratio restricted to the deep layer f_{deep} (Equation A7). It is thus located within the intervals of 38.45–38.8 and 29.062–29.075 kg.m^{-3}. Therefore, the algorithm considers WMDW as the remaining fractions in the deep layer minus those of TDW (Equation A8),

endly implying that the fraction of WMDW can be seen as the deep layer fraction deprived of the intermediate salinity fraction: $f_{WMDW} = f_{deep}*(1 - tmp_{EIW})$. The WIW is included in the mAW tagging and to sort them, we built another temporary function that gives what remains in the lighter θ-S space of fractions: $tmp = f_{frW} + f_{AW} + f_{EIW}$ (Equation A9). This temporary amalgam effectively excludes (and thus gathers) the mAW, WIW, shelf waters, and diluted EIW (Figure 2, right panel, ∼38.45 and 13°C) since frW, AW, EIW, and deep waters have already been defined. The mAW fraction is in the upper layer with a temperature sub-partitioning to discriminate WIW: a temporary mixing ratio (tmp_{WIW}) between $\theta_{WIW} = 13°C$ and $\theta_{mAW} = 13.5°C$ when σ_θ is lower than σ_{EIW} (Equations A10–A12). This WIW labeling is an intermediate method between a fixed range detection and the geometry-based method of Juza et al. (2019). Last, we define a pool of intermediate mixed waters, called mIW, as the unity deprived of the sum of all previously computed fractions (Equation A13). Given the location of the highest fraction of the mIW (see Figure A1g for an illustration of the finite method), with regard to the right panel of Figure 2, this pool seems to be composed of the most desalinated EIW in the Algero-Provencal basin.

2.2.3. Application Example: A One-Day Cross-Section of the Water Masses

Figure 3 shows an illustrative example of the θ-S diagrams of fractions and Figure 4 shows the corresponding vertical distribution of the so-tagged water masses for a zonal section at 40°N in early summer 2002 (see Figure 1). Higher fraction values properly match the known θ-S ranges of each water mass, mixing trends between each and vertical distributions. Waters above $\sigma_\theta = 29.062$ kg.m^{-3} are mainly AW and mAW, showing a zonal transition between the Balearic Sea, where mAW are mostly found, and the central area where the signature of AW is slightly more pronounced. Both are tagged in the upper 300 m and well above the EIW. WIW is located (Figure 4b) between mAW and EIW and preferentially in the Balearic Sea in a vein of low temperature (13–13.3°C) and moderate salinity (38.1–38.4) along the Iberian shelf slope (f_{WIW} greater than 70%). EIW is tagged between 200 and 800 m depth, preferentially on the Sardinian coast. The TDW is mainly located in the range 400–1,500 m with fractions that do not exceed 50% and display deeper remnant fractions of 10% at depths of around 2,200 m. The WMDW is labeled at depth (f_{WMDW} greater than 75% below 800 m) and mainly below the 29.10 kg.m^{-3} isopycnal. The mIW is highly tagged with fractions on the mixing layer of low fractions of EIW, centered on 29.062 kg.m^{-3} isopycnal with a larger extent at a depth of 800 m.

By marking the water masses in this way, we were able to calculate several diagnostic quantities (see Appendix B for details on the calculations) to first check the robustness and efficiency of the algorithm in the entire reanalysis, and second to extract the distributions and transports of each water mass. Based on the fact that the sum of the water mass fractions is always constrained to unity, these are first used as weighting factors to extract the volume-averaged thermohaline characteristics of each water mass over the study area. The core characteristics of each water mass are calculated similarly but using only the local maximum within the water column of the corresponding fraction. We also calculated the depth range occupied by each water mass by averaging the minimum and maximum depths of each water column where the corresponding fraction is greater than 5%. Still based on a sum of fractions equal to unity, the water mass fractions are then used to partition the peculiar volumes and advective fluxes for each grid cell. When averaged over time, this produces circulation maps. It also allows us to calculate water mass volumes and transports from the water column level to the regional scale. This enables us to obtain time series of total volumes in the domain and of transport through selected sections.

3. Results

3.1. Average Characteristics, Volumes, and Circulation of Water Masses

This section presents the climatological averages (i.e., 20-year averages) of the thermohaline characteristics, volumes, and transports of each water mass as labeled by the algorithm. Table 2 presents the average characteristics (θ, S, σ_θ, z) for comparison with known literature values given in Table 1. Figure 5 presents the calculated peculiar volumes and transports. Reported per square meter for each model grid point, the estimated volumes (in m3) can also be interpreted roughly as a thickness of the water mass layer (in meters). The integration of volume fractions corresponds to a water column more extensive than this thickness, reduced to a constant fraction of 100%. Table 3 gives transport values computed at selected sections (see Figure 1) to facilitate the comparisons with known transports of the major currents in the literature.

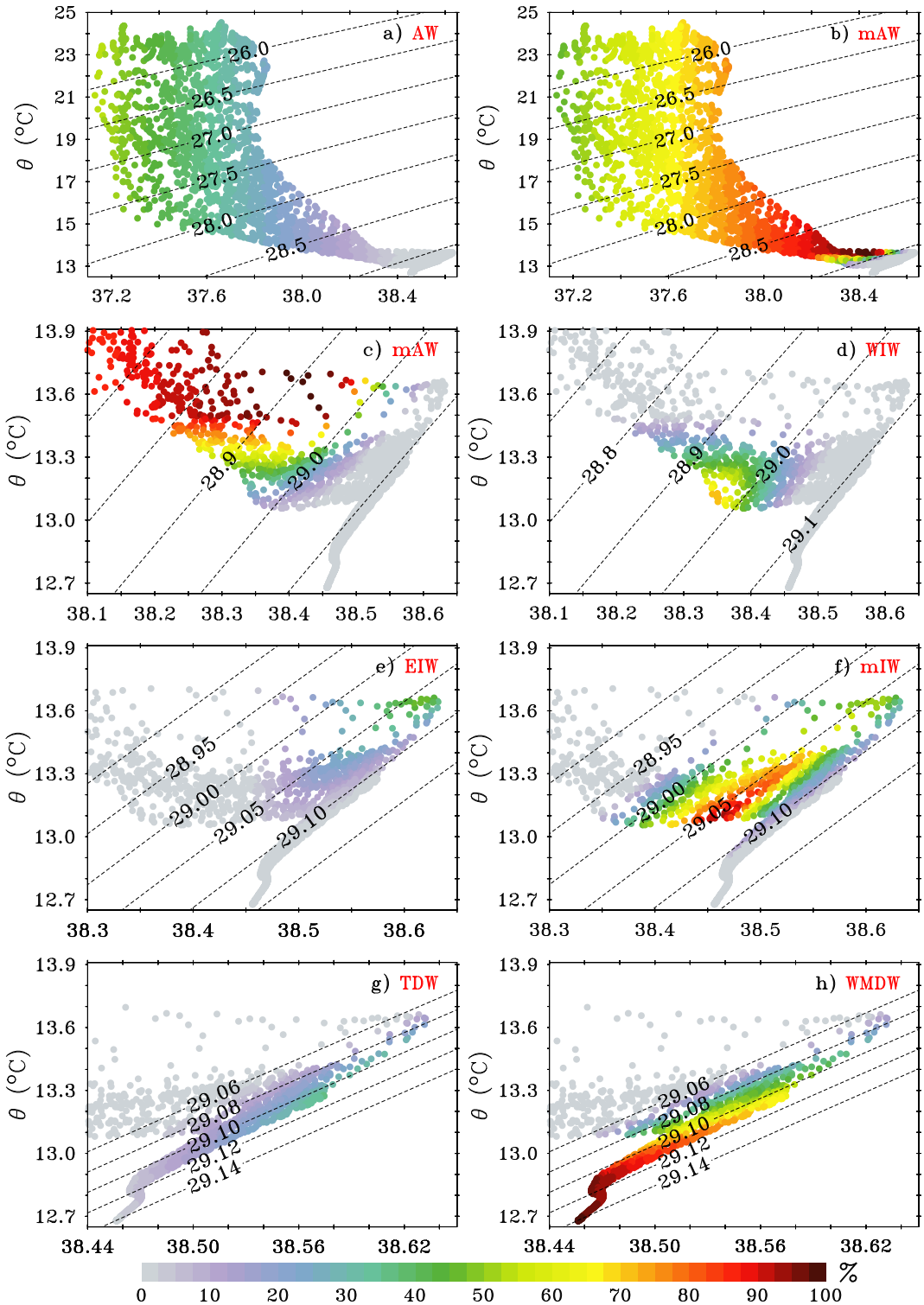

Figure 3. θ-S diagrams of the water mass fractions (%) along 40°N for 30 June 2002 (corresponding to shown NW1 section of Figure 1 and water mass vertical sections of Figure 4) for (a) Atlantic Water, (b and d) modified Atlantic Water, (c) Western Intermediate Water, (e) Eastern Intermediate Water, (f) mixed Intermediate Water, (g) Tyrrhenian Deep Water and (h) Western Mediterranean Deep Water. Some critical dashed isopycnals are shown (kg.m^{-3}). The panel (c) is a zoom of panel (b).

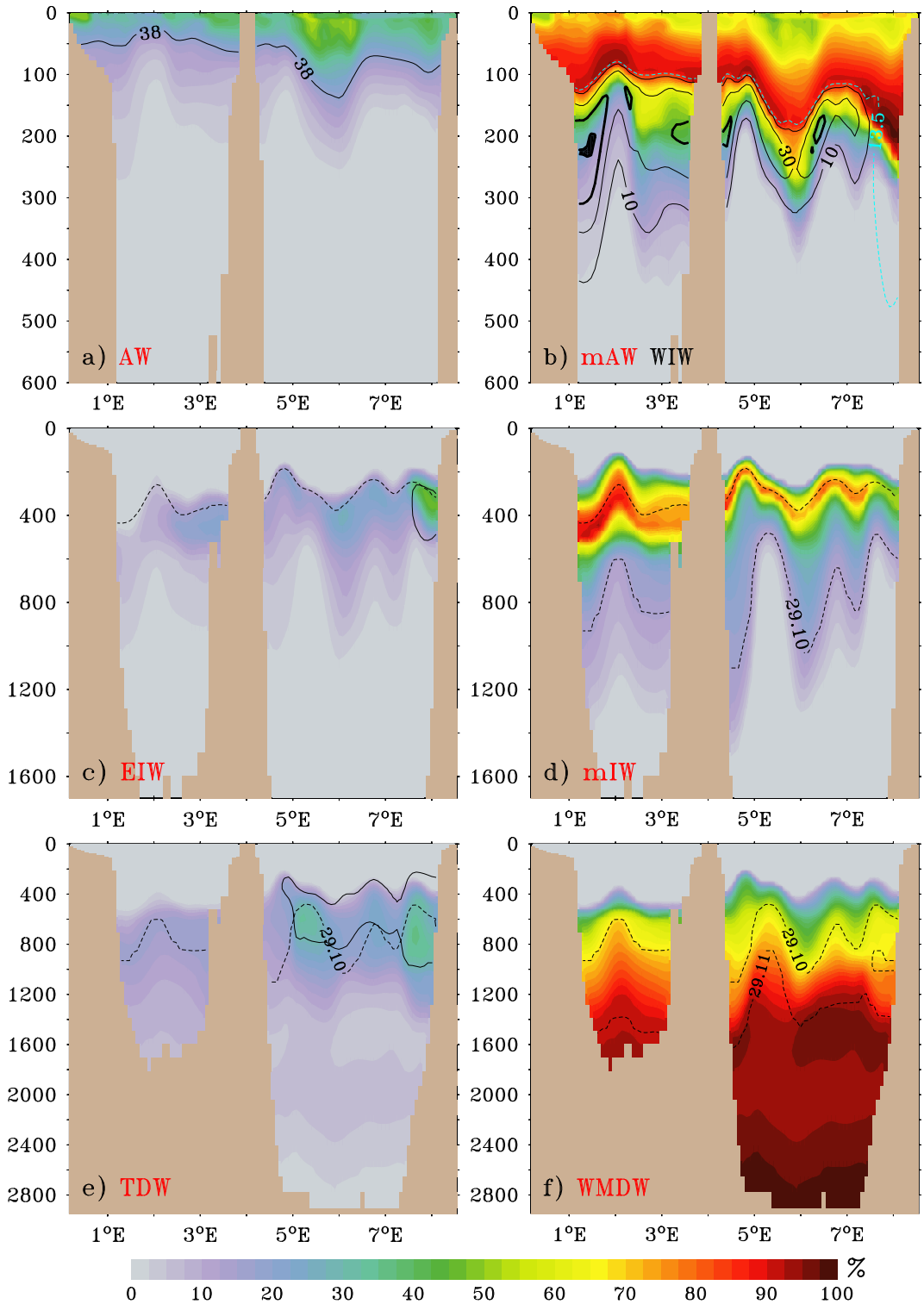

Figure 4. Vertical (m) sections of the water mass fractions (%) along 40°N for 20 June 2002 (corresponding to NW1 section of Figure 1 and θ-S diagrams of Figure 3.). Some critical isolines are shown on vertical section panels: (a) solid isohaline of 38.00; (b) solid contours of fractions of WIW for 10%, 30% and bold for 50% and 70%, light blue dashed isotherm of 13.5°C; (c) dashed isopycnal of 29.05 kg.m^{-3} and isohaline of 38.59; (d) dashed isopycnals of 29.05 and 20.10 kg.m^{-3}; (e) dashed isopycnal of 20.10 kg.m^{-3} and solid isohaline of 38.55; (f) dashed isopycnals of 29.10 and 20.11 kg.m^{-3}.

Table 2
Calculated (20y and Spatial Average, Standard Deviation in Brackets) Values of Potential Temperature, Salinity, Potential Density Anomaly, and Depth Location of the Water Masses in the Algero-Provencal Basin

Water mass		θ (°C)	S	σ_θ (kg.m^{-3})	Depth (m)
frW	Full	16.851 (3.80)	27.885 (2.997)	20.037 (2.489)	min 0 (0)
					ave 2 (1)
					max 2.6 (1.6)
	Core	16.941 (3.798)	24.759 (3.653)	17.621 (2.928)	ave 0.5 (0.1)
AW	Full	15.954 (1.32)	37.565 (0.071)	27.702 (0.338)	min 1 (1)
					ave 34 (2)
					max 138 (16)
	Core	16.907 (1.849)	37.289 (0.123)	27.273 (0.507)	ave 22 (9)
mAW	Full	14.510 (0.607)	38.105 (0.04)	28.460 (0.148)	min 3 (7)
					ave 63 (8)
					max 253 (36)
	Core	13.796 (0.354)	38.300 (0.041)	28.778 (0.09)	ave 114 (26)
WIW	Full	13.203 (0.084)	38.357 (0.05)	28.954 (0.024)	min 131 (29)
					ave 152 (51)
					max 257 (33)
	Core	13.216 (0.074)	38.358 (0.038)	28.953 (0.016)	ave 165 (32)
EIW	Full	13.332 (0.058)	38.539 (0.015)	29.069 (0.007)	min 256 (25)
					ave 425 (34)
					max 576 (89)
	Core	13.438 (0.053)	38.556 (0.015)	29.059 (0.006)	ave 339 (34)
mIW	Full	13.137 (0.085)	38.495 (0.018)	29.075 (0.006)	min 206 (27)
					ave 535 (145)
					max 1336 (403)
	Core	13.287 (0.054)	38.514 (0.014)	29.059 (0.001)	ave 332 (57)
TDW	Full	13.055 (0.041)	38.508 (0.010)	29.103 (0.006)	min 428 (94)
					ave 945 (131)
					max 1590 (465)
	Core	13.212 (0.068)	38.543 (0.020)	29.097 (0.005)	ave 644 (130)
WMDW	Full	12.904 (0.032)	38.475 (0.013)	29.109 (0.007)	min 371 (60)
					ave 1407 (85)
					max 2229 (25)
	Core	12.781 (0.027)	38.460 (0.010)	29.122 (0.009)	ave 2203 (130)

Note. frW and mIW respectively denote freshwater and mixed Intermediate Water.

3.1.1. The Fresh Water

The average characteristics of frW are consistent (warmest, least salty, lightest, and at the surface, Table 1) and its transport through cross-sections is less than 10–4 Sv (so not shown in Table 2). frW merges river plumes, precipitation, and evaporation, but it is mainly represented by the plume of the Rhône (Figure 5h, ∼2 mSv, Gangloff et al., 2017) and the Ebro (∼0.5 mSv, Ludwig et al., 2009). Schauer and Losch (2019) have demonstrated that the freshwater fraction is not relevant. No further results will be discussed concerning this water mass even if some are shown.

3.1.2. The Atlantic Water

The mean salinity of the AW is estimated to be 37.565 ± 0.071 (average ± one standard deviation), with a slight decrease but more variations within the core of the water mass computed with the maximum fraction value

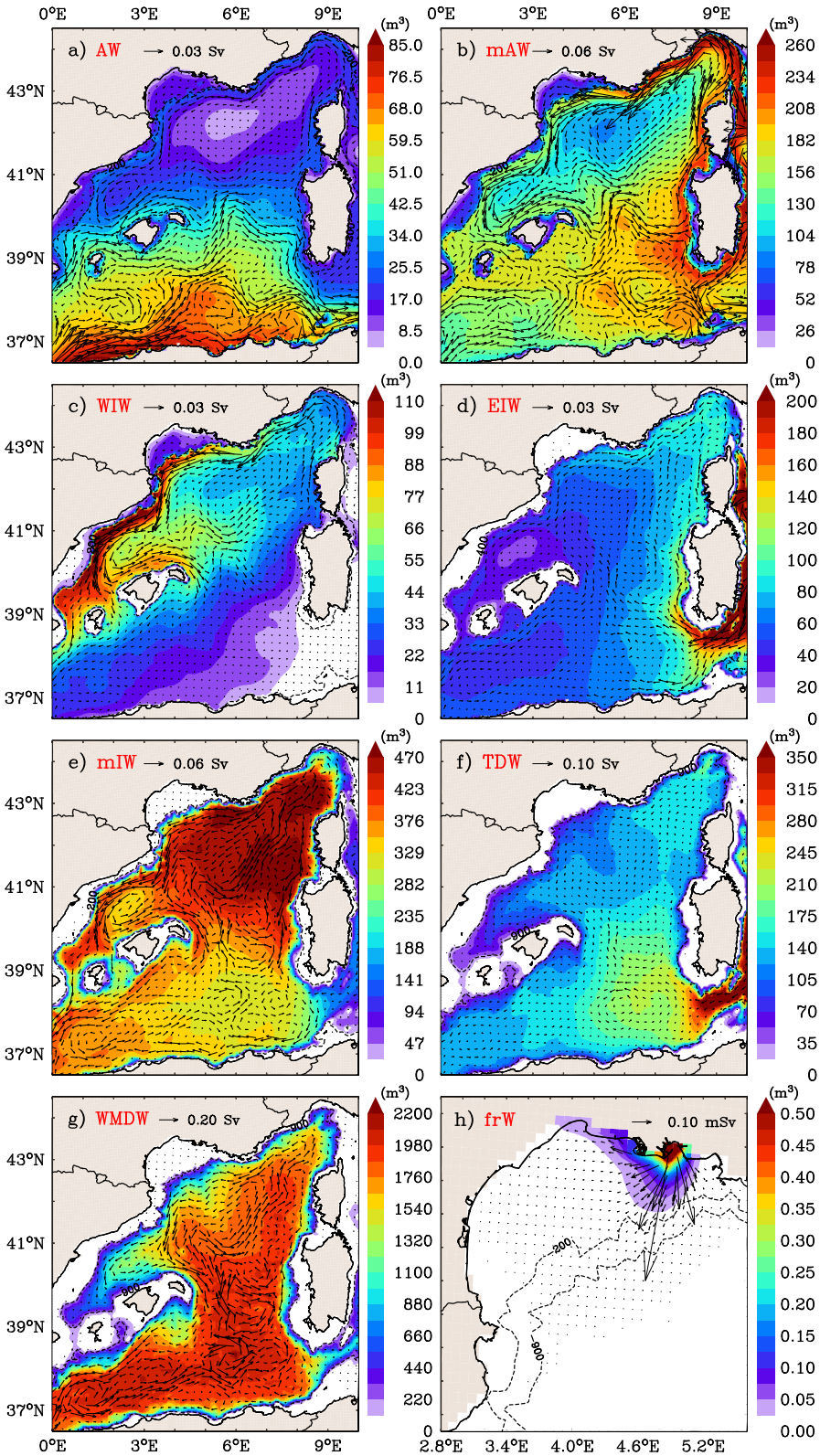
a) AW → 0.03 Sv
b) mAW → 0.06 Sv
c) WIW → 0.03 Sv
d) EIW → 0.03 Sv
e) mIW → 0.06 Sv
f) TDW → 0.10 Sv
g) WMDW → 0.20 Sv
h) frW → 0.10 mSv
(m³)
0°E 3°E 6°E 9°E
2.8°E 3.4°E 4.0°E 4.6°E 5.2°E
43°N 41°N 39°N 37°N

Figure 5.

Table 3
20y Averaged Water Mass Transports (cSv = 104 $m^3.s^{-1}$) and Standard Deviations (Below) Calculated Across the Sections Shown on Figure 1

CS #	Current	Location	AW	mAW	WIW	EIW	mIW	TDW	WMDW	All
CS1	AC	Alb. Sea	45.8	5, 8	−8, 9	−5, 6	−35, 7	7, 2	−63, 7	−69, 5
			49, 8	55, 6	10, 3	6, 6	38, 7	12, 4	132, 0	227, 3
CS2	AC	Tun.-Sard.	37.3	36, 7	0, 0	−17, 6	−4, 7	−12, 9	−1, 8	37, 2
			25.4	45, 9	1, 0	17, 0	11, 4	19, 4	40, 1	38, 9
CS3	SSC	S-W Sard.	12, 1	30, 9	0, 7	1, 5	−8, 3	−1, 7	−30, 0	5, 1
			30, 3	71, 8	7, 1	13, 0	45, 3	20, 6	167, 9	285, 2
CS4	WSC	N-W Sard.	1, 9	17, 6	0, 1	1, 2	−14, 1	−2, 5	−23, 5	15, 5
			6, 1	36, 2	6, 3	11, 5	39, 3	8, 3	72, 4	48, 4
CS5	WCC	W Corsica	6, 2	48, 5	9, 0	4, 6	13, 0	4, 3	33, 1	118, 6
			4, 8	40, 7	14, 1	11, 8	38, 8	15, 0	83, 4	172, 5
CS6	ECC	E Corsica	3, 4	29, 1	0, 6	1, 5	0, 3	0, 1	0, 0	35, 0
			4, 4	31, 0	3, 7	2, 3	1, 0	0, 2	0, 1	36, 5
CS7	NC	Off Nice	−7, 5	−71, 8	−14, 2	−4, 8	−14, 8	−5, 9	−32, 8	−151, 9
			5, 0	42, 7	22, 0	10, 3	38, 2	18, 0	82, 6	175, 8
CS8	NC	Off Pyrenees	−4, 1	−30, 7	−18, 4	−2, 4	−23, 1	−4, 1	−36, 0	−118, 9
			8, 7	46, 2	31, 6	4, 5	34, 0	9, 2	80, 3	153, 3
CS9	IC	Bal. channels	8, 2	−2, 5	−8, 4	−1, 1	−13, 7	−0, 6	−5, 8	−23, 8
			15, 4	35, 1	11, 6	2, 3	20, 2	1, 6	14, 5	77, 5
CS10	BC	N-W Menorca	6, 2	16, 9	5, 9	0, 1	4, 5	−0, 1	−8, 1	25, 4
			11, 1	41, 9	15, 6	3, 3	32, 2	9, 7	88, 1	154, 7
CS11	BC	E Menorca	14, 2	27, 4	4, 4	1, 0	18, 4	6, 9	93, 8	166, 0
			36, 9	92, 6	20, 9	14, 0	74, 0	33, 3	311, 5	511, 2

Note. The sections of the Alboran Sea and the Sardinia Channel are positive eastward; all others are positive northward. Transports between Corsica and Sardinia are not shown (lower than 10^{-5} Sv). AC, SSC, WSC, WCC, ECC, NC, IC, and BC, respectively, denote the Algerian, South Sardinia, West Sardinia, West Corsica, East Corsica, Northern and Islands' and Balearic Currents.

(37.289 ± 0.123). These values are approximately 1.5 units higher than those of the AW entering through the Strait of Gibraltar (S ∼ 36). This reflects the progressive mixing with the underlying Mediterranean's saltier waters initiated in the Alboran gyre system and further east in the AC instabilities by associated AEs. The AW mean temperature is ca 15.954 ± 1.32°C, which is close to the mean values for the inflowing AW. The standard deviation is 1.32–1.85°C (core and whole estimates, respectively), which accounts for the seasonal cycle of surface layers in the area. The AW is the lightest water mass (neglecting freshwater), with average potential density values less than 28.0 $kg.m^{-3}$. Its maximum depth is 138 ± 16 m, and its core's mean depth is close to the surface (22 ± 9 m).

The AW is primarily detected (Figure 5a) in the Algerian basin, in the AC zone and in the AEs' spreading zone up to 40–41°N, with some intrusions in the Balearic Sea through the Ibiza Channel (see Millot, 1987; Pinot et al., 1995). The AW transport exiting the Alboran Sea is estimated to be 0.46 ± 0.50 Sv (CS1 in Table 3), from which a little part passes the Ibiza channel (0.08 ± 0.15 Sv, CS9), whereas the largest part flows eastward through the Sardinia Channel toward the Tyrrhenian (0.37 ± 0.25 Sv, CS2). In both cases, the standard deviations reflect a

Figure 5. Climatology of model grid water mass volumes (m3, also roughly the thickness of the water mass in meters) and transports (Sv) averaged over the 1993–2013 period. Reported per square meter for each model grid point, the estimated volumes may reflect a thickness but the fractions are not equal to unity along the water column. The panels correspond to (a) Atlantic Water, (b) modified Atlantic Water, (c) Western Intermediate Water, (d) Eastern Intermediate Water, (e) mixed Intermediate Water, (f) Tyrrhenian Deep Water, (g) Western Mediterranean Deep Water, and (h) Rhone river plume's freshwater. A scale arrow for transport values is shown on each panel. Volume contours of (a, b, c, d, e, h) 200 and (f, g, h) 900 m depth.

high variability (0.15–0.25 Sv), undoubtedly due to the mesoscale activity that prevails in the AC and AEs and their well-known seasonal variabilities. There is no significant AW transport north to 41°N. The only values that can be considered are very low (lower than 2.10–3 Sv) due to traces of tagged AW (fAW under 5%), left by the use of a linear salinity dilution ratio between AW and mAW in the algorithm rather than a fixed threshold. The imbalance in AW transport between the inflow from Alboran and the outflow through the Sardinia Channel is compensated by a significant eastward flow of mAW through the Sardinia Channel (see below), highlighting the mixing of AW with the resident Mediterranean waters in the instabilities of the AC and the AEs.

3.1.3. The Modified Atlantic Water

The labeled mAWs show higher mean salinities of 38.105 in the whole and 38.300 in the core, with a low standard deviation in both cases (ca 0.04). The mean temperatures are lower than that for the AWs (13.796°C and 14.510°C for the core and the whole, respectively), and less variable (standard deviation less than 0.354–0.607°C), mainly due to their more northerly and deeper distribution (see Figure 3). Mean densities are higher (28.460–28.778 $kg.m^{-3}$), as are the whole's maximum (253 ± 36 m) and the core's mean (114 ± 26 m) depths.

The algorithm labels an eastward and increasing volume of mAW in the Algerian basin in response to the salinity increase along the path of AW toward the Tyrrhenian and, coherently, a higher volume of mAW in the Tyrrhenian. The Sardinia Channel transports show both eastward and westward flows for the mAW, but the net balance is eastward (0.37 ± 0.46 Sv), compensating for the imbalance of AW transport between the Alboran exit and the Sardinia Channel. In the northern part of the basin (north of 40°N), the mAW is identified along the shelf's slope, showing the well-known cyclonic circulation from the West Sardinia to the Balearic Sea, with an offshore undulating return flow between Mallorca and Sardinia around 40°N. The lower amount of mAW in the center of this gyre is consistent with the well-known isopycnal doming in the wintertime convective areas (e.g., Prieur et al., 2020).

The mean transport of mAW at southwest of Sardinia (CS3) is northward but highly variable 0.31 ± 0.72 Sv. It decreases to 0.18 ± 0.36 Sv along the shelf's slope of West Sardinia (CS4) and increases to 0.49 ± 0.41 Sv in the WCC off Calvi (CS5). The mAW flow is reinforced by the ECC from the Tyrrhenian (+0.29 ± 0.31 Sv, CS6), reaching 0.72 ± 0.43 Sv in the NC off Nice (CS7). However, it clearly decreases off the GoL before entering the Balearic Sea (0.30 ± 0.46 Sv, CS8). This decrease comes from the long-term average effect of winter when mAW temporarily vanishes due to their conversion in new WIW during the coldest months and ultimately in WMDW during deep convection events.

3.1.4. The Western Intermediate Water

The average WIW's thermohaline characteristics are close to those of the mAW, showing only a slightly higher salinity (38.357 ± 0.05) and a slight decrease in temperature (13.203 ± 0.084°C). There is no significant difference between the full and core estimates. The low standard deviations of the mean temperatures of the WIWs are due to the narrow range of temperatures that define them and their short period of contact with the ocean-atmosphere interface. The 20-year average encompasses all days of the year, not merely winter season when the recent WIW is at its coldest. Consequently, the "pure" WIW of winter is in fact colder than 13°C. Juza et al. (2019) and Vargas-Yanez et al. (2020) have demonstrated a warming trend in the WIW of 0.5°C over the past decade, a comparable warming evident in the final years of the period (+0.2°C in 2010–2013). The corresponding mean potential density of the WIW (28.954 $kg.m^{-3}$) is slightly higher than that of the mAW's core (28.778 $kg.m^{-3}$), leading to a depth range (131 ± 29 to 257 ± 33 m) that lies between the mAW and EIW cores (114 and 425 m).

The average total volume of WIW over the Algero-Provencal domain is 16.8×103 km^3, distributed mainly along the Gulf of Lion shelf-slope and over most of the Catalano-Balearic area. This is in agreement with estimates of Juza et al. (2013, 2019). The WIW yearly averaged transport off the Catalan coast (CS8) is estimated to be 0.18 ± 0.32 Sv. A portion of this escapes from the Balearic Sea through the BC (0.06 ± 0.16 Sv, CS10), whereas a lesser amount continues through the channels of Ibiza and Mallorca toward the Alboran Sea (0.08 ± 0.12 Sv, CS9). These estimates align with those of Juza et al. (2013), though they use a more detailed model (1/40°) and a shorter period. It is worth noting that the algorithm categorizes WIW as cold mAW. WIWs' volume and transport mainly mirror the decline of those of mAW from the Gulf of Lion to the Balearic Sea. The combined transport of both partially compensates for the loss of mAW between Nice and the Balearic Sea.

3.1.5. The Eastern Intermediate Water

The algorithm gives the EIW mean salinity to be 38.539 ± 0.015, with only a slightly higher value for the core (38.556 ± 0.015). These low values indicate a −0.25 PSU loss due to the EIW dilution from the Strait of Sicily to the Tyrrhenian Sea and Algero-Provencal basin (e.g., Millot, 2013; Schroeder et al., 2020). The algorithm diagnoses a dilution with colder water masses, such as the loss of 0.1°C in its mean temperatures (13.332°C, 13.4°C bound for pure EIW at the Strait). The EIW core is properly warmer (13.438°C). The calculated depth range (256 ± 25 m to 576 ± 89 m) and overall potential density (29.07 $kg.m^{-3}$) of the EIW match the main EIW vein flowing along western Sardinia at about a depth of 400 m in Bosse et al. (2015), with salinities over 38.56, temperatures over 13.39°C, and a potential density of 29.075 $kg.m^{-3}$. This latter value is slightly higher than the one used in the algorithm (29.062 $kg.m^{-3}$) as a specific characteristic of the original EIW, but closer to the one usually found in the northwestern Mediterranean (e.g., Puig et al., 2013; Schroeder et al., 2020).

The largest EIW volume is in the Sardinia Channel, given the proximity of the Tyrrhenian, where EIW is known to spread (e.g., Sammari et al., 1999). EIW volumes decrease rapidly westward, with lowest (or even null) volumes over the shallowest areas, namely the GoL shelf and the Balearic Islands. This ensures that the algorithm effectively identifies them as intermediate waters. The associated transports show a weak cyclonic flow (~0.05 Sv, CS5, and CS7) along the shelf slope over most of the western basin. This cyclonic flow along the shelf slope is consistent with historical findings about the EIW behavior (e.g., Millot & Taupier-Letage, 2005a, 2005b). The absence of a significant EIW flow along Corsica north of 41°N is coherent with the detachment of the "SUddies" northwest of Sardinia, as observed by Bosse et al. (2015).

3.1.6. The Tyrrhenian Deep Water

The calculated mean potential temperatures of the TDW (13.06°C and 13.21°C for the core) fit with the known range about the water mass of the Algero-Provencal basin (greater than 12.86°C). Its average salinities and densities (38.51–38.54, 29.1 $kg.m^{-3}$) are also coherent. The mean depth boundaries of the TDW are slightly above those in the literature but its average depths (945 and 644 m for the core) and the maximum depth of the full TDW (1590 ± 465 m) are included in 600–1900 m. The average circulation of TDW (Figure 5f) shows an inflow through the Sardinian Channel of 0.13 ± 0.19 Sv (CS2) with a westward mixing in the eastern Algerian deep gyre and a northward accumulation in the Ligurian Sea, both in alignment with the TDW detection in Send and Testor (2017). Southwest of Sardinia, the deep transports and entrainment of TDW in the anticyclonic gyre that extends northwestward to the island of Menorca reflects the average turbulent eddy-like propagation of the SEs drift and the mixing of EIW with WMDW (high standard deviation in CS3), concomitant to the EIW vein (e.g., Bosse et al., 2015; Testor, Béranger, & Mortier, 2005). The greatest average transports of TDW are in the sections east of Menorca and next to the Alboran Sea (0.07 ± 0.12 Sv and 0.07 ± 0.33 Sv, CS11 and CS1, respectively). These are high values, but they are low for the TDW circulation, and have much higher variabilities.

3.1.7. The Western Mediterranean Deep Water

The mean density of the detected WMDW is close to the usual definition value of 29.10 $kg.m^{-3}$, both for the total (29.109 ± 0.007 $kg.m^{-3}$) and the core estimates (29.122 ± 0.009 $kg.m^{-3}$). The WMDW is detected at a depth greater than 371 ± 60 m (fractions greater than 5%) with a maximum depth (2229 ± 25 m) and a core depth (2203 ± 130 m), which closely follows the average bottom depth of the area. Its density-based tagging gives mean salinities of 38.475 (full) and 38.460 (core) with small standard deviations (0.010–0.013), close to the usually observed range (see Table 1). The mean temperatures are also close to the usual estimates, being 12.904 ± 0.032°C and 12.781 ± 0.027°C for the full and core, respectively.

The WMDW volume is of a higher order than other water mass volumes due to its greater vertical extent. They closely follow the bathymetry of the basin, with the higher values being in the southern deepest area. The highest volume is not found in the DWF area, which is not surprising, given the rapid southward spreading of newly formed WMDW next to Menorca following the general increase in bathymetry to the south. This process occurs rapidly, within a few months (e.g., Beuvier et al., 2012). This is coherent with the high standard deviation and the significant northward flowback (0.9 ± 3.1 Sv, CS11). The WMDW transports (Figure 5g) reveal a turbulent eddy-like circulation between southern Sardinia and the Balearic Archipelago and two cyclonic circulations over the southwestern basin between the Balearic Archipelago and North Africa and the northwestern Liguro-Provencal area (~0.3 Sv, CS5, CS7, and CS8). The associated transports (Table 3) are of the same order as those of the

mAW. The greater depth range of the WMDW (thousands of meters) compensates for the lower velocities (below 5 cm/s) that prevail in the deeper layers. The high (0.6 ± 1.3 Sv, CS1) average westward transport of WMDW toward the Alboran Sea is discussed later in Section 3.2.

3.1.8. The Mixed Intermediate Water (or Modified Eastern Intermediate Water)

The mIW fraction is not a clearly defined water mass. Rather, it is a residual mixture that comprises the remnant of the isopycnal dilution of EIW along its path in the Tyrrhenian and the Algero-Provencal basin. In summary, mIW within the algorithm is primarily desalinated EIW, mixed with mAW and warmed, salinized WIW, and incorporates certain heavier fractions, including TDW (see Section 2.2, Equation A13 and Figure A1g). It can be conceptualized as a modified EIW, as proposed in Millot (2013) and Schroeder et al. (2020). This allows us to appreciate all the intermediate water mixings in the Algero-Provencal, following those in the Tyrrhenian Sea that passed through the Sardinian Channel, beginning with a pure water mass at the Sicilian Channel. It is thus not feasible to conduct an objective comparison with the existing literature. However, it is imperative that the characteristics are consistent with the surrounding water masses (mAW/WIW, EIW, and TDW).

The mean salinities of the mIW (full: 38.495 ± 0.018, core: 38.514 ± 0.014) are midway between those of the EIW and WIW and between those of EIW and WMDW, thus on the mixing line between EIW and WIW and close to the salinity of full TDW. The mean temperatures (13.13 ± 0.086 and 13.287 ± 0.054) are slightly warmer than the average temperature between TDW and WMDW, which is more likely 13°C. The average potential density of the entire mIW is 29.075 $kg.m^{-3}$, close to that of the EIW. The core is strictly the same to that of the EIW at 29.059 $kg.m^{-3}$. This reflects the fact that mIW is primarily located in the intermediate layer between the mAW/WIW and the EIW, with only a few in the deep layer below the EIW (see Figure 4d). The calculated mIW depths is consistent with these findings, showing a minimum of 206 ± 27 m, close to the maximum depths of the mAW and WIW, a core depth of 332 ± 57 m close to the EIW's, and a maximum depth of 1336 ± 403 m.

The mIW volumes are the second highest, twice as high as mAW or TDW but four times lower than those of WMDW. Their average spatial distribution is opposite to TDW and WMDW, with higher values in the most northeastern part of the area. The circulation patterns are similar to those of WIW and EIW in the north and also similar to the one of WMDW in the south but less pronounced (Figure 5e). The corresponding transport values in the cross-sections show a greater outflow toward the Alboran Sea (0.35 ± 0.39 Sv), confirming the idea of a modified EIW (mEIW) exiting through the Strait of Gibraltar, highly varying east of Menorca (0.74 Sv). The strongest representation of this water mass close to Corsica is the mixing of desalinated EIW with warmed WIW. The main flow at the entrance to the Balearic Sea (0.2 Sv, CS8) has an offshore separation somewhat linked to the WCC by a wide mIW vein midway between Menorca and Corsica. This flow follows the WIW and mAW recirculations in the closure of the northern gyre.

3.2. Time Series of Characteristics, Volumes, and Circulation of Surface Water Masses

Given the general consistency with the literature of the long-term average of the water mass characteristics, volumes, and circulations described in the previous section, we now look for their variability over the whole 20 year of the reanalysis. To do so, we first present the time series of the characteristics (Figure 6), the peculiar volumes (Figures 7b–7d) of the water masses with the corresponding maximum mixed layer depth (MLD, calculated using σ-$\sigma_{surface}$ lower than 0.01 $kg.m^{-3}$ and considered only if greater than 600 m) and DWF area extent (Figure 7a), and the peculiar transports through the straits of the domain open boundaries (Figure 8). The temperature variability on the surface water masses (AW, mAW) is first driven by the seasonal radiative cycles and enforced by strongest winds in winter time, that is, classically, a cooling in autumn and winter and a warming in spring and summer (Figures 6a and 6b). The mAW salinity shows a weaker (and even sometimes unclear) seasonal variability, whereas the AW salinity does not show any seasonal cycles, coherently with the almost constant salinity transport of AW through the strait of Gibraltar (Figure 8a). This nearly constant AW flow also explains the low variability of the AW volume (Figure 7d). The seasonal variability of densities of the water masses then mainly depends on their temperatures. By contrast, the mAW volumes exhibit a marked seasonal cycle with winter drops that mirror the increases of WIW volumes (Figure 7d), materializing the conversion of mAW to WIW in winter time. The AW + mAW transports through the Straits of Sardinia and Corsica also vary seasonally (0.71 ± 0.65 Sv, 0.31 ± 0.34 Sv, respectively), which is well known in the literature and due to the

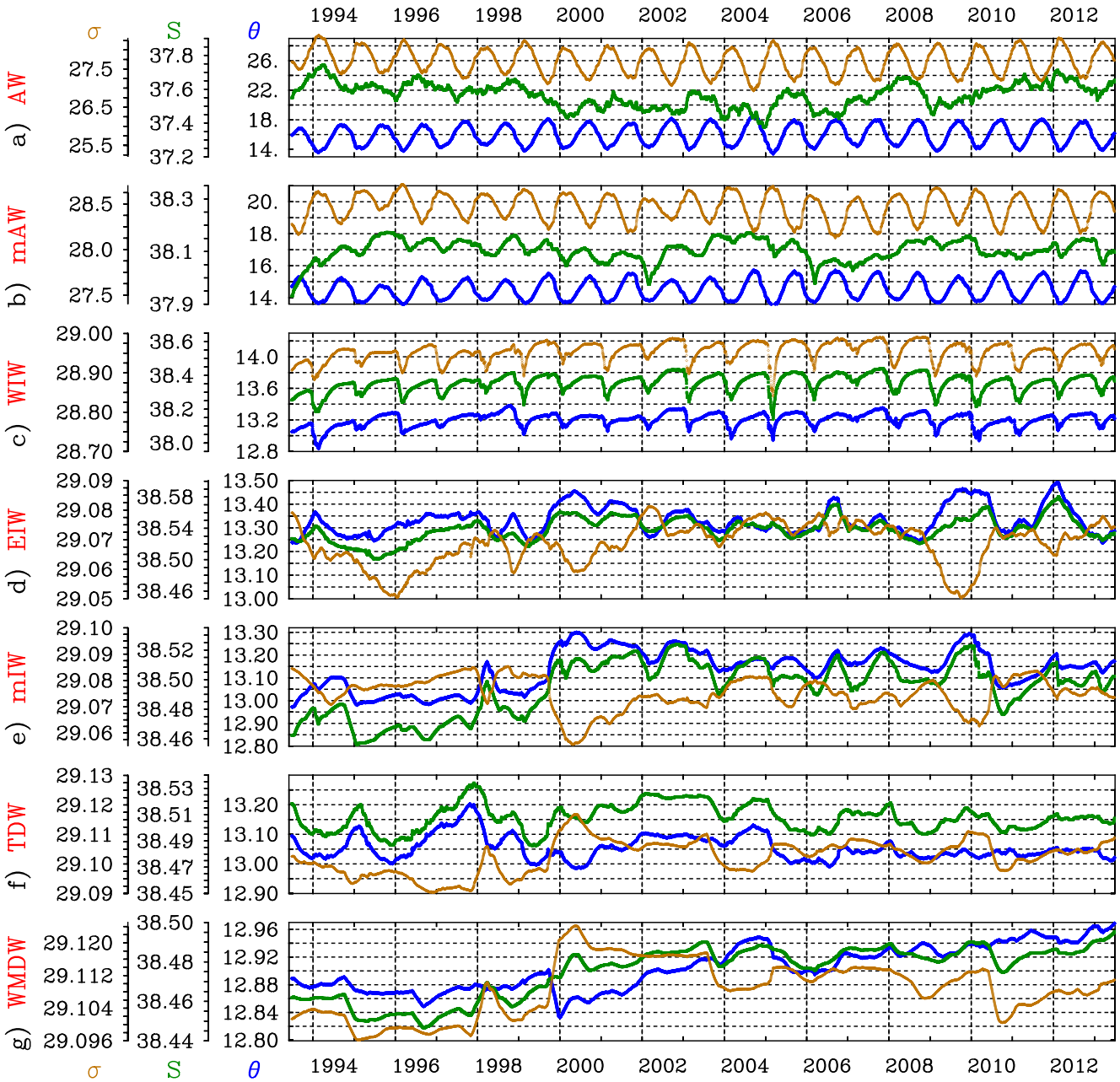

Figure 6. Time series of average potential density anomaly (kg.m^{-3}, brown), potential temperature (°C, blue), and salinity (green) characteristics for (a) Atlantic Water, (b) modified Atlantic Water, (c) Western Intermediate Water, (d) Eastern Intermediate Water, (e) mixed Intermediate Water, (f) Tyrrhenian Deep Water, and (g) Western Mediterranean Deep Water.

difference in the atmospheric conditions between the Algero-Provencal basin and Tyrrhenian Sea (Figures 8b and 8c). However, previous estimates of the intermediate water transport through the Corsican channel range 12%–20% of the total transport (deeper than 200 m depth, Astraldi & Gasparini, 1992; Manzella, 1984), whereas the transport of mIW + EIW is around 6 ± 4%. This bias is later discussed in Section 4.2. Coherently with the mAW volume drops, all WIWs' thermohaline characteristics show strong seasonal variations (Figure 6c) with minimum temperature and salinity in winter (ca 13.0°C and 38.25) and increasing values from spring to summer due to its mixing with surrounding warmer water masses from below (mIW/EIW) and from above (mAW and AW), given the summertime stratification of the surface layers. As such, the WIW volume ranges from 10 × 10^3 km^3 in summer to 28 × 10^3 km^3 in winter, which is close to the range estimated by Juza et al. (2019) for the period

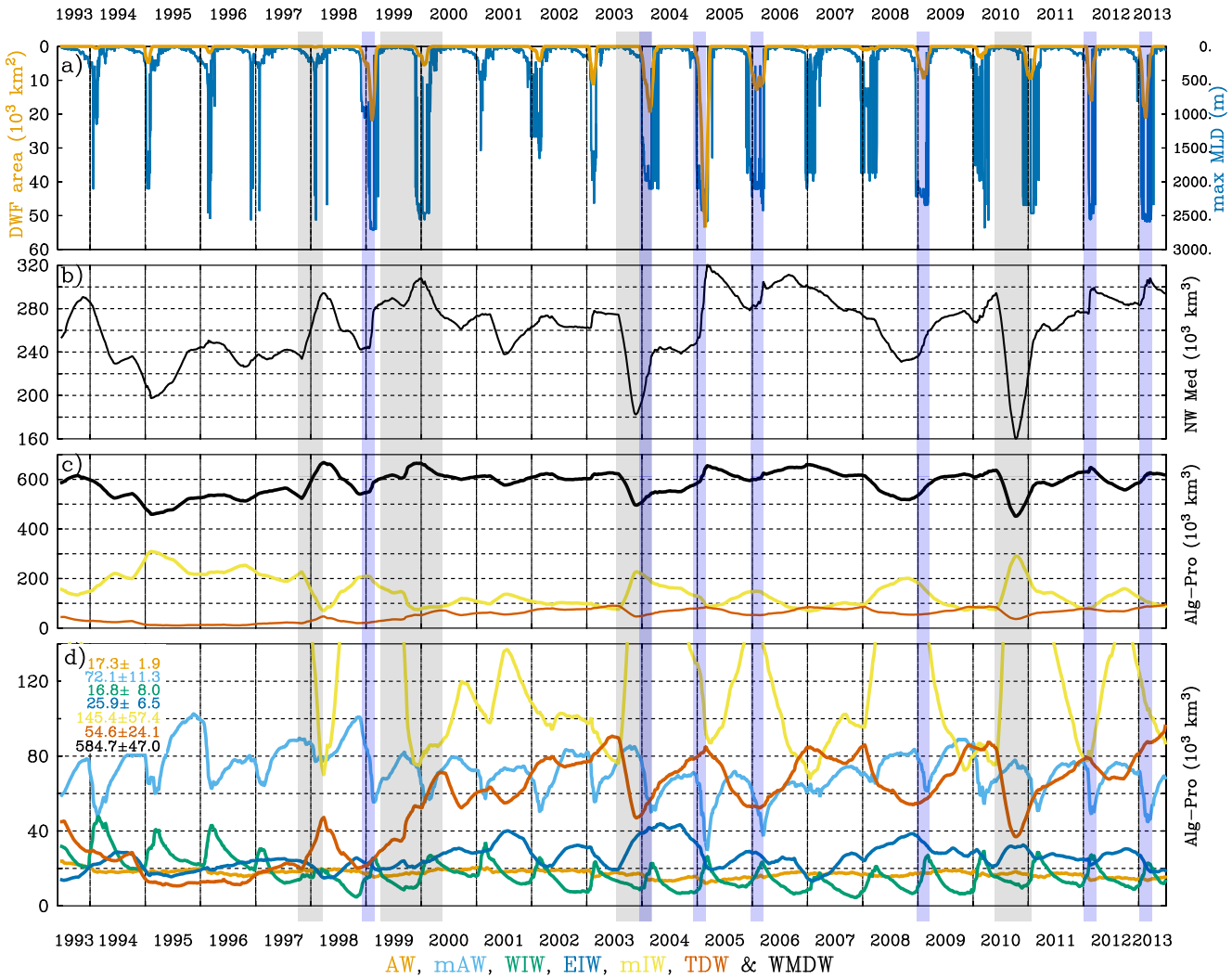

Figure 7. (a) Time series of the MLD (using σ-$\sigma_{surface}$ lower than 0.01 kg.m^{-3} and greater than 600 m) maximum (in meters, no smoothing) and area (in 10^3 km^2, monthly smoothed) of the DWF calculated in MEDRYS1V2, over the NWMED area as for the calculation in Somot et al. (2018) (see Figure 1). (b) Volumes of WMDW in the NWMED area and of (c, d) all the water masses (color codes at the bottom of the figure) over the Algero-Provencal domain (between CS1, CS2, and CS6 in Figure 1). Vertical blue rectangles locate the DWF periods, whereas vertical gray rectangles locate the spurious events (1997–1998 WMDW production, 1999 TDW accumulation, and 2003 and 2010 WMDW destructions). Averages and standard deviations of total peculiar volumes (in 10^3 km^3) in the Algero-Provencal domain are listed on panel (d).

2011–2013 (10×10^3–50×10^3 km^3). In strong DWF years (1999, 2005, 2006, 2013), some WIWs enter the Algero-Provencal basin through the Strait of Corsica, as if they were produced in the Bonifacio dipole (Napolitano et al., 2019). Note that the most severe drops in mAW volumes, which exceed the increase in WIW, occur during the DWF years (e.g., 1999 and 2005), affecting the WIW thermohaline characteristics.

On longer time scales, the mAW and AW salinities' time series show periods of alternating increase and decrease, but of limited amplitude (0.15) and are not concomitant in time. Maxima of mAW volumes also tend to increase during the periods with several years of low or no convection (1996–1998, 2001–2003, and 2007–2009) and, conversely, stay nearly constant during periods of consecutive medium to strong convection (1999–2000, 2004–2006, and 2010–2013). This suggests that the destruction of the mAW by DWF in the northern sub-basin is generally balanced later in the year by its production by mesoscale mixing in the AEs, whereas several consecutive years of low or no convection may favor the accumulation of mAW over the whole basin. However, there are some exceptions to this global rule in 2000–2001 (stagnating mAW maximum volume instead of an increase) and in 2009 (increasing summer's mAW maximum volume instead of a stagnation). In the first case, it seems that from summer to summer, the period of no or low convection was too short to significantly affect the

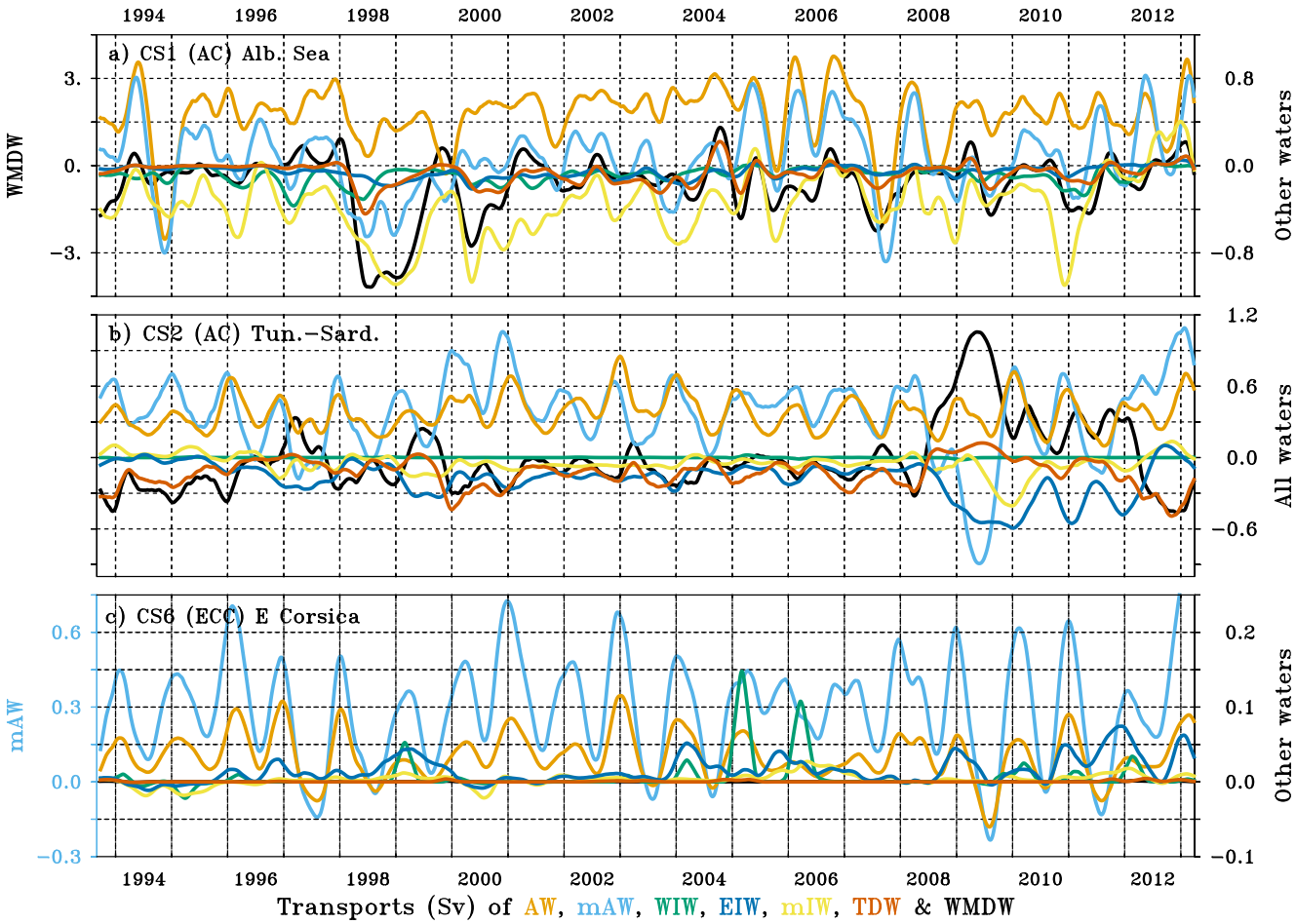

Figure 8. Time series of the water mass transports (Sv) through the cross-sections of (a) the Alboran Sea, (b) the strait of Tunisia-Sardinia and (c) the east Corsica channel (CS1, CS2, and CS6 on Figure 1, triangle smoothing). Left axes correspond to (a) WMDW and (c) mAW transports. The transports are positive to the east (CS1, CS2) and north (CS6).

mAW volume. The year 2009 is an exceptional case that will be explained later (Section 4). Lastly, the AW volume exhibits similar, but lower, drops during years of medium to strong convection followed by relaxing periods during low or no convection years. This similarity between the AW and mAW pluri-annual variability is likely due to the use of a salinity ratio in the algorithm that retains a small amount of AW over the northern part of the basin. As the years of medium to strong convection are more frequent during the second half of the reanalysis, this leads to a general tendency of decreasing AW amount (−25%) over the whole area.

3.3. Time Series of Characteristics, Volumes, and Circulation of Deep Water Masses

3.3.1. Long-Term Changes and Deep Water Formation Events

In contrast, the characteristics, volumes, and transports of intermediate (EIW and mIW) and deep (TDW and WMDW) water masses do not vary seasonally, but rather show two different dynamics before and after the 1998–2000 period (Figures 6d–6g, 7b–7d, 8a and 8b). The early years of the simulations show ambiguous thermohaline variations, mainly a period of slow temperature increase for EIW, mIW, and TDW (one after the other during 1993–1995). Recalling that the reanalysis was initiated with results from a twin free run, a longer spin-up than 9 months initially considered (see Section 2.1) could probably explain the questionable variability observed in the very early years of the reanalysis (1993–1994).

However, this is followed by an increase of both temperature and salinity peaking in late 1997–early 1998 (EIW, mIW, and TDW), and alternating increases and decreases until the end of 1999. At the same time, the TDW volume started to slowly increase after 1995, more suddenly in 1999–2000 and again slowly until 2003

(Figure 7d, gray rectangle). It is constantly high later (about 3 times the initial volume of 20×10^3 km^3) but still with some interannual variations ($\pm 20 \times 10^3$ km^3). Deep transports of WMDW also show instabilities during 1998–1999, with a strong outflow toward the Alboran and alternating fluxes with the Tyrrhenian (Figures 8a and 8b). The thermohaline characteristics and volumes of EIW, mIW, and WMDW are more stable during the first 4 years, but clearly evolve during 1998–2000 toward a higher salinity that remains for the rest of the reanalysis (+0.04, +0.04, and +0.02, respectively) and an increased variability. This sudden change starts the discussion in Section 4.1. That being said, the increase in TDW volume in 1999–2000 does not coincide with the gradual salinization of TDW that starts earlier and drops off sharply in 1998. Rather, it coincides with an increase of the EIW/TDW flux through the Sardinia Channel (Figure 8b, both −0.3 Sv), beginning in 1999 for EIW and peaking in late 1999 to early 2000 for TDW. This increased flux mainly comes from a slight increase of salinity (+0.04) of the incoming from the Tyrrhenian, while velocities of the intermediate layers (200–600 m) only show a very slight acceleration (+0.01 cm.s^{-1}). Discussion in the origin of this volume increase follows in Section 4.1.

After 2000, all intermediate to deep water masses show more stabilized characteristics with a variability that is mostly driven by the interannual variability of DWF, as evidenced by the conversion of mAW/mIW to WMDW (1999, 2005–2006, and 2012–2013) and, conversely, a slow decrease (increase) in WMDW (mAW/mIW) volume during periods without DWF (2001–2002 and 2007–2008). The effect of DWF is less pronounced on EIW volume, probably because the algorithm tends to retain the memory of the mIW salinity anomaly within the newly formed WMDW. The WMDW volume is estimated to be $585 \pm 47 \times 10^3$ km^3 for the entire area (0–10°E) and about $263 \pm 29 \times 10^3$ km^3 when calculated during 1993–2013 for the same NWMED area as in Somot et al. (2018) (see Figure 1). This baseline of WMDW volume is a little higher than in Rixen et al. (2005) and Somot et al. (2018) (185×10^3 km^3 over 1980–2002), mainly due to the algorithm that uses a density fraction, rather than a fixed density threshold, but the increases in deep-water volume during 2005 and 2013 DWF events ranging about $20–80 \times 10^3$ km^3 are in good agreement with Somot et al. (2018), Beuvier et al. (2012), Waldman et al. (2016), and Testor et al. (2018) ($\sim 50 \times 10^3$ km^3).

3.3.2. Detection of Four Spurious Dynamics: 1998–1999, 2003, 2009, and 2010

Conversely, some years make exceptions to this behavior, especially 2003 and 2010 showing high losses of the TDW (−48% and −56%) and WMDW (−19% and −28%) volumes mirrored by gains in mIW volume (about +175% and +250%, Figures 7c and 7d). Likewise, the year 1998 inversely shows increases (decrease) of the TDW and WMDW (mIW) volumes (+135%, +28%, −68%) while it is widely recognized that 1998 is not a DWF year (e.g., Somot et al., 2018). These dubious events of TDW + WMDW productions (1998) and mixings or destructions (2003 and 2010) are detailed in Figure 9.

For 1998, the TDW + WMDW volume anomaly (by reference to the climatological one) suggests that the problem originates mostly from the southwestern area (likely in the Alboran Sea) and propagates northeastward on a large part of the basin (Figure 9a). The associated transport anomalies show a considerably strengthened circulation (+2 Sv) establishing a large anticyclonic gyre over the eastern Algerian basin, which is in contradiction with the well-known cyclonic gyre prevailing in this area (e.g., Send & Testor, 2017). In addition, as it evidences an increase in salinity, an input of TDW from the Alboran Sea is also impossible. Spatially averaged θ-S time series, over the southwestern area where the anomaly emerges, show that the TDW + WMDW volume anomaly indeed mainly originates from a sudden increase of salinity (+0.02), near the bottom in December 1997 that reaches 1000 m in some months (Figure 9g). It is followed by a cooling (−0.15 to −0.27°C) of similar vertical extent (Figure 9d). These thermohaline changes cause a drastic increase in density over a wide depth range with the 29.12 kg.m^{-3} isopycnal reaching 600 m from mid-February to June 1998 (Figure 9j), this being too shallow to be realistic in this region. Consequently, the algorithm also diagnoses higher WMDW fractions, leading to dubious increased volumes. This rapid inflow (about +3 Sv during 3 months) is later compensated by a strong and longer flowback of TDW + WMDW toward the Alboran Sea (Figure 8a, about −4 Sv during the second half of 1998). This to-and-fro is also visible for the Algerian and Provencal basins between the Islands of Menorca and Sardinia (daily WMDW peaks of +13.3 and −16.6 Sv, 5-month lag).

The years 2003 and 2010 are inverted situations with the TDW + WMDW volume anomalies showing destructions located over the whole Provencal basin (Figures 9b and 9c). The TDW + WMDW transport anomalies are not marked over the volume anomaly area, likely due to lowered fractions, but reach ca 1 Sv in numerous eddy-like structures over a large part of the Algerian basin. These anomalies are due to two similar events of

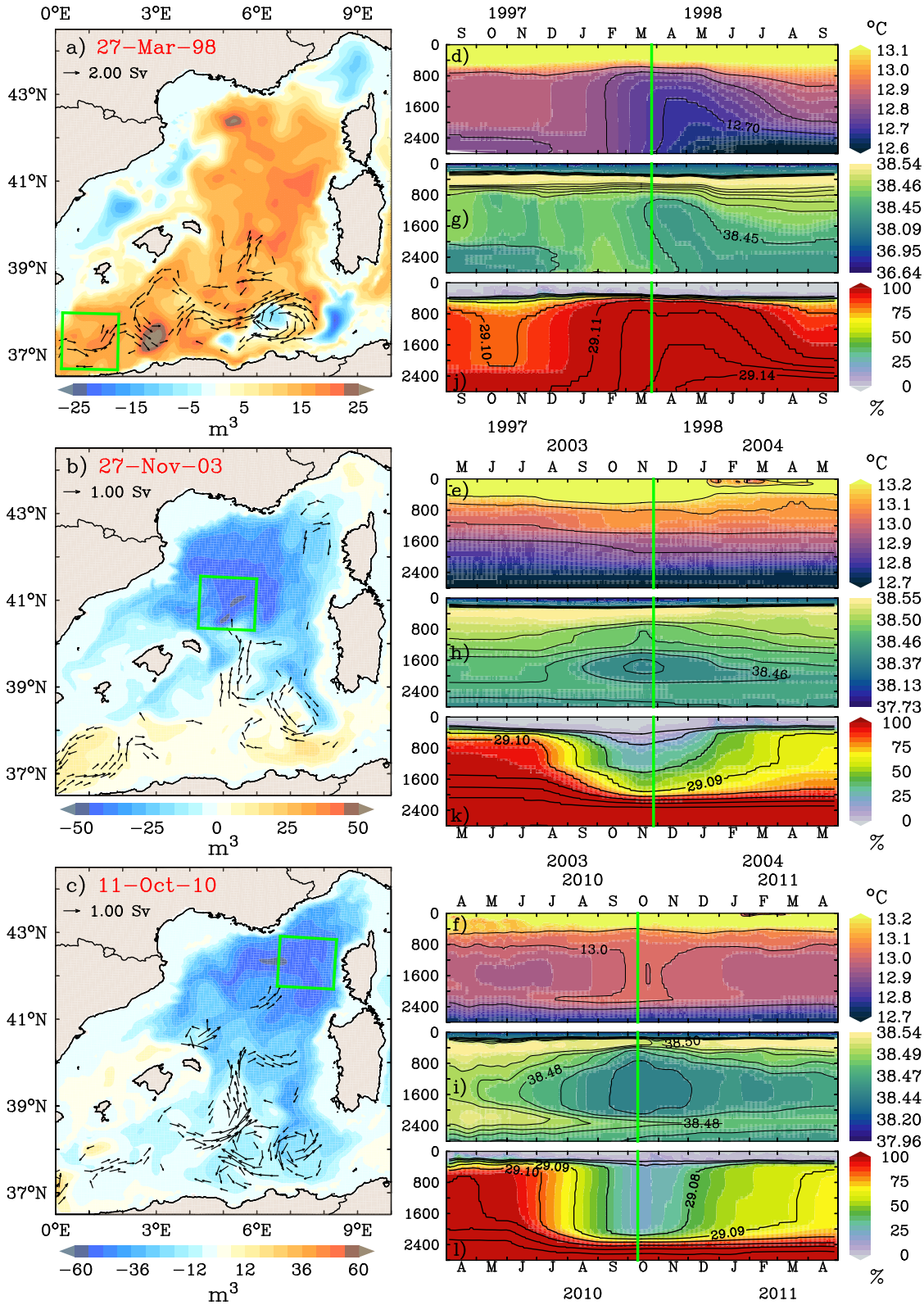
a) 27−Mar−98
→ 2.00 Sv
b) 27−Nov−03
→ 1.00 Sv
c) 11−Oct−10
→ 1.00 Sv
0°E
3°E
6°E
9°E
43°N
41°N
39°N
37°N
−25 −15 −5 5 15 25
−50 −25 0 25 50
−60 −36 −12 12 36 60
m3
1997
1998
2003
2004
2010
2011
S O N D J F M A M J J A S
M J J A S O N D J F M A M
A M J J A S O N D J F M A
d)
e)
f)
g)
h)
i)
j)
k)
l)
12.70
38.45
29.10
29.11
29.14
13.0
38.46
38.48
38.50
29.09
29.08
°C
%

Figure 9.

desalination in the 600–2,200 m range lasting several months (Figures 9h and 9i). The drop in salinity reached −0.02 in the core (1,800 m) of the anomaly in 2003 and -0.03 between 800 and 2,000 m in 2010. There are no significant deep temperature changes in 2003, but an increase in 2010 reached +0.08°C, strengthening the drop in potential density (Figures 9e and 9f). In both cases, the isopycnals of 29.10 kg.m^{-3} fall from 600 to 2,000 m (Figures 9k and 9l), leading the algorithm to diagnose much lower TDW + WMDW fractions (less than 30%) and consequently lower volumes over a large part of the water column. The possible origins of these three fallacious deep dynamics are discussed in Section 4.1.

The year of 2005 is known as the most convective year of this period (Schroeder, Ribotti, et al., 2008; Somot et al., 2018). The consequences of this significant production of WMDW volume, deep heat and salt inputs, and denser signature of the WMDW at the seafloor yielded in warming and salinization in the deep and intermediate layers, the so-called WMT. The latter's effects continued years afterward and even as late as 2013, firstly quickly spreading in the Algerian basin (a few months) but reaching the Tyrrhenian and the Atlantic only after 2008 and 2010, respectively (Piñeiro et al., 2019; Schroeder et al., 2016). Leaving aside the Alboran Sea, this very late impact in the Tyrrhenian is attributed to the deposition on the seafloor in 2005 of the newly formed WMDWs, followed by several moderate DWF events in 2006, 2008, and in 2009. Each of these DWF events results in successive WMDW deposition, year after year, with the top of accumulated WMDW reaching 1,900 m in 2009, the depth of Sardinia Channel sill (e.g., Ben Ismail et al., 2021; Li & Tanhua, 2020; Schroeder et al., 2016). This well-documented dynamic is represented in the Algero-Provencal basin of the reanalysis since a major overflow of WMDW toward the Tyrrhenian is obvious in Figure 8b through the Strait of Sardinia in 2009. This year has the largest effect on the annual circulations of surface and intermediate water masses in the Algero-Provencal because this overflow of WMDW toward the Tyrrhenian induced a strong return current at the surface and intermediate layers. This return current is clearly visible on Figure 8b, as westward transports of mAW and EIW, whereas the 2009 regional circulation event is presented in Figure 10: the water mass anomalies of volume and transport of 2009 facing the climatology of Figure 5. The transports of WMDW and mAW-EIW in the Sardinia Channel differ from the rest of the time series, from mid-2008 to the end of 2009, both in intensity (larger than 1 Sv for WMDW) and sign, and are almost perfectly opposite. The two transport anomalies peak in late-June 2009, 4 months after the 2009 DWF event, a time scale for WMDW propagation that is consistent with Schroeder, Ribotti, et al. (2008) and Beuvier et al. (2012). However, even if the time series of AW transport shows that it is not modified in the Channel of Sardinia in comparison with the previous years (still stronger in winter than summer, Figure 8b), its spatial distribution is more strongly affected leading to a significant redistribution of the amount of AW over the whole basin (Figure 10a). This redistribution shows a smaller volume of AW over the Balearic Islands, contrasting with an accumulation in the eastern Algerian sub-basin in several AEs. In addition, part of the AW is driven by the northward flow of mAW from the center of the Algerian basin into the WCC (Figures 10a and 10b). The northward influx of mAW is reversed facing climatology, to the southwest of Sardinia (Figure 5b), where the surface current is usually oriented southeastwards. The transports of EIW, mIW, and TDW through the Sardinia Channel are also modified during this exceptional event, at a lower level in a 6-month delay. Again, the impact is more pronounced on their regional circulations throughout the basin. The positive (negative) anomaly of WMDW/TDW (mIW) volume over the Provencal basin (Figures 10c, 10e, and 10f) is coherent with Figure 7b as 2009 is a DWF year. The greater amount of TDW in the Ligurian is likely due to the northward accumulation and entrainment by the mAW/EIW flow (Figures 10b and 10d), whereas the negative TDW volume anomaly in the Sardinia Channel may reflect the thinning of the TDW layer due to the thicker layers of mAW/EIW entering the Algero-Provencal basin and WMDW leaving.

This return current of surface and intermediate waters in the Strait of Sardinia is induced by the Tyrrhenian circulation of the reanalysis in 2009 (not shown). The reanalysis produces an anticyclonic and barotropic gyre which is located at the southeast of Sardinia and fully developed at the surface and intermediated layers by the entrainment of the recently entered WMDW. The WMDW inflow in the Tyrrhenian veers off sharply to the north

Figure 9. Anomalies of the TDW + WMDW volumes (by reference to the climatology of Figure 5) at the dates of maximum of the anomalous events of (a) 1998, (b) 2003, and (c) 2010, and corresponding year-long centered times series of spatially averaged (d–f) temperatures, (g–i) salinities, and (j–l) fractions of TDW + WMDW in the most impacted areas. The black arrows on the left panels show the TDW + WMDW transports (greater than 0.8 Sv for 1998 and 0.4 Sv for 2003 and 2010). The green squares show the spatial domains used for averaging time series. The vertical green lines on right panels indicate the same day as on the left panels. The right panels display contours for the isotherms in 0.01°C steps from (d) 12.7°C–12.9°C, and (e, f) 12.9°C–13.1°C, (g–i) isohalines from 35.45 to 38.50 in 0.01 steps and (j–l) isopycnals in 0.01 kg.m^{-3} steps.

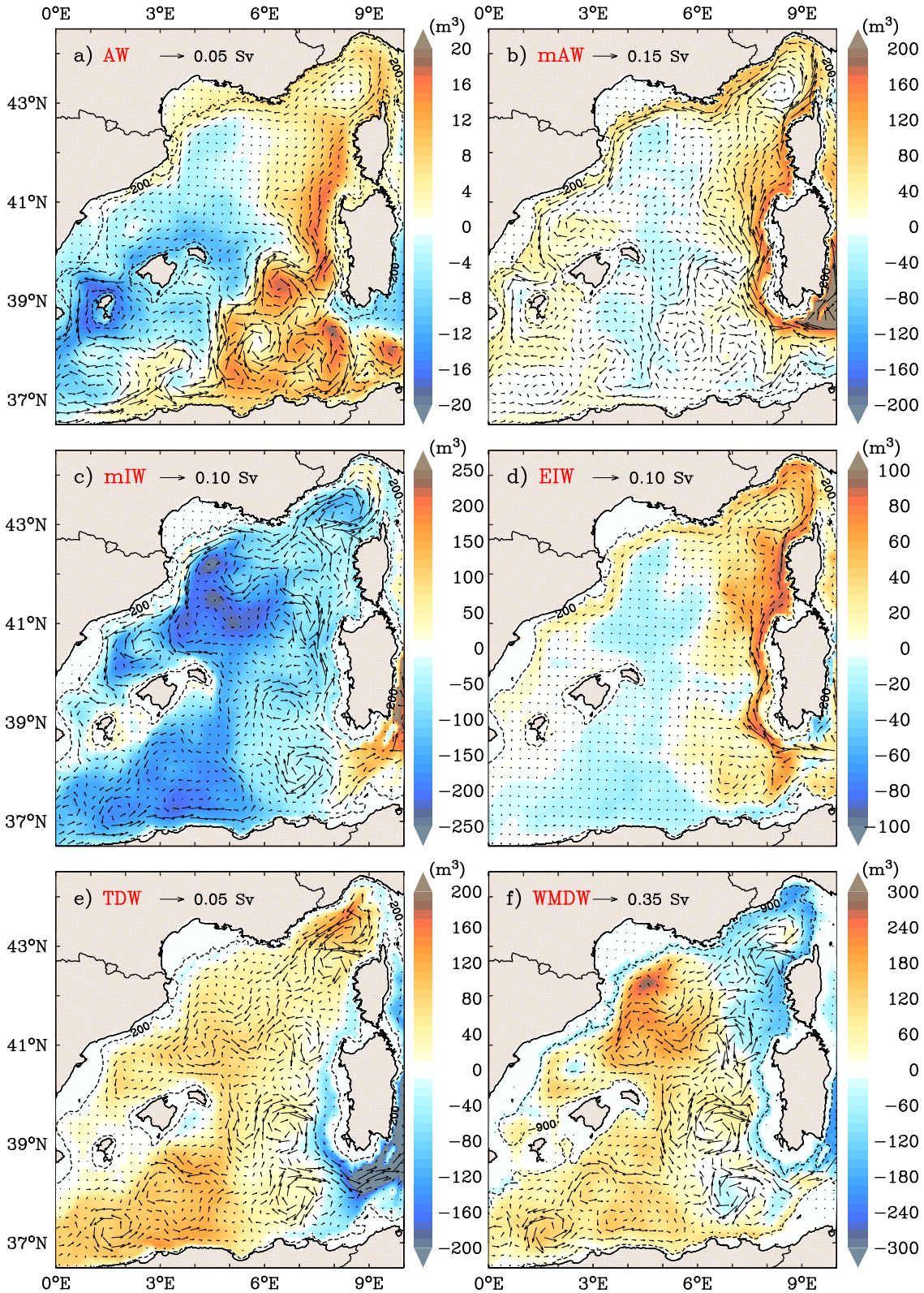

Figure 10. Volume and water mass transport anomalies in 2009 in comparison with the climatology of Figure 5 for (a) Atlantic Water, (b) modified Atlantic Water, (c) mixed Intermediate Water, (d) Eastern Intermediate Water, (e) Tyrrhenian Intermediate Water, and (f) Western Mediterranean Deep Water. Volume contours of (a–e) 200 and (f) 900 m depth.

and then loops back on itself clockwise. The mAW and EIW are strongly trapped in the gyre—the mAW fractions are present deeper than 1,000 m depths in its center—and redistributed westward toward the Algero-Provencal basin along the southern coasts of Sardinia. Even if the overtopping of WMDW above the sill is documented and its hydrological characteristics at this location in the reanalysis seem coherent with deep observations in 2009 (not shown), the mAW fractions in the Tyrrhenian are way too deep to be reliable, and the realistic and well-known circulation at the southeast of Sardinia should actually be composed of a cyclonic and baroclinic gyre, whether at the scale of the general circulation (Iacono et al., 2021; Marullo et al., 1994; Pinardi et al., 2015; Sorgente et al., 2011; Vara et al., 2019) or especially during the year of 2009 (Iacono et al., 2013; Napolitano et al., 2014). Possible clues to the origin of this spurious event are given in the next section.

4. Discussion

4.1. Possible Origins of Spurious Deep Water Mass Dynamics in Reanalysis

Here we discuss the six weaknesses in the water mass dynamics of the reanalysis that were detected, thanks to the sorting algorithm and its analysis metrics. In particular, we investigate the different possible origins of the TDW volume increases in 1999–2000 suddenly, slowly during 1995–2003, the impact of the DWF in the Alboran Sea during 1998–1999, the destruction of the WMDW during the summers of 2003 and 2010 in the Provencal basin, and the effect of the Tyrrhenian gyre and its return current during 2009.

With a first regard to the TDW volume increase in 1999–2000, the salinization of the middle and deep layers during 2000 was already noted by Hamon et al. (2016) in a previous version of the reanalysis (MEDRYS1V1). They attributed it to a biased volume correction term of the SLA model equivalent. This misfit tends to compensate for the SLA error by densifying the water columns. As the assimilation system is more constrained on temperature (due to better data coverage) than on salinity, this adjustment has a stronger effect on salinity, especially at depth due to the very low number of data assimilated below the depth of 600 m before 2005. The increase in these deep salinities may therefore have led to a sudden increase in the volume of TDW. However, taking a broader view at the time series, the TDW volume actually increases from 1995 to 2003, and seems to be due to increased salinities and velocities in the Strait of Sardinia. This suggests that the accumulation of TDW in the Algero-Provencal basin may also be related to the EMT that slowly propagated higher deep salt content toward the western Mediterranean from 1997 to 2004 (Amitai et al., 2021; Schneider et al., 2014). However, this statement must be qualified because the transport of EIW from the Channel of Sicily does not increase as much as the TDW in the Channel of Sardinia and remains almost constant (not shown). Both processes (i.e., a biased SLA adjustment or the westward EMT propagation) may have occurred simultaneously but would be difficult to distinguish since the biased SLA adjustment also affects the eastern Mediterranean (see Beuvier et al., 2016; Hamon et al., 2016).

Then, regarding the 1998–1999 DWF in the Alboran Sea that reversed the eastern Algerian deep gyre and the summers of 2003 and 2010 where Liguro-Provencal deep waters lightened up, in all of these three cases, there is no physical process that can be invoked to explain such changes in the salinity and heat contents of deep and intermediate waters over such large areas. Those are more likely due to biases in the assimilation processes, either through subregional SLA adjustments or local vertical profiles adjustments that can propagate over large areas. It is not in the scope of this study to clearly identify these biases or malfunctioning of the assimilation processes, but we note that the 1998 event just follows a short period of intensive CTD operations in the Alboran Sea during the ALMOFRONT-2 campaign (Prieur et al., 2003) while the availability of CTD profiles in the Mediterranean was generally low before the Argo era (i.e., before 2005) and limited to the 0–1,000 m range (Hamon et al., 2016). The sudden arrival of a higher level of information at depth in the assimilation system may have over-constrained the model. Likewise, the 2003 event just follows the 2003 marine heat wave that has been shown to markedly impact the SST over the northwestern Mediterranean and the circulation in the Central Mediterranean (García-Herrera et al., 2010; Olita et al., 2007). It is not unlikely that the model and/or the assimilation system may have poorly or differently handled the steric effect of this exceptional heat wave, leading to a destabilization of the assimilation system for the SLA. Note that WMDW volume calculations using a fixed threshold (such as 29.10, 29.11, or 29.12 $kg.m^{-3}$, e.g., Somot et al., 2018) yielded much more unrealistic estimates during these anomalous events, with stronger and more sudden variations (a few days, not shown).

Thirdly, the fallacious gyre during 2009 in the Tyrrhenian Sea, even if being consequent to a documented overtopping of the WMDW, induced a large impact over the Algero-Provencal surface and intermediate circulations that were also spurious. That said, these circulations in the Algero-Provencal and Tyrrhenian sub-basins

may be the result of a combination of one, several, or even more of the following factors. First, the choice not to trust observations of SST and SLA within the 50 km off all the coasts (Section 2.2, Hamon et al., 2016) may have allowed the strong coastal currents in the Strait of Sardinia and the Algero-Provencal basin to develop. Meanwhile, a lack in observational data in the center of the Tyrrhenian in the year of 2008 and 2009 (almost none XBT and Argo data, Napolitano et al., 2019), and therefore in the CORA database, can also have allowed the offshore anticyclonic gyre to develop and maintain itself off southeast Sardinia, instead of being cyclonic. Otherwise, the mAW fractions that were excessively deep in the center of the gyre may also indicate that a bias in salinity in the assimilation scheme also occurred, as in the previous cases.

All these events highlight a general weakness of contemporary reanalyses, which most often start in 1993 to benefit from the availability of altimetry data, but thus cover periods of very heterogeneous availability of in situ data. In the Mediterranean, the start of the Argo era between 2000 and 2005 has led to a five-fold increase in available in situ profiles, but with still insufficient coverage of deep layers, especially for salinity (e.g., Hamon et al., 2016). Because deep salinity is the least constrained variable in assimilation systems, it is most likely to suffer from assimilation bias. In any case, all these hypotheses, whatever the event cited above, indicate that the problems do not stem from the water mass detection algorithm, and rather support the hypothesis of accidental biases in the assimilation system.

4.2. Weaknesses and Strengths of the Water Mass Detection Algorithm

4.2.1. The mIW Case, the TIW Absence, and a False AW Formation by the frW

Nevertheless, even if the times series reveal spurious anomalies in mIW-deep coupled nonphysical variability during 1998–1999, 2003, and 2010 that have been assigned to assimilation biases, those are due to subtle variations of salinity (0.02–0.04), slightly lowering (for the 2003 and 2010 cases) or hardly increasing (for the 1998–1999 case) potential density on a large part of the intermediate and deep waters. From this point, the somewhat fuzzy definition of the mIW may appear as the main shortcoming of our approach and should be discussed first. The mIW aggregates the mixings of EIW with several water masses of diverse origins, such as mAW, WIW, TDW (which itself has diverse origins, e.g., Buffett et al., 2017; Fuda et al., 2002; Iacono et al., 2021; Li & Tanhua, 2020) and any waters possibly formed during intermediate or moderate convective events that do not fall into the typical WMDW category (such as the Winter Deep Water, WDW in Bosse et al., 2016). The different intermediate mixed water masses included in the mIW may have similar thermohaline characteristics and are distributed mainly along the EIW mixing path. As such, they do not generate an inflection point on the θ-S diagram that could help to clearly discriminate them (e.g., the TDW). Similarly, the algorithm does not distinguish Tyrrhenian Intermediate Water (TIW), a slightly warmer equivalent of the WIW formed in winter due to the Mistral channeled through the Strait of Bonifacio (Iacono et al., 2021; Napolitano et al., 2019). The TIW flows northward to the Corsican Channel and dilutes in the NC with average characteristics ($\theta \sim 14°C$, $S \sim 38.3$, and $\sigma_\theta \sim 28.8$ kg.m^{-3} in the reanalysis) that are very similar to the mAW, even though it was slightly detected as WIW in the Strait of Corsica during the major events of Provencal DWF. A better method to effectively sort the TIW from the mAW/WIW amalgam would be Lagrangian tracking of this water type along its trajectory from the Bonifacio dipole to the Liguro-Provencal basin. This method has a development and computational cost that was quite prohibitive given the encouraging results we obtained with very early versions of the θ-S-based algorithm (see Barral et al., 2020). Apart from the TIW, the presently defined mIW pool may be related to the finding of Millot (2013). It is representative of the mixing of all intermediate waters in the Tyrrhenian and Algero-Provencal basins with the EIW on its path from the Strait of Sicily, such as for all intermediate waters produced in areas of intermediate convection in the eastern basin that mix on their path to be defined as the EIW at the Strait of Sicily. As so, it has an oceanographic sense, even if an oversimplified one, and mIW is not at the origin of the detected problems. On the contrary, it was its definition and use that enabled us to identify the events of 1998–1999, 2003, and 2010. Besides this asset, based on all previous results (Section 3.1.8) and discussions, it is clear that the mIW is the vanishing part of the EIW by mixing with overlying and underlying water masses on its path to the west, just as the mAW is for the AW by air-sea interactions and mixing with underlying water masses on its path to the east. It is important to note that if the algorithm remains unchanged, the mIW would have been, and should have been, therefore designated the modified EIW (the mEIW).

The frW fraction produces a false AW detection in the region of frW influence (RoFI) of rivers, where frW from rivers would rather mix with the resident and saltier mAW. These false AW detections are of very limited extent due to the sharpness of the salinity fronts on the edges of the frW plumes and have virtually no effect on the volumes and

transports estimates made later on. Let's note that shelf's water is mainly labeled frW whatever its temperature and between 0 and 36 in the RoFI because of its origin from rivers. However, when it is well mixed and falsely becomes AW on the shelves, as it is cooler than mAW, its buoyancy causes it to float to the surface and suffer harsh winds in winter, thus cooling, sinking, and becoming directly WIW, and this, even if less salinity can counteract intermediate convection (e.g., Vargas-Yanez et al., 2012). This explains why between 36 and 38.45 and below 13.5°C the mixing is considered AW-WIW even if it is frW-WIW and ultimately correctly becomes WIW in winter. If we had separated these two types of mixings to obtain an frW-WIW one below 13.5°C, we would have obtained an unwelcome discontinuity and WIW directly incoming from the rivers for more than half the year which is also unfortunate.

4.2.2. A Bias in the mAW-EIW Ratios and Sub-Sorting the WMDW

Two other issues about the water mass algorithm need to be addressed, namely the salinity bounds between EIW and mAW/WMDW and the water masses that are subdivided in WMDW. Describing EIW's salt anomaly dilution with the surrounding water masses led to the setting of a lower bound of 38.45 for both upper and underneath salinity bounds. Given the fact that averaging the salinity minimum of the inflection point that locates WMDW on a θ-S diagram is 38.45, the salt dilution description is coherent and led to proper detection and validation of the volumes and transports of WMDW. However, the average salinity of mAW in the surface Liguro-Provencal basin (38.0–38.5 in Table 1) should be smaller than 38.45 (38.45 at 100 m and 38.3 at 50 m, in Prieur et al., 2020). For example, by using a mAW salinity bound of 38.3 instead of 38.45 in the mixing of AW-mAW (mAW-EIW), the gain (loss) in mAW fraction would have been 6% (30%). Although the bias with AW is small, the one with EIW suggests that the ratio of mAW is overestimated by about one-third by the algorithm to the detriment of EIW. Apart from this example, the impact of such a bias in mAW-EIW mixing would be mainly on the EIW path from the southwest coast of Sardinia toward the northern extent of the AEs where SEs outcrop near Menorca, along the western coasts of Sardinia and Corsica and in the Corsica channel. The first location (39.5°N–8°E) indeed shows large volumes of mAW (Figure 11b) but mixing with AWs in larger AEs also contributes to this. The second location shows low volumes of EIW while this vein also appears to undergo westward propagation of eddies at 41°N (the SUddies, Bosse et al., 2016). Thirdly, the ECC would have increased EIW transport to feed the NC but, as calculated previously in Section 3.2, the bias against the literature indicates a shortfall of around 6%–14% in intermediate transport through the Strait of Corsica. This low transport can also be explained by both the low resolution of the reanalysis above. Whatever, if we want to differentiate salinity dilutions between above and below the EIW, the difference between the two salinity bounds forces to separate them by a threshold in potential density, which ultimately creates a unwelcome discontinuity instead of a smoothed sorting between water masses, the principle of the algorithm. In addition, using 38.45—both because of the summer surface salinity in the Ligurian Sea (mAW fraction at 100%, see Figure A1b in Appendix A) and of the WMDW salinity—instead of a lower value means that the algorithm is prepared for the greater salinization tendency of the surface in the western Mediterranean (see next paragraph). The second issue concerning the WMDW sorting is that, given the period and events of the reanalysis, the water mass could have been subdivided into the nWMDW, oWMDW, and cWMDW (Piñeiro et al., 2019; Schroeder et al., 2006) by salinity and density ratios but the same problem of creating a discontinuity would have arisen, and given the WMDW volumes involved, would have had a significant impact on the calculations (all the more so as the separation of each deep water layer according to its year of formation is not the subject of this study). In the end, these two controversies are brought to a close by these undesirable discontinuities (tried, not shown), whereas the algorithm presented here has demonstrated its ability to meet the study's objective.

4.2.3. The Climatological Trends to Warming, Salinization, and Densification

The regime shift suggested by the marked increase of the estimated TDW volume (discussed in Section 4.1) call for a discussion on the fact that the current algorithm does not take into account the warming and salinization trends observed throughout the Mediterranean in recent decades (e.g., Fedele et al., 2022; Iona et al., 2018; Schroeder et al., 2017; Skliris et al., 2018; Vargas-Yanez et al., 2021). Warming would not significantly affect water mass sorting when based on salinity ratio (i.e., for AW, mAW, and EIW), but would eventually lead WIW to be less marked and even disappearing, at least relative to their current definition. Previous estimates showed a warming increase (trend) in WIW of 0.14–0.5°C (0.014–0.064°C/yr) over the last decade (Barcelo-Llull et al., 2019; Juza et al., 2019; Vargas-Yanez et al., 2021), but our results do not show a significant decrease in the amount of WIW over the 1993–2013 period. This can be explained by recalling that the current algorithm

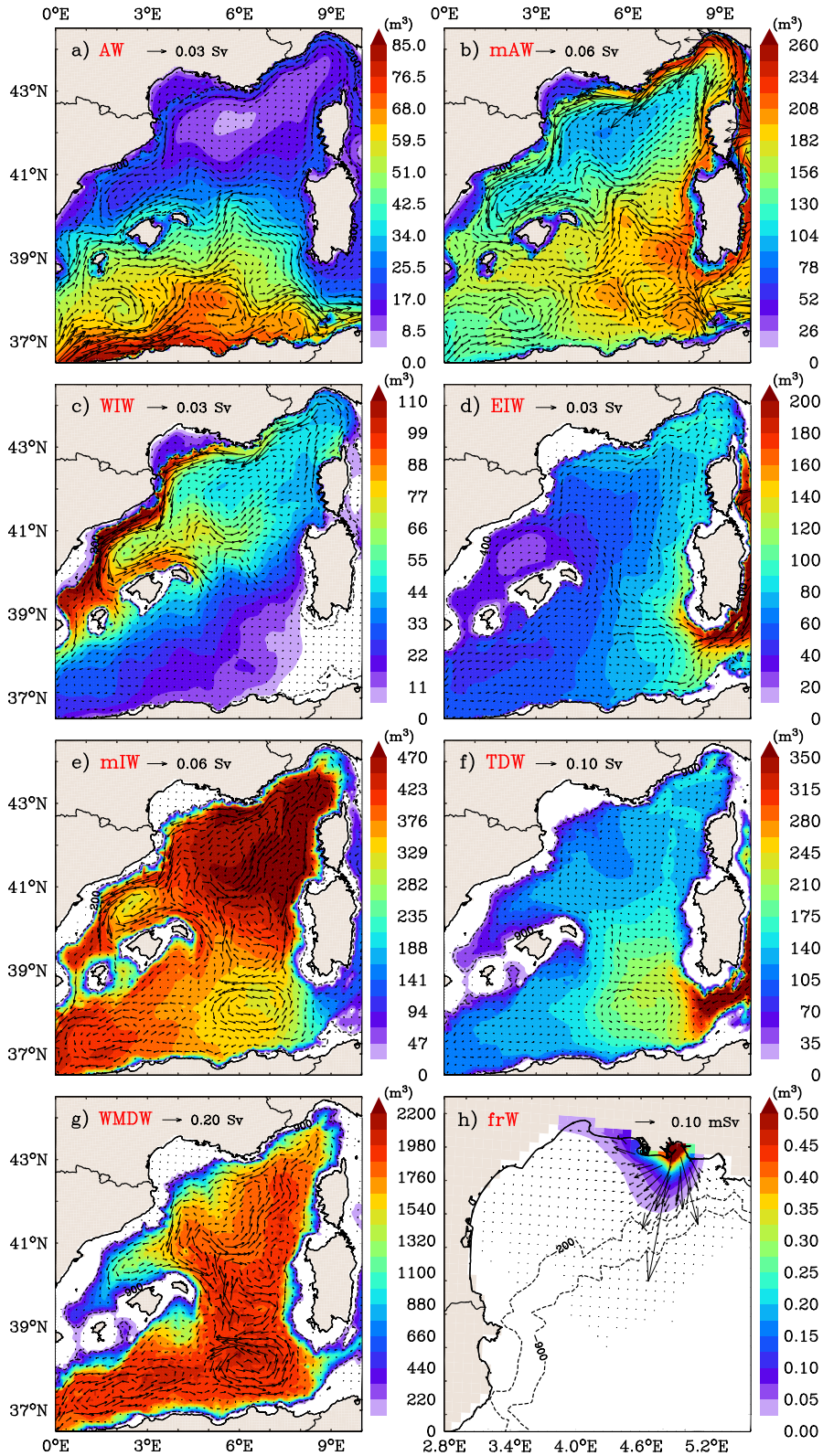

Figure 11. Same as Figure 4, without the years 1998–1999, 2003, 2009, and 2010. Volume contours of (a, b, c, d, e, and h) 200 and (f, g, and h) 900 m depth.

progressively marks the WIW for a temperature below 13.5°C, whereas the usual temperature threshold used to identify it is 13°C. Preliminary tests using lower thresholds led to large underestimations of WIW volumes. The WIW temperature threshold was then set to keep the WIW volume estimates within the range of previous estimates and it appears, therefore, to implicitly parameterize the recent warming of the WIW. The most recent estimates of salinization trends in the western Mediterranean range from 0.001 to 0.007 yr^{-1} depending on the area, depth, and period covered (Fedele et al., 2022; Iona et al., 2018; Skliris et al., 2018; Vargas-Yanez et al., 2021). Taking the most extreme estimates, salinity changes over a 20-year period remain small (0.04–0.14) relative to the salinity ranges used by the algorithm to differentiate AW from mAW (2.35) and mAW/WMDW from EIW (0.35). Furthermore, this trend appears to be more pronounced for mAW (0.04–0.06 yr^{-1}) than that of EIW (0.012–0.035 yr^{-1}) or AW (−0.01 yr^{-1}) in the Algero-Provencal basin (Fedele et al., 2022; Vargas-Yanez et al., 2021) so we do not expect serious bias in their fraction estimates. The problem is more questionable for the density-based water column partitioning, mainly for mIW-TDW-WMDW sorting which is very sensitive to small changes in potential density, as seen with the three anomalous events detected with the algorithm. Nevertheless, due to the nonlinear and antagonistic impact of salinity versus temperature changes on the sea state equation, the potential density increases (trends) observed for EIW or WMDW (0.01 $kg.m^{-3}$, 2.10^{-4} $kg.m^{-3}$/yr) in the western Mediterranean are small or insignificant (Schroeder et al., 2016; Vargas-Yanez et al., 2021) compared to the potential density ranges used in the algorithm to partition the intermediate to deep part of the water column (0.0455 $kg.m^{-3}$). Therefore, we conclude that these warming, salinization, and densification trends would not have biased the estimated water mass fractions, and thus the subsequent volume and transport estimates. Nevertheless, it is clear that careful a priori consideration will be required for application on a longer time scale than the present 20-year analysis.

Validation or evaluation of a reanalysis is most often based on global statistics for heat and salt content, model misfit or assimilation increment, etc. (e.g., Aznar et al., 2016; Hamon et al., 2016). The approach we used goes further in this necessary assessment exercise as it allows us to identify at least three unrealistic events over the deep and intermediate layers that would be undetectable from global statistics given the small value of the salinity and temperature biases involved (fewer than 0.1 and 0.3°C). In fact, similar biases are likely to occur throughout the water column, but their impact would be much lower in the surface layers given the higher range of salinity and temperature variability between AW, mAW, and WIW.

4.3. Rectified Climatology and the Link Between Surface and Deep Dynamics

Beyond the possible origins of the spurious events, and the fact that mIW is more an asset than a weakness because it has made it possible to detect them, the reanalysis seems to resist the artifacts, which do not last more than a few months for 2003 and 2010 in terms of water mass characteristics, peculiar volumes and transports (Figures 6–8). The impact in terms of deep-water transport is more questionable for the 1998 event for which the increase in transport over the Algerian basin and the inverted quasi-barotropic gyre lasted a few more than 2 years (Figure 9), and in terms of intermediate and surface circulations for the 2009 event when exceptional circulation occurred for a year throughout the Algero-Provencal basin (Figure 10). We therefore recalculated the long-term mean volumes and transports for each water mass without the years 1998–1999, 2003, 2009, and 2010, as shown in Figure 11. The removal of the year 2009 only led to a little more southeastward mAW transport at the southwest of Sardinia; hence, following the path of AW in the AC to the Tyrrhenian but there are no other significant differences in the volumes and transports of AW, mAW, and WIW between Figures 5 and 11, showing that the 2003, 2009, and 2010 dubious events have almost had no effects on the surface water mass climatological circulations. The new estimates for mIW, TDW, and WMDW better highlight a deep cyclonic gyre in the eastern Algerian basin (Figures 11e–11g) that is much more consistent with the literature (Send & Testor, 2017; Testor, Send, et al., 2005). This mean cyclonic gyre was hidden by the strong anticyclonic gyre generated by the suspicious 1998–99 deep event, maintained until early 2000. The mIW and TDW now also exhibit this deep cyclonic circulation (Mallil et al., 2021), leading to cumulative 20-year climatological transports of deep and intermediate water mass of about 2.5 ± 0.5 Sv, only slightly lower than those reported by Send and Testor (2017) during the 1997–2002 period (4.0 ± 1.0 Sv). For the seven water masses, the largest volume differences from the first guess appear primarily in the western Algerian basin, consistent with the removal of the 1998 TDW + WMDW event, but do not exceed 10% (hence the invisibility between Figures 5g and 11g).

The corrected climatology of water mass circulations (Figure 11) highlights a deep gyre in the eastern Algerian basin in controlling the dynamics of deep and intermediate water masses. It has been suggested previously that

this deep gyre may also control the surface path of AEs (Escudier et al., 2016; Isern-Fontanet et al., 2006; Mallil et al., 2021; Pessini et al., 2018). Although clearly an artifact, the 1998 TDW + WMDW production event in the Alboran Sea suggests that the deep gyre of the eastern Algerian basin may be highly sensitive to the arrival of newly formed deep water. In addition, Barral et al. (2021) showed that the DWF over the northern sub-basin can shift the northern boundary of the AWs, that is, the Balearic-Sardinian frontal zone, one degree southward. They hypothesized that this would be due to a weakening in the formation and northward propagations of AEs during DWF years. To reexamine this hypothesis, we recomputed the mean water mass volumes and transports by separating the years with (2004–2006, 2011–2012, 5 years mean) and without DWF (1993–1997, 2000–2002, and 2007–2008, 10 years mean) based on the maximum MLD and DWF area (Figure 7a).

For each water mass, the difference in mean volumes and transports between the two regimes are presented in Figure 12. Years with DWF correctly show larger volumes of WMDW in the northwestern part of the basin, mainly in the known DWF area around 42°N–5°E, as well as increased transport of WMDW from the DWF area to northeastern Menorca and southward. The volume differences over the central Liguro-Provencal area for the mAW, WIW, mIW, and EIW illustrate the conversion of surface and intermediate waters to WMDW when DWF occurs. The TDW volume is higher over the entire basin during DWF years in contradiction with the usual finding of its destruction during DWF events. This is due to the 1999 increase in TDW volume (Section 3.3.1), as all of the used DWF years occur after 2004. Furthermore, the differences in transport estimates show an acceleration of the along-slope cyclonic circulation over the Liguro-Provencal area for mAW, WIW, EIW, mIW, and TDW. This acceleration of the regional cyclonic circulation has been suggested for a long time, based on heat and water budget (e.g., Astraldi & Gasparini, 1994; Bethoux et al., 1982) or dynamical considerations (e.g., Crépon & Boukthir, 1987; Madec et al., 1991) and clearly evidenced in dedicated modeling study (e.g., Herrmann et al., 2008) but, to our knowledge, never on such climatological mean. The water mass volumes over the northern along-slope circulation are not significantly affected (along the 200 m isobath), showing that the response is only an enhanced current. Conversely, there are significant changes in the AW (mAW) volumes around and east of the Balearic Sea (east of the Balearic Sea to the northwest of Sardinia), showing that the shape of the northern (southeastern) extension of the AW (mAW) reservoir is modified toward less AW north of 39°N. This is consistent with our previous study that shows a DWF-induced meridional shift of the haline frontal zone that prevails between Menorca and Sardinia (Barral et al., 2021). This regime shift also largely affects the amount of mAW at the west/northwest of Sardinia and above the deep Algerian gyre, suggesting that less mAW may be produced by mixing in the AEs, such as a lesser northward extent and activity of the AEs following a DWF event.

The difference in transports estimates between the two regimes also shows a marked inversion of the deep circulation in the area of the eastern deep Algerian gyre when DWF occurs, comforting the hypothesis of a disruption, or at least, a marked weakening of the barotropic gyre in response to the increased southward flow of the WMDW. Except WIW which is not detectable in this region, all the surface (AW and mAW), intermediate (EIW, and mIW), and deep (TDW and WMDW) water masses show the same tendency. For EIW and mIW, this is likely due to the algorithm that maintains a link between the intermediate water masses and the TDW and WMDW through the use of salinity and potential density fractions, but it is also coherent with Send and Testor (2017).

Note that this deep gyre is not a true permanent feature in the reanalysis, but the average effect of the paths of several smaller (50–100 km) anticyclonic eddies. The velocities (and hence transports) in these eddies are about half the velocities of the southward spreading cyclonic eddies of the newly formed WMDW (about 5 $cm.s^{-1}$ vs. 10 $cm.s^{-1}$, Beuvier et al., 2012; Testor, Send, et al., 2005). The resulting eddy-eddy interactions are complex and chaotic (e.g., Testor et al., 2018; Waldman et al., 2018), so the disturbance of the deep gyre may simply reflect the mean of a more turbulent deep circulation.

The alignment between the circulations of surface (AW and mAW) and deep water masses over the eastern deep Algerian gyre is less intuitive, but not so surprising if this long term mean is seen as retaining the long-term average of the paths of the AEs as guided by the deep barotropic gyre (Escudier et al., 2016; Isern-Fontanet et al., 2006; Mallil et al., 2021; Pessini et al., 2018). The weakening of the deep eastern Algerian gyre would induce a lesser northern extent of the AEs, as suggested above regarding the differences in AW and mAW volumes; hence, a weakened signature of the cyclonic path of their surface circulation and a low but detected AW retention in its center.

Of the 15 years used to compute the two average regimes (i.e., after elimination of the five biased ones), five are DWF years whereas 10 are not and DWF years occur more often at the end of the reanalysis, so that the two

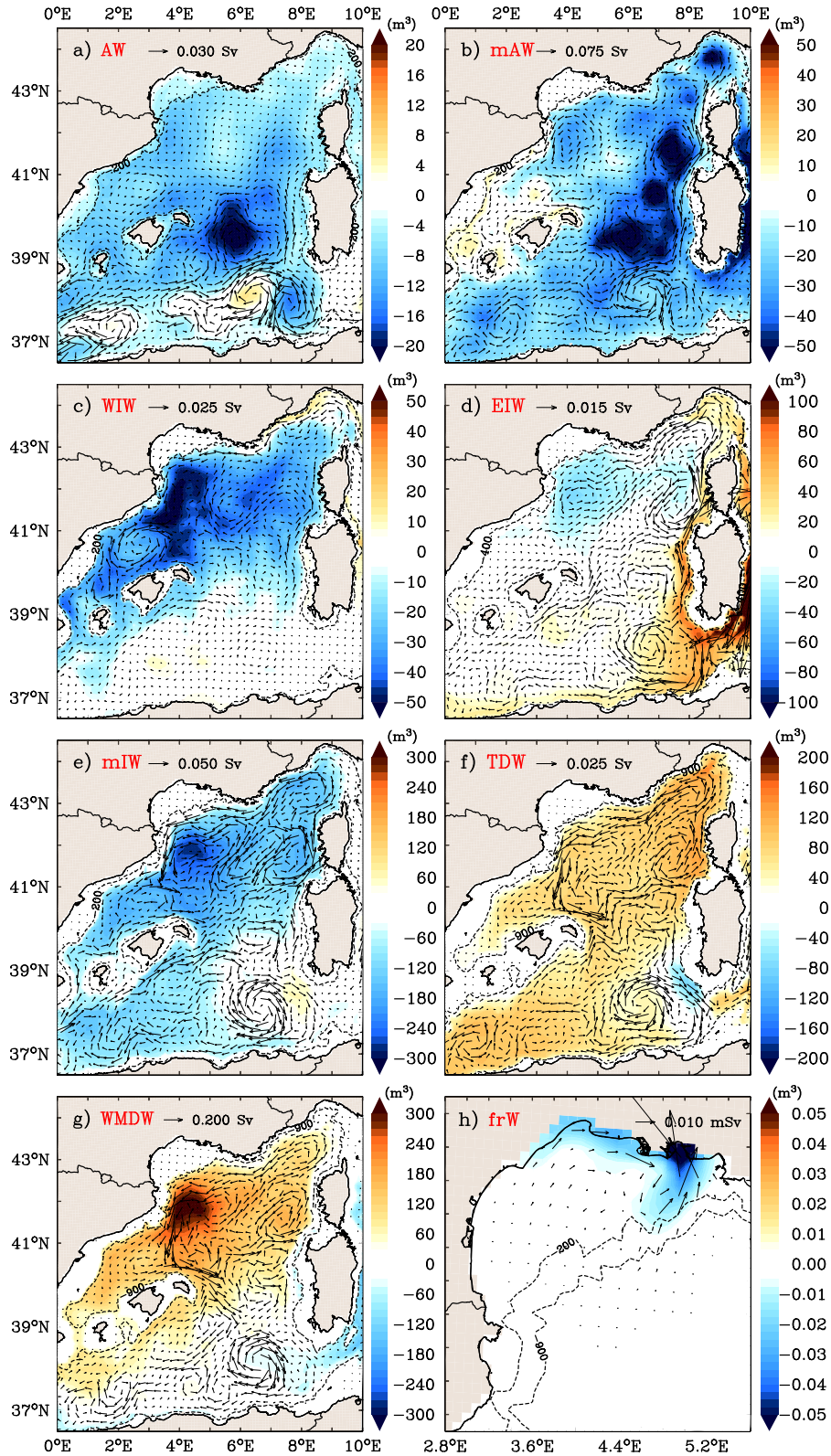

Figure 12. Differences of water mass volumes and transports between the average of 10 years without DWF and the average of 5 years with DWF (i.e., DWF minus no DWF) for Atlantic Water (a), modified Atlantic Water (b), Western Intermediate Water (c), Eastern Intermediate Water (d), mixed Intermediate Water (e), Tyrrhenian Deep Water (f), Western Mediterranean Deep Water (g), and freshwater (h). A scale arrow for transport values is shown on each panel. Volume contours of (a, b, c, d, e, and h) 200 and (f, g, and h) 900 m depth.

climatological regimes do not have the same statistical robustness. Nevertheless, the differences between the two regimes (DWF or no DWF) are coherent with the known acceleration of the northern cyclonic circulation of the surface (mAW), subsurface (WIW), and intermediate (EIW, mIW, and TDW) layers (e.g., Herrmann et al., 2008; Madec et al., 1991), and with the southern shift of the AW/mAW main frontal zone suggested in Barral et al. (2021) during DWF years.

5. Conclusion

The main objective of this study was to extract from a 20-year reanalysis of the western Mediterranean a coherent climatological picture of the water mass dynamics, focusing on the Algero-Provencal basin. To do this, we built a θ-S-based algorithm that discriminates the main seven water masses (AW, mAW, WIW, EIW, mIW, TDW, and WMDW) in order to estimate the corresponding volumes and transports. Prior to the actual analysis, the calculated water mass mixing fractions were also used to estimate the mean thermohaline characteristics and depth range of each water mass. This allowed us to validate the behavior of the algorithm, that is, to ensure that it could indeed report the correct water mass at the correct depth. Averaged over the 20 years of the reanalysis, the results give consistent distributions of the volumes and transports of the different water masses in the Algero-Provencal basin. The analysis of the time series of temperature, salinity, and volumes brought several other positive elements, such as the coherent seasonally driven variability of AW, mAW, and WIW, and the realistic inter-annual variability of WMDW production, particularly in 2005, which is known to be the major DWF event of the last three decades, given its impact on the intermediate and deep thermohaline characteristics (Schroeder, Ribotti, et al., 2008; Schroeder, Taillandier, et al., 2008).

Fine-tuning the algorithm between the intermediate and deep water masses has enabled us to conceptualize that the mIW is in fact the modified EIW (mEIW, by analogy with the mAW) and to identify several spurious events. The first is a slow increase in TDW volume over the long term, in addition to a sudden rise in 1999. Secondly, a DWF in the Alboran Sea occurs at the end of 1997 and induces a reversal of the deep gyre in eastern Algerian until 1999. In the summers 2003 and 2010, two WMDW destructions happen by lightening in the Provencal basin. Finally, a documented overflow of WMDW into the Tyrrhenian Sea due to the WMT induced a strong inflow of surface and intermediate waters through a false return current during 2009. Discussions on the possible origins of these problems focused on the assimilation of small salinity biases associated with a lack of deep observations. Above all, these episodes highlight the lack (and hence the need) for deep observations to constrain the deep layer of reanalyses, which is then likely to become an adjustment variable for model assimilation deviations.

The elimination of these abnormal events has had virtually no impact on surface volumes and flows. In addition, we have shown that bypassing the biased periods allowed us to improve the average circulation scheme of the intermediate and deep water masses, mainly by retrieving the well-known eastern Algerian barotropic gyre. This shows that the reanalysis is robust to accidental assimilation biases and we can expect deep-sea dynamics to be better constrained as more and more in situ deep-sea data become available for assimilation. Ultimately, these detections testify to the algorithm's ability to go further than the usual calculations of heat and salt content, which only validate the average or long-term assessment of simulations, and are unable to highlight these anomalies in circulation and transformations between water masses. Plus, the study showed that the method overcomes the need for a large number of variables in an OMP analysis and the need for high computing power for large database analyses with other methods.

Beyond the assessment exercise, this study suggests a new finding regarding the impact of the WMDW dynamics on surface and intermediate waters. It is a possible breakdown of the eastern Algerian barotropic gyre in response to the arrival of new WMDW in the southern part of the basin following significant DWF events occurring in the northern part. This disturbance of the Algerian gyre has not been documented before from in situ data, but can be seen in Beuvier et al. (2012) who describes the southward propagation of WMDW cyclonic eddies after the strong DWF event of 2005 leading to a similar destabilization of the gyre in a model.

Further studies are currently underway to overcome these anomalies and attempt to validate the latest results by analyzing the satellite altimetry observations and, with the same algorithm of water mass sorting and derived proxies (volumes, transports), the twin free run of MEDRYS and another longer and finer reanalysis of the Mediterranean (1987–2019, 1/24°, Escudier et al., 2021). This should allow us to compare the impact of the detected assimilation biases, to get more robust climatological estimates and to enlarge the studied area to the Alboran and Tyrrhenian Seas.

Appendix A: The Water Mass Detection Algorithm in the Algero-Provencal Basin

First step of the algorithm, the partitioning of the water column involves the definitions of surface and deep layers. To locate the surface layer, two densities bound a linear function between the mAW (σ_{mAW}) and the EIW (σ_{EIW}). Above this σ_{mAW}, the surface fraction is set to one while below σ_{EIW}, it is set to zero as:

$$f_{surf} = \begin{cases} 1, \ \sigma < \sigma_{mAW} \\ \dfrac{\sigma_{EIW} - \sigma}{\sigma_{EIW} - \sigma_{mAW}}, \ \sigma_{mAW} \leq \sigma \leq \sigma_{EIW} \\ 0, \ \sigma > \sigma_{EIW} \end{cases} \tag{A1}$$

where $\sigma_{mAW} = 28.9643$ kg.m^{-3} (computed from $S_{mAW} = 38.45$, $\theta_{mAW} = 13.5$°C, see Sections 2.2 and 4.2 and Equation A5) and $\sigma_{EIW} = 29.0624$ kg.m^{-3} ($S_{EIW} = 38.8$, $\theta_{EIW} = 14.3$°C at the Strait of Sicily), standing for the lower bound of the surface layer and the well-known core of the intermediate layer, respectively. It should be noted that, whatever the water mass, the temperature and salinity that define the bounds of linear mixing have been chosen both in accordance with the literature first (Table 1) and then in accordance with the daily climatology of the θ-S diagram of the reanalysis (see the monthly climatology in Figure A1). The separation of the deep layer of the water column from the intermediate is carried out in the same way, but between the EIW and WMDW:

$$f_{deep} = \begin{cases} 0, \ \sigma < \sigma_{EIW} \\ \dfrac{\sigma - \sigma_{EIW}}{\sigma_{WMDW} - \sigma_{EIW}}, \ \sigma_{EIW} \leq \sigma \leq \sigma_{WMDW} \\ 1, \ \sigma > \sigma_{WMDW} \end{cases} \tag{A2}$$

where σ_{EIW} remains as previously, and $\sigma_{WMDW} = 29.1075$ kg.m^{-3} is computed from $S_{WMDW} = 38.45$ and $\theta_{WMDW} = 12.815$°C. The second step sorts the freshwater as a water with a salinity which is lower than that of the AW salinity minimum ($S_{AW} = 36$):

$$f_{fresh} = \begin{cases} \dfrac{S_{AW} - S}{S_{AW}}, \ S \leq S_{AW} \\ 0, \ S > S_{AW} \end{cases} \tag{A3}$$

The fraction of AW hence uses a salinity ratio built to represent the AW-mAW mixing in the surface layer (Figure A1a):

$$f_{AW} = \begin{cases} \left(1 - f_{fresh}\right) \cdot f_{surf}, \ S < S_{AW} \\ \dfrac{S_{mAW} - S}{S_{mAW} - S_{AW}} \cdot f_{surf}, \ S_{AW} \leq S \leq S_{mAW} \\ 0, \ S > S_{mAW} \end{cases} \tag{A4}$$

A temporary salinity fraction is defined for EIW assuming 38.8 at the Strait of Sicily and that it dilutes along a salinity gradient from 38.8 to 38.45 (both the average minimum of salinity of WMDW and the maximum surface salinity of the mAW in the Ligurian Sea):

$$tmp_{EIW} = \begin{cases} 0, \ S < S_{WMDW} \\ \dfrac{S - S_{WMDW}}{S_{EIW} - S_{WMDW}}, \ S_{WMDW} \leq S \leq S_{EIW} \\ 1, \ S > S_{EIW} \end{cases} \tag{A5}$$

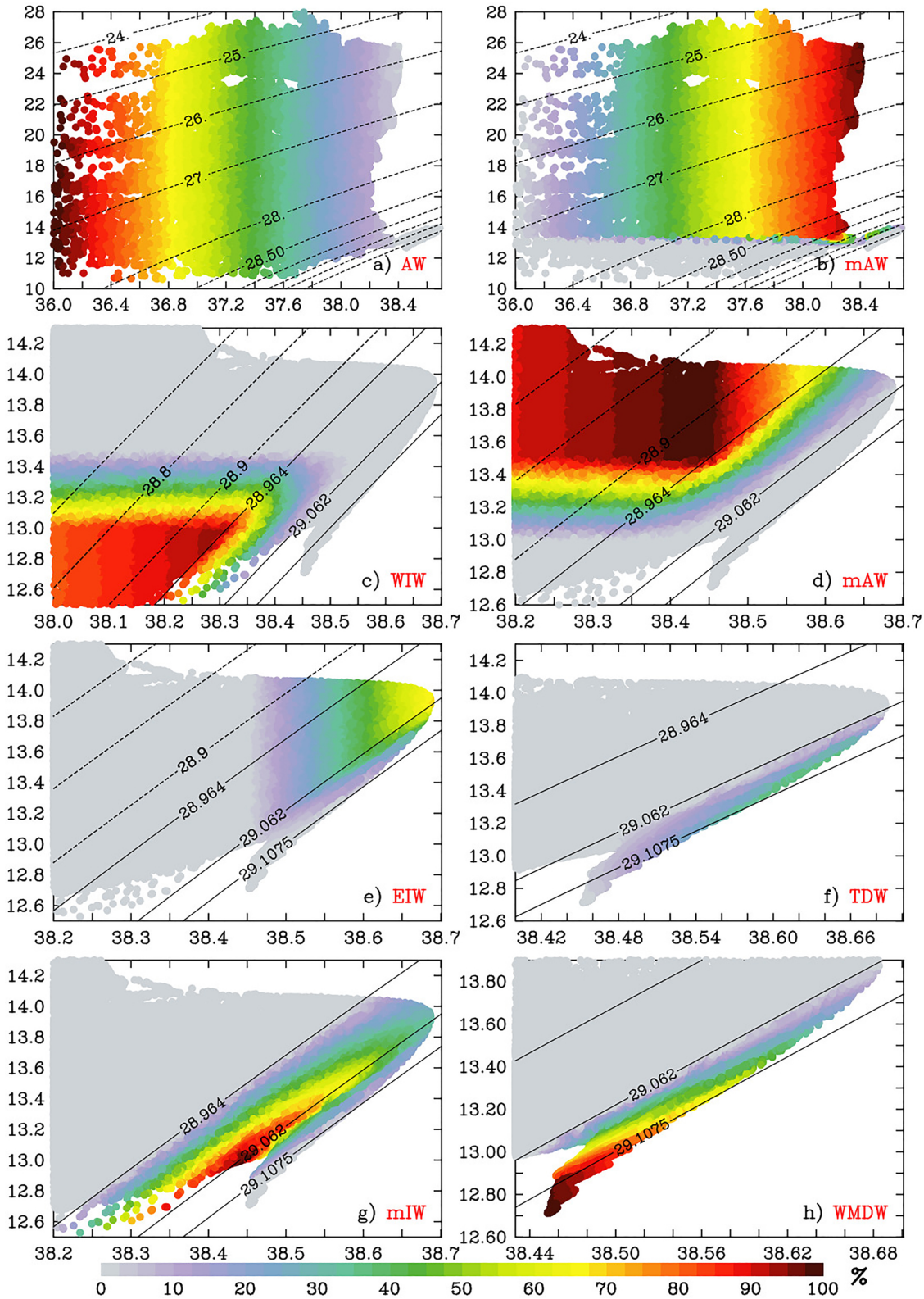

Figure A1. θ-S diagrams of the water mass fractions (%), computed over the monthly climatology of the Algero-Provencal domain (excluding the Alboran and Tyrrhenian Seas) for (a) Atlantic Water, (b and d) modified Atlantic Water, (c) Western Intermediate Water, (e) Eastern Intermediate Water, (f) Tyrrhenian Deep Water, (g) mixed Intermediate Water and (h) Western Mediterranean Deep Water. The panel (d) is a zoom of the panel (b).

As the EIW mixes with the deeper WMDW and they together produce the TDW in between them, the final fraction of EIW is defined as the salinity sorting out of the deep layer:

$$f_{\mathrm{EIW}} = \mathrm{tmp}_{\mathrm{EIW}} \cdot \left(1 - f_{\mathrm{deep}}\right) \tag{A6}$$

Note that this produces a simple salinity sorting below σ_{EIW} while a multiplication of two fractions above (Figure A1e). Then, to the opposite, the fraction of TDW is the salinity fraction of EIW (Equation A5) that spreads in the deep layer (Equation A2) (Figure A1f):

$$f_{\mathrm{TDW}} = \mathrm{tmp}_{\mathrm{EIW}} \cdot f_{\mathrm{deep}} \tag{A7}$$

Then, the fraction of WMDW is considered to be what remains in this deep layer (Figure A1h):

$$f_{\mathrm{WMDW}} = f_{\mathrm{deep}} - f_{\mathrm{TDW}} \tag{A8}$$

This ultimately suggests that the WMDW is in the deep-water layer (Equation A2), but deprived of the salinity fraction of the EIW (Equation A5) that built the TDW by mixing (i.e., $f_{\mathrm{WMDW}} \sim f_{\mathrm{deep}}{}^{*}(1 - \mathrm{tmp}_{\mathrm{EIW}})$). To consider the water masses above EIW, the sum of previous water mass fractions that can be lower than σ_{EIW} (Equations A3, A4, and A6) defines a temporary fraction that allows only the remaining ratios to be treated:

$$\mathrm{tmp} = f_{\mathrm{fresh}} + f_{\mathrm{AW}} + f_{\mathrm{EIW}} \tag{A9}$$

For the third step, sorting the mAW (Figures A1b and A1d) and WIW (Figure A1c) assumes that they are pooled in the remaining (Equation A9) surface waters (Equation A1) and can be discriminated using a temperature ratio:

$$f_{\mathrm{WIW}} = f_{\mathrm{surf}} \cdot (1 - \mathrm{tmp}) \cdot \mathrm{tmp}_{\mathrm{WIW}} \tag{A10}$$

$$f_{\mathrm{mAW}} = f_{\mathrm{surf}} \cdot (1 - \mathrm{tmp}) \cdot \left(1 - \mathrm{tmp}_{\mathrm{WIW}}\right) \tag{A11}$$

where the temperature ratio between mAW ($\theta_{\mathrm{mAW}} = 13.5°\mathrm{C}$) and WIW ($\theta_{\mathrm{WIW}} = 13°\mathrm{C}$) is:

$$\sigma < \sigma_{\mathrm{EIW}} \Rightarrow \mathrm{tmp}_{\mathrm{WIW}} = \begin{cases} 1, \ \theta < \theta_{\mathrm{WIW}} \\ \dfrac{\theta_{\mathrm{mAW}} - \theta}{\theta_{\mathrm{mAW}} - \theta_{\mathrm{WIW}}}, \ \theta_{\mathrm{WIW}} \le \theta \le \theta_{\mathrm{EIW}} \\ 0, \ \theta > \theta_{\mathrm{mAW}} \end{cases} \tag{A12}$$

With all known water masses defined, the mIW is defined as the remainder of all previous water mass fractions. It is in this case along the 29.062 $\mathrm{kg.m}^{-3}$ isopycnal and with a maximum percentage near the lowest salinities (Figure A1g):

$$f_{\mathrm{mIW}} = 1 - \left(f_{\mathrm{fresh}} + f_{\mathrm{AW}} + f_{\mathrm{mAW}} + f_{\mathrm{WIW}} + f_{\mathrm{EIW}} + f_{\mathrm{TDW}} + f_{\mathrm{WMDW}}\right) \tag{A13}$$

Appendix B: Characteristics, Volumes, and Transports of the Water Mass

The mean characteristics (θ, S, $\sigma_{\theta,}$ and depth) of each water mass is computed as fraction and volume weighted means, as for example, for the mean potential temperature:

$$\overline{\theta}_i(t) = \frac{\sum_{xyz} \left(f_i \cdot \Delta x \Delta y \Delta z \cdot \theta\right)}{\sum_{xyz} \left(f_i \cdot \Delta x \Delta y \Delta z\right)} \tag{B1}$$

where "i" is the water mass index (from 1 to 7: AW, mAW, WIW, EIW, mIW, TDW, and WMDW) and dx, dy, and dz are the spatial increments defining the finite volume of one grid mesh. Note that the model grid being

curvilinear and bottom adjusted for the deepest wet grid meshes (partial step discrete mesh), the grid meshes dimensions vary in space. Indexes of spatial increments have been omitted for simplification in this and the following equations (except when essential). The estimate for the core of a water mass is similarly computed but retaining only the value of the maximum fraction inside each vertical profile.

Starting with a simple water column (i.e., at a fixed longitude and latitude location), the water mass volume is computed as:

$$V_i(x,\ y,\ t) = \int_z f_i \cdot dV = \sum_z f_i(x,\ y,\ z,\ t) \cdot \Delta x \Delta y \Delta z \tag{B2}$$

This first quantity allows us to construct daily maps of the volumes of the different water masses. Summing over the whole domain (or a subdomain like for the NWMed area) leads to the total volume of each water mass. As the local (x, y, z, and t) sum of all the water mass fractions is always one, it is straightforward to show that summing the overall water masses gives the constant water column volume that is only bathymetry dependent, neglecting the dynamic height (SSH) that is only about tens of centimeters over the western Mediterranean.

Using the same fractions based distribution principle, each water mass transport (Sv) over a water column is computed as:

$$\vec{M}_i(t) = \iint \left(f_i \cdot \vec{U}\right) ds \approx \vec{i} \sum_k \left(f_i \cdot u_\theta \cdot \Delta x_\theta \Delta z_\theta\right) + \vec{j} \sum_k \left(f_i \cdot v_\theta \cdot \Delta y_\theta \Delta z_\theta\right) \tag{B3}$$

where "u_θ" and "v_θ" stand for the velocity components interpolated at the scalar (temperature and salinity) grid points, according to the used curvilinear and Arakawa C mesh grid. Similarly, the across-section transports are computed as:

$$M_i^S(t) = \iint \left(f_i \cdot \vec{U} \circ \hat{n}\right) ds \approx \sum_{N_S} \sum_k \left[f_{i,\,S} \cdot \left(u_S \cdot \Delta x_u \Delta z_u + v_S \cdot \Delta y_v \Delta z_v\right)\right] \tag{B4}$$

where "S" is the chosen section and "NS" stands for the total number of grid points along the section. The velocities u_S and v_S and corresponding increments (dxu, dzu, dyv, and dz) are the original Arakawa C grid (no interpolation) following the rule of positive signs to the north and east. This grid-specific computation was necessary to obtain a precise budget of the total transport when applied over all frontiers of a sub-region. As previously shown for the volumes, summing those transports on all water masses conserves the total transports, either on a water column or a boundary section.

Abbreviations

Water Masses

AW	Atlantic Water
EIW	Eastern Intermediate Water
frW	freshwater
LIW	Levantine Intermediate Water
mAW	modified Atlantic Water
mIW	mixed Intermediate Water
TDW	Tyrrhenian Deep Water
TIW	Tyrrhenian Intermediate Water
WIW	Western Intermediate Water
WMDW	Western Mediterranean Deep Water

Currents

AC	Algerian Current
AE	Algerian Eddy
BC	Balearic Current
ECC	East Corsican Current
NC	Northern Current
SE	Sardinian Eddy
WCC	West Corsican Current

Others

DWF	Deep Water Formation
EMT	Eastern Mediterranean Transient
GoL	Gulf of Lion
MDT	Mean Dynamic Topography
MEDRYS	MEDiterranean ReanalYSis
MLD	Mixed Layer Depth
MTHC	Mediterranean ThermoHaline Circulation
SLA	Sea Level Anomaly
WMT	Western Mediterranean Transition

Data Availability Statement

[Dataset] The bathymetry ETOPO1 data set used for the first figure is available at the NOAA National Geophysical Data Center. 2009: ETOPO1 1 Arc-Minute Global Relief Model. NOAA National Centers for Environmental Information. https://www.ngdc.noaa.gov/mgg/global/. [Software] The software used to compute and visualize all the results is PyFerret, developed by the National Oceanic and Atmospheric Administration and available at the Ferret User Guide website. https://ferret.pmel.noaa.gov/Ferret/.

Acknowledgments
This work was part of the PhD thesis of Q.-B. Barral funded by the French Ministère de l'Enseignement Supérieur, de la Recherche et de l'Innovation (MESRI). It is a contribution to the MISTRALS (Mediterranean INtegrated STudies at Regional And Local Scales) program through the CLOSCHEMED (CLOsure SCHEme of the MEDiterranean gyre) project funded by the French CNRS/INSU program LEFE-GMMC.

References

Adloff, F., Somot, S., Sevault, F., Jordà, G., Aznar, R., Déqué, M., et al. (2015). Mediterranean Sea response to climate change in an ensemble of twenty first century scenarios. *Climate Dynamics*, *45*(9), 2775–2802. https://doi.org/10.1007/s00382-015-2507-3

Amitai, Y., Ashkenazy, Y., & Gildor, H. (2021). The effect of the source of deep water in the eastern Mediterranean on western Mediterranean intermediate and deep water. *Frontiers in Marine Science*, *7*. https://doi.org/10.3389/fmars.2020.615975

Astraldi, M., & Gasparini, G. P. (1992). The seasonal characteristics of the circulation in the north Mediterranean basin and their relationship with the atmospheric-climatic conditions. *Journal of Geophysical Research*, *97*(C6), 9531–9540. https://doi.org/10.1029/92JC00114

Astraldi, M., & Gasparini, G. P. (1994). The seasonal characteristics of the circulation in the Tyrrhenian Sea. In *Seasonal and interannual variability of the western Mediterranean Sea* (pp. 115–134). American Geophysical Union (AGU). https://doi.org/10.1029/CE046p0115

Aznar, R., Sotillo, M. G., Cailleau, S., Lorente, P., Levier, B., Amo-Baladrón, A., et al. (2016). Strengths and weaknesses of the CMEMS forecasted and reanalyzed solutions for the Iberia–Biscay–Ireland (IBI) waters. *Journal of Marine Systems*, *159*, 1–14. https://doi.org/10.1016/j.jmarsys.2016.02.007

Balmaseda, M. A., Hernandez, F., Storto, A., Palmer, M. D., Alves, O., Shi, L., et al. (2015). The ocean reanalyses intercomparison project (ORA-IP). *Journal of Operational Oceanography*, *8*(1), s80–s97. https://doi.org/10.1080/1755876X.2015.1022329

Barceló-Llull, B., Pascual, A., Ruiz, S., Escudier, R., Torner, M., & Tintoré, J. (2019). Temporal and spatial hydrodynamic variability in the Mallorca channel (Western Mediterranean Sea) from 8 years of underwater glider data. *Journal of Geophysical Research: Oceans*, *124*(4), 2769–2786. https://doi.org/10.1029/2018JC014636

Barral, Q.-B., Zakardjian, B., Dumas, F., Garreau, P., & Beuvier, J. (2020). Analysis of specific water masses transports in the Western Mediterranean in the MEDRYS1V2 twenty-one-year reanalysis. https://doi.org/10.5194/egusphere-egu2020-21979

Barral, Q.-B., Zakardjian, B., Dumas, F., Garreau, P., Testor, P., & Beuvier, J. (2021). Characterization of fronts in the Western Mediterranean with a special focus on the North Balearic Front. *Progress in Oceanography*, *197*, 102636. https://doi.org/10.1016/j.pocean.2021.102636

Bauch, D., & Cherniavskaia, E. (2018). Water mass classification on a highly variable Arctic shelf region: Origin of Laptev Sea water masses and implications for the nutrient budget. *Journal of Geophysical Research: Oceans*, *123*(3), 1896–1906. https://doi.org/10.1002/2017JC013524

Ben Ismail, S., Schroeder, K., Chiggiato, J., Sparnocchia, S., & Borghini, M. (2021). Long term changes monitored in two Mediterranean Channels. In K. von Schuckmann, P. Y. Le Traon, N. Smith, A. Pascual, S. Djavidnia, J. P. Gattuso, et al. (Eds.), *Copernicus marine service ocean state report, issue 5* (Vol. 14, pp. 1–185). Journal of Operational Oceanography. sup1. https://doi.org/10.1080/1755876X.2021.1946240

Ben Ismail, S., Schroeder, K., Sammari, C., Gasparini, G. P., Borghini, M., & Aleya, L. (2014). Interannual variability of water mass properties in the Tunisia–Sicily Channel. *Journal of Marine Systems*, *135*, 14–28. https://doi.org/10.1016/j.jmarsys.2013.06.010

Bensoussan, N., Cebrian, E., Dominici, J.-M., Kersting, D.-K., Kipson, S., Kizilkaya, Z., et al. (2019). Using CMEMS and the Mediterranean Marine Protected Areas sentinel network to track ocean warming effects in coastal areas. In K. von Schuckmann, P. Y. Le Traon, N. Smith, A. Pascual, S. Djavidnia, J. P. Gattuso, et al. (Eds.), *Copernicus marine service ocean state report, issue 3* (Vol. 12, pp. S1–S123). Journal of Operational Oceanography. sup1. https://doi.org/10.1080/1755876X.2019.1633075

Béranger, K., Mortier, L., & Crépon, M. (2005). Seasonal variability of water transport through the Straits of Gibraltar, Sicily and Corsica, derived from a high-resolution model of the Mediterranean circulation. *Progress in Oceanography*, *66*(2–4), 341–364. https://doi.org/10.1016/j.pocean.2004.07.013

Béranger, K., Mortier, L., Gasparini, G.-P., Gervasio, L., Astraldi, M., & Crépon, M. (2004). The dynamics of the sicily strait: A comprehensive study from observations and models. *Deep Sea Research Part II: Topical Studies in Oceanography*, *51*(4–5), 411–440. https://doi.org/10.1016/j.dsr2.2003.08.004

Bergamasco, A., & Malanotte-Rizzoli, P. (2010). The circulation of the Mediterranean Sea: A historical review of experimental investigations. *Advances in Oceanography and Limnology*, *1*(1), 11–28. https://doi.org/10.1080/19475721.2010.491656

Bethoux, J. (1980). Mean water fluxes across sections in the mediterranean-sea, evaluated on the basis of water and salt budgets and of observed salinities. *Oceanologica Acta*, *3*(1), 79–88.

Bethoux, J. P., & Gentili, B. (1999). Functioning of the Mediterranean Sea: Past and present changes related to freshwater input and climate changes. *Journal of Marine Systems*, *20*(1–4), 33–47. https://doi.org/10.1016/S0924-7963(98)00069-4

Béthoux, J.-P., Gentili, B., & Tailliez, D. (1998). Warming and freshwater budget change in the Mediterranean since the 1940s, their possible relation to the greenhouse effect. *Geophysical Research Letters*, *25*(7), 1023–1026. https://doi.org/10.1029/98GL00724

Bethoux, J. P., Prieur, L., & Nyffeler, F. (1982). The water circulation in the North-Western Mediterranean Sea, its relations with wind and atmospheric pressure. In J. C. J. Nihoul (Ed.), *Elsevier oceanography series* (Vol. 34, pp. 129–142). Elsevier. https://doi.org/10.1016/S0422-9894(08)71240-6

Beuvier, J., Béranger, K., Lebeaupin Brossier, C., Somot, S., Sevault, F., Drillet, Y., et al. (2012). Spreading of the Western Mediterranean Deep Water after winter 2005: Time scales and deep cyclone transport. *Journal of Geophysical Research*, *117*(C7). https://doi.org/10.1029/2011JC007679

Beuvier, J., Hamon, M., Greiner, E., Drévillon, M., & Lellouche, J. (2016). New version of MEDRYS, A Mediterranean Sea reanalysis during 1992–2013. *1*.

Bond, G., Showers, W., Cheseby, M., Lotti, R., Almasi, P., de Menocal, P., et al. (1997). A pervasive millennial-scale cycle in north Atlantic Holocene and glacial climates. *Science*, *278*(5341), 1257–1266. https://doi.org/10.1126/science.278.5341.1257

Bosse, A., Testor, P., Houpert, L., Damien, P., Prieur, L., Hayes, D., et al. (2016). Scales and dynamics of submesoscale coherent vortices formed by deep convection in the northwestern Mediterranean Sea. *Journal of Geophysical Research: Oceans*, *121*(10), 7716–7742. https://doi.org/10.1002/2016JC012144

Bosse, A., Testor, P., Mortier, L., Prieur, L., Taillandier, V., d'Ortenzio, F., & Coppola, L. (2015). Spreading of Levantine Intermediate Waters by submesoscale coherent vortices in the northwestern Mediterranean Sea as observed with gliders. *Journal of Geophysical Research: Oceans*, *120*(3), 1599–1622. https://doi.org/10.1002/2014JC010263

Bryden, H. L., Candela, J., & Kinder, T. H. (1994). Exchange through the Strait of Gibraltar. *Progress in Oceanography*, *33*(3), 201–248. https://doi.org/10.1016/0079-6611(94)90028-0

Buffett, G. G., Krahmann, G., Klaeschen, D., Schroeder, K., Sallarès, V., Papenberg, C., et al. (2017). Seismic oceanography in the Tyrrhenian Sea: Thermohaline staircases, eddies, and internal waves. *Journal of Geophysical Research: Oceans*, *122*(11), 8503–8523. https://doi.org/10.1002/2017JC012726

Cabanes, C., Grouazel, A., von Schuckmann, K., Hamon, M., Turpin, V., Coatanoan, C., et al. (2013). The CORA dataset: Validation and diagnostics of in-situ ocean temperature and salinity measurements. *Ocean Science*, *9*(1), 1–18. https://doi.org/10.5194/os-9-1-2013

Cacho, I., Grimalt, J. O., Canals, M., Sbaffi, L., Shackleton, N. J., Schönfeld, J., & Zahn, R. (2001). Variability of the western Mediterranean Sea surface temperature during the last 25,000 years and its connection with the Northern Hemisphere climatic changes. *Paleoceanography*, *16*(1), 40–52. https://doi.org/10.1029/2000PA000502

Cacho, I., Grimalt, J. O., Sierro, F. J., Shackleton, N., & Canals, M. (2000). Evidence for enhanced Mediterranean thermohaline circulation during rapid climatic coolings. *Earth and Planetary Science Letters*, *183*(3–4), 417–429. https://doi.org/10.1016/S0012-821X(00)00296-X

Cardin, V., Civitarese, G., Hainbucher, D., Bensi, M., & Rubino, A. (2015). Thermohaline properties in the Eastern Mediterranean in the last three decades: Is the basin returning to the pre-EMT situation? *Ocean Science*, *11*(1), 53–66. https://doi.org/10.5194/os-11-53-2015

Carracedo, L. I., Gilcoto, M., Mercier, H., & Pérez, F. F. (2014). Seasonal dynamics in the Azores–Gibraltar Strait region: A climatologically-based study. *Progress in Oceanography*, *122*, 116–130. https://doi.org/10.1016/j.pocean.2013.12.005

CIESM. (2001). Round table session on Mediterranean water mass acronyms. In *36Th CIESM Congress, Monte Carlo, 26 September 2001*. Retrieved from http://ciesm.org/events/RT5-WaterMassAcronyms.pdf

CIESM. (2002). Tracking long-term hydrological change in the Mediterranean Sea. In *Workshop Series* (Vol. 16). Retrieved from http://www.ciesm.org/online/monographs/Monaco02.html

CIESM. (2022). C2 COMMITTEE—Physics and Climate of the Ocean. Revision and update of the water mass acronyms. In *Hybrids meetings of 26 August 2022 and 5 October 2022*. Retrieved from https://ciesm.org/MWM_Acronyms/MedWaterMassAcronyms.pdf

Colin, J., Déqué, M., Radu, R., & Somot, S. (2010). Sensitivity study of heavy precipitation in limited area model climate simulations: Influence of the size of the domain and the use of the spectral nudging technique. *Tellus A: Dynamic Meteorology and Oceanography*, *62*(5), 591–604. https://doi.org/10.1111/j.1600-0870.2010.00467.x

Cortina-Guerra, A., Gomez-Navarro, J. J., Martrat, B., Montávez, J. P., Incarbona, A., Grimalt, J. O., et al. (2021). Northern Hemisphere atmospheric pattern enhancing Eastern Mediterranean Transient-type events during the past 1000 years. *Climate of the Past*, *17*(4), 1523–1532. https://doi.org/10.5194/cp-17-1523-2021

Crépon, M., & Boukthir, M. (1987). Effect of deep water formation on the circulation of the Ligurian Sea. *Effect of Deep Water Formation on the Circulation of the Ligurian Sea*, *5*(1), 43–48.

Darmaraki, S., Somot, S., Sevault, F., Nabat, P., Cabos Narvaez, W. D., Cavicchia, L., et al. (2019). Future evolution of Marine Heatwaves in the Mediterranean Sea. *Climate Dynamics*, *53*(3–4), 1371–1392. https://doi.org/10.1007/s00382-019-04661-z

de Brauwere, A., Jacquet, S. H. M., De Ridder, F., Dehairs, F., Pintelon, R., Schoukens, J., & Baeyens, W. (2007). Water mass distributions in the Southern Ocean derived from a parametric analysis of mixing water masses. *Journal of Geophysical Research*, *112*(C2), C02021. https://doi.org/10.1029/2006JC003742

Dee, D. P., Uppala, S. M., Simmons, A. J., Berrisford, P., Poli, P., Kobayashi, S., et al. (2011). The ERA-Interim reanalysis: Configuration and performance of the data assimilation system. *Quarterly Journal of the Royal Meteorological Society*, *137*(656), 553–597. https://doi.org/10.1002/qj.828

de Sherbinin, A. (2014). Climate change hotspots mapping: What have we learned? *Climatic Change*, *123*(1), 23–37. https://doi.org/10.1007/s10584-013-0900-7

Escudier, R., Clementi, E., Cipollone, A., Pistoia, J., Drudi, M., Grandi, A., et al. (2021). A high resolution reanalysis for the Mediterranean Sea. *Frontiers in Earth Science*, *9*, 1060. https://doi.org/10.3389/feart.2021.702285

Escudier, R., Mourre, B., Juza, M., & Tintoré, J. (2016). Subsurface circulation and mesoscale variability in the Algerian subbasin from altimeter-derived eddy trajectories. *Journal of Geophysical Research: Oceans*, *121*(8), 6310–6322. https://doi.org/10.1002/2016JC011760

Estournel, C., Marsaleix, P., & Ulses, C. (2021). A new assessment of the circulation of Atlantic and intermediate Waters in the Eastern Mediterranean. *Progress in Oceanography*, *198*, 102673. https://doi.org/10.1016/j.pocean.2021.102673

Falco, P., Trani, M., & Zambianchi, E. (2016). Water mass structure and deep mixing processes in the Tyrrhenian Sea: Results from the VECTOR project. *Deep Sea Research Part I: Oceanographic Research Papers*, *113*, 7–21. https://doi.org/10.1016/j.dsr.2016.04.002

Fedele, G., Mauri, E., Notarstefano, G., & Poulain, P. M. (2022). Characterization of the Atlantic Water and Levantine Intermediate Water in the Mediterranean Sea using 20 years of Argo data. *Ocean Science*, *18*(1), 129–142. https://doi.org/10.5194/os-18-129-2022

Flament, P. (2002). A state variable for characterizing water masses and their diffusive stability: Spiciness. *Progress in Oceanography*, *54*(1–4), 493–501. https://doi.org/10.1016/S0079-6611(02)00065-4

Fox-Kemper, B., Adcroft, A., Böning, C. W., Chassignet, E. P., Curchitser, E., Danabasoglu, G., et al. (2019). Challenges and prospects in ocean circulation models. *Frontiers in Marine Science*, *6*. https://doi.org/10.3389/fmars.2019.00065

Fuda, J.-L., Etiope, G., Millot, C., Favali, P., Calcara, M., Smriglio, G., & Boschi, E. (2002). Warming, salting and origin of the Tyrrhenian Deep Water: Warming, salting and origin of the Tyrrhenian deep water. *Geophysical Research Letters*, *29*(19), 4-1–4-4. https://doi.org/10.1029/2001GL014072

Fuda, J. L., Millot, C., Taupier-Letage, I., Send, U., & Bocognano, J. M. (2000). XBT monitoring of a meridian section across the western Mediterranean Sea. *Deep Sea Research Part I: Oceanographic Research Papers*, *47*(11), 2191–2218. https://doi.org/10.1016/s0967-0637(00)00018-2

Gangloff, A., Verney, R., Doxaran, D., Ody, A., & Estournel, C. (2017). Investigating Rhône River plume (Gulf of Lions, France) dynamics using metrics analysis from the MERIS 300m Ocean Color archive (2002–2012). *Continental Shelf Research*, *144*, 98–111. https://doi.org/10.1016/j.csr.2017.06.024

Gao, Y., Huang, R. X., Zhu, J., Huang, Y., & Hu, J. (2020). Using the Sigma-Pi diagram to analyze water masses in the northern south China Sea in spring. *Journal of Geophysical Research: Oceans*, *125*(7), e2019JC015676. https://doi.org/10.1029/2019JC015676

García-Herrera, R., Díaz, J., Trigo, R. M., Luterbacher, J., & Fischer, E. M. (2010). A review of the European summer heat wave of 2003. *Critical Reviews in Environmental Science and Technology*, *40*(4), 267–306. https://doi.org/10.1080/10643380802238137

Gasparini, G. P., Ortona, A., Budillon, G., Astraldi, M., & Sansone, E. (2005). The effect of the Eastern Mediterranean Transient on the hydrographic characteristics in the Strait of Sicily and in the Tyrrhenian Sea. *Deep Sea Research Part I: Oceanographic Research Papers*, *52*(6), 915–935. https://doi.org/10.1016/j.dsr.2005.01.001

Giorgi, F. (2006). Climate change hot-spots. *Geophysical Research Letters*, *33*(8), L08707. https://doi.org/10.1029/2006GL025734

Hamon, M., Beuvier, J., Somot, S., Lellouche, J.-M., Greiner, E., Jordà, G., et al. (2016). Design and validation of MEDRYS, a Mediterranean Sea reanalysis over the period 1992–2013. *Ocean Science*, *12*(2), 577–599. https://doi.org/10.5194/os-12-577-2016

Hassoun, A. E. R., Guglielmi, V., Gemayel, E., Goyet, C., Saab, M. A.-A., Giani, M., et al. (2015). Is the Mediterranean Sea circulation in a steady state. *Journal of Water Resources and Ocean Science*, *4*(1), 6. https://doi.org/10.11648/j.wros.20150401.12

Herrmann, M., Estournel, C., Déqué, M., Marsaleix, P., Sevault, F., & Somot, S. (2008). Dense water formation in the Gulf of Lions shelf: Impact of atmospheric interannual variability and climate change. *Continental Shelf Research*, *28*(15), 2092–2112. https://doi.org/10.1016/j.csr.2008.03.003

Hjelmervik, K. T., & Hjelmervik, K. (2013). Estimating temperature and salinity profiles using empirical orthogonal functions and clustering on historical measurements. *Ocean Dynamics*, *63*(7), 809–821. https://doi.org/10.1007/s10236-013-0623-3

Houpert, L., Durrieu de Madron, X., Testor, P., Bosse, A., D'Ortenzio, F., Bouin, M. N., et al. (2016). Observations of open-ocean deep convection in the northwestern Mediterranean Sea: Seasonal and interannual variability of mixing and deep water masses for the 2007-2013 Period. *Journal of Geophysical Research: Oceans*, *121*(11), 8139–8171. https://doi.org/10.1002/2016JC011857

Huang, R. X., Yu, L.-S., & Zhou, S.-Q. (2018). New definition of potential spicity by the least square method. *Journal of Geophysical Research: Oceans*, *123*(10), 7351–7365. https://doi.org/10.1029/2018JC014306

Iacono, R., Napolitano, E., Marullo, S., Artale, V., & Vetrano, A. (2013). Seasonal variability of the Tyrrhenian Sea surface geostrophic circulation as assessed by altimeter data. *Journal of Physical Oceanography*, *43*(8), 1710–1732. https://doi.org/10.1175/JPO-D-12-0112.1

Iacono, R., Napolitano, E., Palma, M., & Sannino, G. (2021). The Tyrrhenian Sea circulation: A review of recent work. *Sustainability*, *13*(11), 6371. https://doi.org/10.3390/su13116371

Incarbona, A., Martrat, B., Mortyn, P. G., Sprovieri, M., Ziveri, P., Gogou, A., et al. (2016). Mediterranean circulation perturbations over the last five centuries: Relevance to past Eastern Mediterranean Transient-type events. *Scientific Reports*, *6*(1), 29623. https://doi.org/10.1038/srep29623

Intergovernmental Panel on Climate Change (IPCC). (2023). *Climate change 2021 – The physical science basis*. https://doi.org/10.1017/9781009157896

Iona, A., Theodorou, A., Sofianos, S., Watelet, S., Troupin, C., & Beckers, J.-M. (2018). Mediterranean Sea climatic indices: Monitoring long-term variability and climate changes. *Earth System Science Data*, *10*(4), 1829–1842. https://doi.org/10.5194/essd-10-1829-2018

Isern-Fontanet, J., García-Ladona, E., & Font, J. (2006). Vortices of the Mediterranean Sea: An altimetric perspective. *Journal of Physical Oceanography*, *36*(1), 87–103. https://doi.org/10.1175/JPO2826.1

Jebri, F., Birol, F., Zakardjian, B., Bouffard, J., & Sammari, C. (2016). Exploiting coastal altimetry to improve the surface circulation scheme over the central Mediterranean Sea. *Journal of Geophysical Research: Oceans*, *121*(7), 4888–4909. https://doi.org/10.1002/2016JC011961

Jordà, G., Von Schuckmann, K., Josey, S. A., Caniaux, G., García-Lafuente, J., Sammartino, S., et al. (2017). The Mediterranean Sea heat and mass budgets: Estimates, uncertainties and perspectives. *Progress in Oceanography*, *156*, 174–208. https://doi.org/10.1016/j.pocean.2017.07.001

Josey, S. A., & Schroeder, K. (2023). Declining winter heat loss threatens continuing ocean convection at a Mediterranean dense water formation site. *Environmental Research Letters*, *18*(2), 024005. https://doi.org/10.1088/1748-9326/aca9e4

Juza, M., Escudier, R., Vargas-Yáñez, M., Mourre, B., Heslop, E., Allen, J., & Tintoré, J. (2019). Characterization of changes in Western Intermediate Water properties enabled by an innovative geometry-based detection approach. *Journal of Marine Systems*, *191*, 1–12. https://doi.org/10.1016/j.jmarsys.2018.11.003

Juza, M., Mourre, B., Lellouche, J.-M., Tonani, M., & Tintoré, J. (2015). From basin to sub-basin scale assessment and intercomparison of numerical simulations in the Western Mediterranean Sea. *Journal of Marine Systems*, *149*, 36–49. https://doi.org/10.1016/j.jmarsys.2015.04.010

Juza, M., Renault, L., Ruiz, S., & Tintoré, J. (2013). Origin and pathways of Winter Intermediate Water in the Northwestern Mediterranean Sea using observations and numerical simulation: Origin and Pathways of WIW in Nwmed. *Journal of Geophysical Research: Oceans*, *118*(12), 6621–6633. https://doi.org/10.1002/2013JC009231

Keller, D., Jr., Givon, Y., Pennel, R., Raveh-Rubin, S., & Drobinski, P. (2022). Untangling the mistral and seasonal atmospheric forcing driving deep convection in the Gulf of Lion: 2012–2013. *Ocean Science*, *18*(2), 483–510. https://doi.org/10.5194/os-18-483-2022

Kim, K., Kim, K.-R., Rhee, T. S., Rho, H. K., Limeburner, R., & Beardsley, R. C. (1991). Identification of water masses in the Yellow Sea and the East China Sea by cluster analysis. In K. Takano (Ed.), *Elsevier oceanography series* (Vol. 54, pp. 253–267). Elsevier. https://doi.org/10.1016/S0422-9894(08)70100-4

Knoll, M., Borrione, I., Fiekas, H.-V., Funk, A., Hemming, M. P., Kaiser, J., et al. (2017). Hydrography and circulation west of Sardinia in June 2014. *Ocean Science*, *13*(6), 889–904. https://doi.org/10.5194/os-13-889-2017

Kubin, E., Poulain, P.-M., Mauri, E., Menna, M., & Notarstefano, G. (2019). Levantine intermediate and Levantine deep Water Formation: An Argo float study from 2001 to 2017. *Water*, *11*(9), 1781. https://doi.org/10.3390/w11091781

Lellouche, J.-M., Le Galloudec, O., Drévillon, M., Régnier, C., Greiner, E., Garric, G., et al. (2013). Evaluation of global monitoring and forecasting systems at Mercator Océan. *Ocean Science*, *9*(1), 57–81. https://doi.org/10.5194/os-9-57-2013

Li, P., & Tanhua, T. (2020). Recent changes in deep ventilation of the Mediterranean Sea; evidence from long-term transient tracer observations. *Frontiers in Marine Science*, *7*, 594. https://doi.org/10.3389/fmars.2020.00594

López-Jurado, J.-L., González-Pola, C., & Vélez-Belchí, P. (2005). Observation of an abrupt disruption of the long-term warming trend at the Balearic Sea, western Mediterranean Sea, in summer 2005. *Geophysical Research Letters*, *32*(24). https://doi.org/10.1029/2005GL024430

Ludwig, W., Dumont, E., Meybeck, M., & Heussner, S. (2009). River discharges of water and nutrients to the Mediterranean and Black Sea: Major drivers for ecosystem changes during past and future decades? *Progress in Oceanography*, *80*(3), 199–217. https://doi.org/10.1016/j.pocean.2009.02.001

Madec, G., Delecluse, P., Crepon, M., & Chartier, M. (1991). A three-dimensional numerical study of deep-water formation in the northwestern Mediterranean Sea. *Journal of Physical Oceanography*, *21*(9), 1349–1371. https://doi.org/10.1175/1520-0485(1991)021<1349:ATDNSO>2.0.CO;2

Mallil, K., Testor, P., Bosse, A., Margirier, F., Houpert, L., Le Goff, H., et al. (2021). The Levantine Intermediate Water in the western Mediterranean and its interactions with the Algerian Gyres: Insights from 60 years of observation. *Ocean Science Discussions*, 1–26. https://doi.org/10.5194/os-2021-120

Mamayev, O. I. (1975). *Temperature-salinity analysis of world ocean waters*. Elsevier.

Manca, B. B., Ibello, V., Pacciaroni, M., Scarazzato, P., & Giorgetti, A. (2006). Ventilation of deep waters in the Adriatic and Ionian Seas following changes in thermohaline circulation of the Eastern Mediterranean. *Climate Research*, *31*(2–3), 239–256. https://doi.org/10.3354/cr031239

Manzella, G. M. R. (1984). Fluxes across the Corsica Channel and coastal circulation in the East Ligurian Sea-North-Western Mediterranean. *Fluxes across the Corsica Channel and Coastal Circulation in the East Ligurian Sea-North-Western Mediterranean*, *8*(1), 29–35.

Manzella, G. M. R., & La Violette, P. E. (1990). The seasonal variation of water mass content in the western Mediterranean and its relationship with the inflows through the straits of Gibraltar and Sicily. *Journal of Geophysical Research*, *95*(C2), 1623–1626. https://doi.org/10.1029/JC095iC02p01623

Margirier, F., Testor, P., Heslop, E., Mallil, K., Bosse, A., Houpert, L., et al. (2020). Abrupt warming and salinification of intermediate waters interplays with decline of deep convection in the Northwestern Mediterranean Sea. *Scientific Reports*, *10*(1), 20923. https://doi.org/10.1038/s41598-020-77859-5

Mariotti, A., Struglia, M. V., Zeng, N., & Lau, K. M. (2002). The hydrological cycle in the mediterranean region and Implications for the water budget of the Mediterranean Sea. *Journal of Climate*, *15*(13), 17–1690. https://doi.org/10.1175/1520-0442(2002)015<1674:thcitm>2.0.co;2

Martínez, J., Leonelli, F. E., García-Ladona, E., Garrabou, J., Kersting, D. K., Bensoussan, N., & Pisano, A. (2023). Evolution of marine heatwaves in warming seas: The Mediterranean Sea case study. *Frontiers in Marine Science*, *10*. https://doi.org/10.3389/fmars.2023.1193164

Marty, J. C., & Chiavérini, J. (2010). Hydrological changes in the Ligurian Sea (NW Mediterranean, DYFAMED site) during 1995–2007 and biogeochemical consequences. *Biogeosciences*, *7*(7), 2117–2128. https://doi.org/10.5194/bg-7-2117-2010

Marullo, S., Santoleri, R., & Bignami, F. (1994). The surface characteristics of the Tyrrhenian Sea: Historical satellite data analysis. In *Seasonal and interannual variability of the western Mediterranean Sea* (pp. 135–154). American Geophysical Union (AGU). https://doi.org/10.1029/CE046p0135

McDougall, T. J., & Krzysik, O. A. (2015). Spiciness. *Journal of Marine Research*, *73*(5), 141–152. https://doi.org/10.1357/002224015816665589

MEDOC GROUP. (1970). Observation of formation of deep water in the Mediterranean Sea, 1969. *Nature*, *227*(5262), 1037–1040. https://doi.org/10.1038/2271037a0

Millot, C. (1987). Circulation in the western mediterranean-sea. *Oceanologica Acta*, *10*(2), 143–149.

Millot, C. (1990). The Gulf of Lions' hydrodynamics. *Continental Shelf Research*, *10*(9–11), 885–894. https://doi.org/10.1016/0278-4343(90)90065-T

Millot, C. (1999). Circulation in the Western Mediterranean Sea. *Journal of Marine Systems*, *20*(1), 423–442. https://doi.org/10.1016/S0924-7963(98)00078-5

Millot, C. (2007). Interannual salinification of the Mediterranean inflow. *Geophysical Research Letters*, *34*(21). https://doi.org/10.1029/2007GL031179

Millot, C. (2009). Another description of the Mediterranean Sea outflow. *Progress in Oceanography*, *82*(2), 101–124. https://doi.org/10.1016/j.pocean.2009.04.016

Millot, C. (2013). Levantine intermediate water characteristics: An astounding general misunderstanding. *Scientia Marina*, *77*(2), 217–232. https://doi.org/10.3989/scimar.03518.13A

Millot, C., Candela, J., Fuda, J.-L., & Tber, Y. (2006). Large warming and salinification of the Mediterranean outflow due to changes in its composition. *Deep Sea Research Part I: Oceanographic Research Papers*, *53*(4), 656–666. https://doi.org/10.1016/j.dsr.2005.12.017

Millot, C., & Taupier-Letage, I. (2005a). Additional evidence of LIW entrainment across the Algerian subbasin by mesoscale eddies and not by a permanent westward flow. *Progress in Oceanography*, *66*(2–4), 231–250. https://doi.org/10.1016/j.pocean.2004.03.002

Millot, C., & Taupier-Letage, I. (2005b). Circulation in the Mediterranean Sea. In A. Saliot (Ed.), *The Mediterranean Sea* (Vol. 5K, pp. 29–66). Springer Berlin Heidelberg. https://doi.org/10.1007/b107143

Napolitano, E., Iacono, R., Ciuffardi, T., Reseghetti, F., Poulain, P.-M., & Notarstefano, G. (2019). The Tyrrhenian Intermediate Water (TIW): Characterization and formation mechanisms. *Progress in Oceanography*, *170*, 53–68. https://doi.org/10.1016/j.pocean.2018.10.017

Napolitano, E., Iacono, R., & Marullo, S. (2014). The 2009 surface and intermediate circulation of the Tyrrhenian Sea as assessed by an operational model. In *The Mediterranean Sea* (pp. 59–74). American Geophysical Union (AGU). https://doi.org/10.1002/9781118847572.ch5

Nof, D. (1979). On man-induced variations in the circulation of the Mediterranean Sea. *Tellus*, *31*(6), 558–564. https://doi.org/10.1111/j.2153-3490.1979.tb00937.x

Nykjaer, L. (2009). Mediterranean Sea surface warming 1985–2006. *Climate Research*, *39*, 11–17. https://doi.org/10.3354/cr00794

Olita, A., Sorgente, R., Natale, S., Gaberšek, S., Ribotti, A., Bonanno, A., & Patti, B. (2007). Effects of the 2003 European heatwave on the Central Mediterranean Sea: Surface fluxes and the dynamical response. *Ocean Science*, *3*(2), 273–289. https://doi.org/10.5194/os-3-273-2007

Onken, R., & Sellschopp, J. (2001). Water masses and circulation between the eastern Algerian Basin and the Strait of Sicily in October 1996. *Oceanologica Acta*, *24*(2), 151–166. https://doi.org/10.1016/S0399-1784(00)01135-X

Ozer, T., Gertman, I., Kress, N., Silverman, J., & Herut, B. (2017). Interannual thermohaline (1979–2014) and nutrient (2002–2014) dynamics in the Levantine surface and intermediate water masses, SE Mediterranean Sea. *Global and Planetary Change*, *151*, 60–67. https://doi.org/10.1016/j.gloplacha.2016.04.001

Parras-Berrocal, I. M., Vázquez, R., Cabos, W., Sein, D. V., Álvarez, O., Bruno, M., & Izquierdo, A. (2022). Surface and intermediate water changes triggering the future collapse of deep water formation in the North Western Mediterranean. *Geophysical Research Letters*, *49*(4), e2021GL095404. https://doi.org/10.1029/2021gl095404

Peliz, A., Boutov, D., & Teles-Machado, A. (2013). The Alboran Sea mesoscale in a long term high resolution simulation: Statistical analysis. *Ocean Modelling*, *72*, 32–52. https://doi.org/10.1016/j.ocemod.2013.07.002

Pellet, V., Aires, F., Munier, S., Fernández Prieto, D., Jordá, G., Dorigo, W. A., et al. (2019). Integrating multiple satellite observations into a coherent dataset to monitor the full water cycle—Application to the Mediterranean region. *Hydrology and Earth System Sciences*, *23*(1), 465–491. https://doi.org/10.5194/hess-23-465-2019

Pessini, F., Olita, A., Cotroneo, Y., & Perilli, A. (2018). Mesoscale eddies in the Algerian basin: Do they differ as a function of their formation site? *Ocean Science*, *14*(4), 669–688. https://doi.org/10.5194/os-14-669-2018

Pinardi, N., Cessi, P., Borile, F., & Wolfe, C. L. P. (2019). The Mediterranean Sea overturning circulation. *Journal of Physical Oceanography*, *49*(7), 1699–1721. https://doi.org/10.1175/JPO-D-18-0254.1

Pinardi, N., Zavatarelli, M., Adani, M., Coppini, G., Fratianni, C., Oddo, P., et al. (2015). Mediterranean Sea large-scale low-frequency ocean variability and water mass formation rates from 1987 to 2007: A retrospective analysis. *Progress in Oceanography*, *132*, 318–332. https://doi.org/10.1016/j.pocean.2013.11.003

Piñeiro, S., González-Pola, C., Fernández-Díaz, J. M., & Balbin, R. (2019). Thermohaline evolution of the western Mediterranean deep waters since 2005: Diffusive stages and interannual renewal Injections. *Journal of Geophysical Research: Oceans*, *124*(12), 8747–8766. https://doi.org/10.1029/2019JC015094

Piñeiro, S., González-Pola, C., Fernández-Díaz, J. M., Naveira-Garabato, A. C., Sánchez-Leal, R., Puig, P., et al. (2021). Persistent, depth-Intensified mixing during the Western Mediterranean Transition's initial stages. *Journal of Geophysical Research: Oceans*, *126*(2). https://doi.org/10.1029/2020JC016535

Pinot, J.-M., Tintoré, J., & Gomis, D. (1995). Multivariate analysis of the surface circulation in the Balearic Sea. *Progress in Oceanography*, *36*(4), 343–376. https://doi.org/10.1016/0079-6611(96)00003-1

Pisano, A., Marullo, S., Artale, V., Falcini, F., Yang, C., Leonelli, F. E., et al. (2020). New evidence of Mediterranean climate change and variability from sea surface temperature observations. *Remote Sensing*, *12*(1), 132. https://doi.org/10.3390/rs12010132

Prieur, L., D'ortenzio, F., Taillandier, V., & Testor, P. (2020). Physical oceanography of the Ligurian Sea. In C. Migon, P. Nival, & A. Sciandra (Eds.), *The Mediterranean Sea in the era of global change 1* (1st ed., pp. 49–78). Wiley. https://doi.org/10.1002/9781119706960.ch3

Prieur, L., Lefevre, D., Gorsky, G., Bianchi, M., Andersen, V., & Gratton, Y. (2003). Frontal processes enhance productivity of the Alboran Sea: A tentative first synthesis of the Almofront 2 experiment results, 14063. In *Presented at the EGS—AGU—EUG Joint Assembly*.

Puig, P., de Madron, X. D., Salat, J., Schroeder, K., Martín, J., Karageorgis, A. P., et al. (2013). Thick bottom nepheloid layers in the western Mediterranean generated by deep dense shelf water cascading. *Progress in Oceanography*, *111*, 1–23. https://doi.org/10.1016/j.pocean.2012.10.003

Puillat, I., Taupier-Letage, I., & Millot, C. (2002). Algerian Eddies lifetime can near 3 years. *Journal of Marine Systems*, *31*(4), 245–259. https://doi.org/10.1016/S0924-7963(01)00056-2

Reynolds, R. W., Smith, T. M., Liu, C., Chelton, D. B., Casey, K. S., & Schlax, M. G. (2007). Daily high-resolution-blended analyses for sea surface temperature. *Journal of Climate*, *20*(22), 5473–5496. https://doi.org/10.1175/2007JCLI1824.1

Rhein, M., Send, U., Klein, B., & Krahmann, G. (1999). Interbasin deep water exchange in the western Mediterranean. *Journal of Geophysical Research*, *104*(C10), 23495–23508. https://doi.org/10.1029/1999JC900162

Rio, M. H., Guinehut, S., & Larnicol, G. (2011). New CNES-CLS09 global mean dynamic topography computed from the combination of GRACE data, altimetry, and in situ measurements. *Journal of Geophysical Research*, *116*(C7). https://doi.org/10.1029/2010JC006505

Rixen, M., Beckers, J.-M., Levitus, S., Antonov, J., Boyer, T., Maillard, C., et al. (2005). The Western Mediterranean deep water: A proxy for climate change. *Geophysical Research Letters*, *32*(12). https://doi.org/10.1029/2005GL022702

Robinson, A. R., & Golnaraghi, M. (1994). The physical and dynamical oceanography of the Mediterranean Sea. In P. Malanotte-Rizzoli & A. R. Robinson (Eds.), *Ocean processes in climate dynamics: Global and Mediterranean examples* (pp. 255–306). Springer Netherlands. https://doi.org/10.1007/978-94-011-0870-6_12

Roether, W., Klein, B., Manca, B. B., Theocharis, A., & Kioroglou, S. (2007). Transient Eastern Mediterranean deep waters in response to the massive dense-water output of the Aegean Sea in the 1990s. *Progress in Oceanography*, *74*(4), 540–571. https://doi.org/10.1016/j.pocean.2007.03.001

Salat, J., & Font, J. (1987). Water mass structure near and offshore the Catalan coast during the winters of 1982 and 1983. *5*(1), 48–54.

Sammari, C., Millot, C., Taupier-Letage, I., Stefani, A., & Brahim, M. (1999). Hydrological characteristics in the Tunisia–Sardinia–Sicily area during spring 1995. *Deep Sea Research Part I: Oceanographic Research Papers*, *46*(10), 1671–1703. https://doi.org/10.1016/S0967-0637(99)00026-6

Sammartino, S., García Lafuente, J., Naranjo, C., Sánchez Garrido, J. C., Sánchez Leal, R., & Sánchez Román, A. (2015). Ten years of marine current measurements in Espartel Sill, Strait of Gibraltar. *Journal of Geophysical Research: Oceans*, *120*(9), 6309–6328. https://doi.org/10.1002/2014JC010674

Schauer, U., & Losch, M. (2019). "Freshwater" in the ocean is not a useful parameter in climate research. *Journal of Physical Oceanography*, *49*(9), 2309–2321. https://doi.org/10.1175/JPO-D-19-0102.1

Schneider, A., Tanhua, T., Roether, W., & Steinfeldt, R. (2014). Changes in ventilation of the Mediterranean Sea during the past 25 year. *Ocean Science*, *10*(1), 1–16. https://doi.org/10.5194/os-10-1-2014

Schröder, K., Gasparini, G. P., Tangherlini, M., & Astraldi, M. (2006). Deep and intermediate water in the western Mediterranean under the influence of the Eastern Mediterranean Transient. *Geophysical Research Letters*, *33*(21), L21607. https://doi.org/10.1029/2006GL027121

Schroeder, K., Chiggiato, J., Bryden, H. L., Borghini, M., & Ben Ismail, S. (2016). Abrupt climate shift in the Western Mediterranean Sea. *Scientific Reports*, *6*(1), 23009. https://doi.org/10.1038/srep23009

Schroeder, K., Chiggiato, J., Josey, S. A., Borghini, M., Aracri, S., & Sparnocchia, S. (2017). Rapid response to climate change in a marginal sea. *Scientific Reports*, *7*(1), 4065. https://doi.org/10.1038/s41598-017-04455-5

Schroeder, K., Cozzi, S., Belgacem, M., Borghini, M., Cantoni, C., Durante, S., et al. (2020). Along-path evolution of biogeochemical and carbonate system properties in the intermediate water of the Western Mediterranean. *Frontiers in Marine Science*, *7*. https://doi.org/10.3389/fmars.2020.00375

Schroeder, K., Josey, S. A., Herrmann, M., Grignon, L., Gasparini, G. P., & Bryden, H. L. (2010). Abrupt warming and salting of the Western Mediterranean deep water after 2005: Atmospheric forcings and lateral advection. *Journal of Geophysical Research*, *115*(C8), C08029. https://doi.org/10.1029/2009JC005749

Schroeder, K., Ribotti, A., Borghini, M., Sorgente, R., Perilli, A., & Gasparini, G. P. (2008). An extensive western Mediterranean deep water renewal between 2004 and 2006. *Geophysical Research Letters*, *35*(18). https://doi.org/10.1029/2008GL035146

Schroeder, K., Taillandier, V., Vetrano, A., & Gasparini, G. P. (2008). The circulation of the western Mediterranean Sea in spring 2005 as inferred from observations and from model outputs. *Deep Sea Research Part I: Oceanographic Research Papers*, *55*(8), 947–965. https://doi.org/10.1016/j.dsr.2008.04.003

Schroeder, K., Tanhua, T., Chiggiato, J., Velaoras, D., Josey, S. A., García Lafuente, J., & Vargas-Yáñez, M. (2023). Chapter 4—The forcings of the Mediterranean Sea and the physical properties of its water masses. In K. Schroeder & J. Chiggiato (Eds.), *Oceanography of the Mediterranean Sea* (pp. 93–123). Elsevier. https://doi.org/10.1016/B978-0-12-823692-5.00005-4

Send, U., & Testor, P. (2017). Direct observations reveal the deep circulation of the Western Mediterranean Sea. *Journal of Geophysical Research: Oceans*, *122*(12), 10091–10098. https://doi.org/10.1002/2016JC012679

Sisma-Ventura, G., Kress, N., Silverman, J., Gertner, Y., Ozer, T., Biton, E., et al. (2021). Post-eastern Mediterranean transient oxygen decline in the deep waters of the Southeast Mediterranean Sea supports weakening of ventilation rates. *Frontiers in Marine Science*, *7*. https://doi.org/10.3389/fmars.2020.598686

Skliris, N., Zika, J. D., Herold, L., Josey, S. A., & Marsh, R. (2018). Mediterranean sea water budget long-term trend inferred from salinity observations. *Climate Dynamics*, *51*(7–8), 2857–2876. https://doi.org/10.1007/s00382-017-4053-7

Somot, S., Houpert, L., Sevault, F., Testor, P., Bosse, A., Taupier-Letage, I., et al. (2018). Characterizing, modelling and understanding the climate variability of the deep water formation in the North-Western Mediterranean Sea. *Climate Dynamics*, *51*(3), 1179–1210. https://doi.org/10.1007/s00382-016-3295-0

Somot, S., Sevault, F., & Déqué, M. (2006). Transient climate change scenario simulation of the Mediterranean Sea for the twenty-first century using a high-resolution ocean circulation model. *Climate Dynamics*, *27*(7), 851–879. https://doi.org/10.1007/s00382-006-0167-z

Somot, S., Sevault, F., Déqué, M., & Crépon, M. (2008). 21st century climate change scenario for the Mediterranean using a coupled atmosphere–ocean regional climate model. *Global and Planetary Change*, *63*(2–3), 112–126. https://doi.org/10.1016/j.gloplacha.2007.10.003

Sorgente, R., Olita, A., Oddo, P., Fazioli, L., & Ribotti, A. (2011). Numerical simulation and decomposition of kinetic energy in the Central Mediterranean: Insight on mesoscale circulation and energy conversion. *Ocean Science*, *7*(4), 503–519. https://doi.org/10.5194/os-7-503-2011

Soto-Navarro, J., Criado-Aldeanueva, F., García-Lafuente, J., & Sánchez-Román, A. (2010). Estimation of the Atlantic inflow through the Strait of Gibraltar from climatological and in situ data. *Journal of Geophysical Research*, *115*(C10), C10023. https://doi.org/10.1029/2010JC006302

Sparnocchia, S., Gasparini, G. P., Astraldi, M., Borghini, M., & Pistek, P. (1999). Dynamics and mixing of the Eastern Mediterranean outflow in the Tyrrhenian basin. *Journal of Marine Systems*, *20*(1–4), 301–317. https://doi.org/10.1016/S0924-7963(98)00088-8

Tailleux, R. (2021). Spiciness theory revisited, with new views on neutral density, orthogonality, and passiveness. *Ocean Science*, *17*(1), 203–219. https://doi.org/10.5194/os-17-203-2021

Testor, P., Béranger, K., & Mortier, L. (2005). Modeling the deep eddy field in the southwestern Mediterranean: The life cycle of Sardinian eddies. *Geophysical Research Letters*, *32*(13). https://doi.org/10.1029/2004GL022283

Testor, P., Bosse, A., Houpert, L., Margirier, F., Mortier, L., Legoff, H., et al. (2018). Multiscale observations of deep convection in the northwestern Mediterranean Sea during winter 2012–2013 using multiple Platforms. *Journal of Geophysical Research: Oceans*, *123*(3), 1745–1776. https://doi.org/10.1002/2016JC012671

Testor, P., Send, U., Gascard, J.-C., Millot, C., Taupier-Letage, I., & Béranger, K. (2005). The mean circulation of the southwestern Mediterranean Sea: Algerian Gyres. *Journal of Geophysical Research*, *110*(C11), C11017. https://doi.org/10.1029/2004JC002861

Theocharis, A. (2008). Do we expect significant changes in the Thermohaline Circulation in the Mediterranean in relation to the observed surface layers warming? *5*.

Theocharis, A., Georgopoulos, D., Lascaratos, A., & Nittis, K. (1993). Water masses and circulation in the central region of the Eastern Mediterranean: Eastern Ionian, South Aegean and Northwest Levantine. *Deep Sea Research Part II: Topical Studies in Oceanography*, *40*(6), 1121–1142. https://doi.org/10.1016/0967-0645(93)90064-T

de la Vara, A., del Sastre, P. G., Arsouze, T., Gallardo, C., & Gaertner, M. Á. (2019). Role of atmospheric resolution in the long-term seasonal variability of the Tyrrhenian Sea circulation from a set of ocean hindcast simulations (1997–2008). *Ocean Modelling*, *134*, 51–67. https://doi.org/10.1016/j.ocemod.2019.01.004

Vargas-Yáñez, M., Jesús García, M., Salat, J., García-Martínez, M. C., Pascual, J., & Moya, F. (2008). Warming trends and decadal variability in the Western Mediterranean shelf. *Global and Planetary Change*, *63*(2–3), 177–184. https://doi.org/10.1016/j.gloplacha.2007.09.001

Vargas-Yáñez, M., Juza, M., Balbín, R., Velez-Belchí, P., García-Martínez, M. C., Moya, F., & Hernández-Guerra, A. (2020). Climatological hydrographic properties and water mass transports in the balearic channels from repeated observations over 1996–2019. *Frontiers in Marine Science*, *7*, 568602. https://doi.org/10.3389/fmars.2020.568602

Vargas-Yáñez, M., Juza, M., García-Martínez, M. C., Moya, F., Balbín, R., Ballesteros, E., et al. (2021). Long-term changes in the water mass properties in the balearic channels over the period 1996–2019. *Frontiers in Marine Science*, *8*. https://doi.org/10.3389/fmars.2021.640535

Vargas-Yáñez, M., Zunino, P., Schroeder, K., López-Jurado, J. L., Plaza, F., Serra, M., et al. (2012). Extreme western intermediate Water formation in winter 2010. *Journal of Marine Systems*, *105–108*, 52–59. https://doi.org/10.1016/j.jmarsys.2012.05.010

Velaoras, D., Kassis, D., Perivoliotis, L., Pagonis, P., Hondronasios, A., & Nittis, K. (2013). Temperature and salinity variability in the Greek seas based on POSEIDON stations time series: Preliminary results. *Mediterranean Marine Science*, *14*(3), 5–18. https://doi.org/10.12681/mms.446

Velaoras, D., Krokos, G., Nittis, K., & Theocharis, A. (2014). Dense intermediate water outflow from the Cretan Sea: A salinity driven, recurrent phenomenon, connected to thermohaline circulation changes. *Journal of Geophysical Research: Oceans*, *119*(8), 4797–4820. https://doi.org/10.1002/2014JC009937

von Schuckmann, K., Le Traon, P.-Y., Smith, N., Pascual, A., Djavidnia, S., Gattuso, J.-P., et al., (2021). Copernicus Marine Service Ocean State Report, Issue 5. *Journal of Operational Oceanography*, *14*(sup1), 1–185. https://doi.org/10.1080/1755876x.2021.1946240

Waldman, R., Brüggemann, N., Bosse, A., Spall, M., Somot, S., & Sevault, F. (2018). Overturning the mediterranean thermohaline circulation. *Geophysical Research Letters*, *45*(16), 8407–8415. https://doi.org/10.1029/2018GL078502

Waldman, R., Herrmann, M., Somot, S., Arsouze, T., Benshila, R., Bosse, A., et al. (2017). Impact of the mesoscale dynamics on ocean deep convection: The 2012–2013 case study in the northwestern Mediterranean Sea. *Journal of Geophysical Research: Oceans*, *122*(11), 8813–8840. https://doi.org/10.1002/2016JC012587

Waldman, R., Somot, S., Herrmann, M., Bosse, A., Caniaux, G., Estournel, C., et al. (2017). Modeling the intense 2012–2013 dense water formation event in the northwestern Mediterranean Sea: Evaluation with an ensemble simulation approach: Modeling the 2012–2013 DWF event. *Journal of Geophysical Research: Oceans*, *122*(2), 1297–1324. https://doi.org/10.1002/2016JC012437

Waldman, R., Somot, S., Herrmann, M., Testor, P., Estournel, C., Sevault, F., et al. (2016). Estimating dense water volume and its evolution for the year 2012–2013 in the Northwestern Mediterranean Sea: An observing system simulation experiment approach: Estimating dense water volume. *Journal of Geophysical Research: Oceans*, *121*(9), 6696–6716. https://doi.org/10.1002/2016JC011694

Wüst, G. (1961). On the vertical circulation of the Mediterranean Sea. *Journal of Geophysical Research*, *66*(10), 3261–3271. https://doi.org/10.1029/JZ066i010p03261

Zhu, J., Zheng, Q., Hu, J., Lin, H., Chen, D., Chen, Z., et al. (2019). Classification and 3-D distribution of upper layer water masses in the northern South China Sea. *Acta Oceanologica Sinica*, *38*(4), 126–135. https://doi.org/10.1007/s13131-019-1418-2